EFFICIENT SPECTRUM SENSING AND UTILIZATION FOR COGNITIVE RADIO

A Dissertation
Presented to
The Academic Faculty

By

Xiangwei Zhou

In Partial Fulfillment
of the Requirements for the Degree
Doctor of Philosophy
in
Electrical and Computer Engineering

School of Electrical and Computer Engineering
Georgia Institute of Technology
December 2011

EFFICIENT SPECTRUM SENSING AND UTILIZATION FOR COGNITIVE RADIO

Approved by:

Dr. Geoffrey Ye Li, Advisor
Professor, School of Electrical and Computer Engineering
Georgia Institute of Technology

Dr. Xiaoli Ma
Associate Professor, School of Electrical and Computer Engineering
Georgia Institute of Technology

Dr. Gordon L. Stüber
Professor, School of Electrical and Computer Engineering
Georgia Institute of Technology

Dr. Xingxing Yu
Professor, School of Mathematics
Georgia Institute of Technology

Dr. Ian F. Akyildiz
Professor, School of Electrical and Computer Engineering
Georgia Institute of Technology

Date Approved: August 8, 2011

To my parents and to my wife.

ACKNOWLEDGMENTS

This dissertation arose out of years of research that has been done since I came to Professor Li's group. I have worked with a great number of people and it is a pleasure to convey my gratitude to them all.

In the first place I would like to record my gratitude to Professor Geoffrey Li for his supervision, advice, and guidance since the beginning of this research. I have learned a lot from his impressive insights and extraordinary experiences in research. He provided me encouragement and support in different ways. He also helped me to improve my academic writing and oral presentation significantly. I appreciate his care and concern for my intellectual and personal growth. I am deeply indebted to him.

Many thanks go in particular to Dr. Anthony Soong, Dr. Dandan Wang, and Dr. Jun Ma. It has been my pleasant experience to work with them. My research has greatly benefited from their valuable advice and constructive comments.

I would also like to express my sincere thanks to Professor Gordon Stüber, Professor Ian Akyildiz, Professor Xiaoli Ma, and Professor Xingxing Yu for serving in my dissertation committee. Their broad perspectives helped me a lot in refining this dissertation.

I gratefully thank Professor Zhaoyang Zhang at Zhejiang University for stimulating my interest in wireless communications. I am thankful for all my labmates in the Information Transmission and Processing Laboratory and all my colleagues in the Centergy One Building for inspiring discussions. I thank all my friends at Georgia Institute of Technology for making this place warm and more attractive.

Finally, I would like to thank my parents. They have been supportive throughout my Ph.D. study. It was they who have shaped my positive attitude in both work and life. Most importantly, I would like to thank my wife Mingxuan for her unconditional love and understanding, without which I could never made this far. This dissertation is dedicated to my parents and to my wife.

TABLE OF CONTENTS

ACKNOWLEDGMENTS iv

LIST OF TABLES viii

LIST OF FIGURES ix

SUMMARY xi

CHAPTER 1 INTRODUCTION 1
1.1 Motivation 1
1.2 Literature Review 3
1.2.1 Spectrum Sensing for Cognitive Radio 3
1.2.2 Spectrum Utilization for Cognitive Radio 7
1.3 Our Approaches and Thesis Outline 10

CHAPTER 2 PROBABILITY-BASED PERIODIC SPECTRUM SENSING . 13
2.1 System Model 14
2.1.1 Licensed User Signal Model 14
2.1.2 General Frame Structure for Periodic Spectrum Sensing 15
2.1.3 Probability Model on Licensed User Appearance 15
2.2 Spectrum Sensing within One Single Frame 16
2.2.1 Optimal Detection Scheme 17
2.2.2 Probability-based Energy Detection Scheme 18
2.2.3 Conventional Energy Detection Scheme 20
2.2.4 Numerical Results 21
2.3 Periodic Spectrum Sensing in Multiple Consecutive Frames 25
2.3.1 Probability Model in Multiple Consecutive Frames 26
2.3.2 Evolution of Probability Sequence 27
2.3.3 Stable Detection Performance of Conventional Scheme 28
2.3.4 Stable Detection Performance of Probability-based Scheme 31
2.3.5 Numerical Results 32
2.4 Conclusion 33

CHAPTER 3 PROBABILITY-BASED OPTIMIZATION OF INTER-SENSING DURATION AND POWER CONTROL 36
3.1 System Model 37
3.2 Strategy within Silent Block 38
3.2.1 Silent Block Length Optimization 38
3.2.2 Numerical Results 40
3.3 Strategies within Data Block 41
3.3.1 Data Block Length Optimization 41
3.3.2 Transmit Power Control 44

3.3.3 Numerical Results . . . 45
3.4 Conclusion . . . 46

CHAPTER 4 PROBABILITY-BASED COMBINATION FOR COOPERATIVE SPECTRUM SENSING . . . 49
4.1 System Model . . . 49
4.2 Optimal Combination for Cooperative Spectrum Sensing . . . 50
4.3 An Equivalent "K_0-Out-of-K" Scheme . . . 54
4.4 Simulation Results . . . 54
4.5 Conclusion . . . 56

CHAPTER 5 BANDWIDTH-EFFICIENT REPORTING FOR COOPERATIVE SPECTRUM SENSING . . . 57
5.1 System Model . . . 58
5.1.1 Local Spectrum Sensing and Processing . . . 58
5.1.2 Combination for Cooperative Spectrum Sensing . . . 59
5.2 Optimal Design with Gaussian Reporting Channel . . . 61
5.2.1 General Principle . . . 61
5.2.2 Probabilistic Information . . . 62
5.2.3 Practical Considerations . . . 64
5.3 Optimal Design with Fading Reporting Channel . . . 64
5.3.1 General Principle . . . 65
5.3.2 Threshold Optimization . . . 66
5.3.3 Probabilistic Information . . . 67
5.3.4 Performance Analysis . . . 68
5.3.5 Practical Considerations . . . 69
5.4 Simulation Results . . . 70
5.5 Conclusion . . . 73

CHAPTER 6 SPECTRUM SHAPING FOR OFDM-BASED COGNITIVE RADIO SYSTEMS . . . 77
6.1 System Model . . . 78
6.2 Low-Complexity Spectrum Shaping . . . 81
6.2.1 Basic Approach . . . 81
6.2.2 Sidelobe Decaying Rate . . . 83
6.2.3 Decoding . . . 84
6.2.4 Two-Level Power Control . . . 84
6.2.5 Simulation Results . . . 85
6.3 Multi-User Spectral Precoding . . . 88
6.3.1 Basic Approach . . . 90
6.3.2 Decoding . . . 91
6.3.3 Selection of Notched Frequencies . . . 92
6.3.4 Simulation Results . . . 94
6.4 Conclusion . . . 97

CHAPTER 7 PROBABILISTIC RESOURCE ALLOCATION FOR OPPORTUNISTIC SPECTRUM ACCESS 98
7.1 System Model 99
7.1.1 Opportunistic Spectrum Access 99
7.1.2 Multi-Channel Spectrum Sensing 100
7.2 Probabilistic Resource Allocation 101
7.2.1 Metrics for Resource Allocation 101
7.2.2 Probabilistic Information from Spectrum Sensing 103
7.3 Resource Allocation for One Single Cognitive Radio User 104
7.4 Resource Allocation for Multiple Cognitive Radio Users 107
7.5 Simulation Results 113
7.6 Conclusion 117

CHAPTER 8 CONCLUSION 120

APPENDIX A PROOF FOR CHAPTER 2 122
A.1 Proof of Proposition 2.2.1 122
A.2 Proof of Proposition 2.3.1 123
A.3 Proof of Proposition 2.3.2 124
A.4 Proof of Proposition 2.3.3 124

APPENDIX B PROOF FOR CHAPTER 4 127
B.1 Proof of Proposition 4.3.1 127

APPENDIX C PROOF FOR CHAPTER 5 128
C.1 Proof of (5.18) 128

APPENDIX D PROOF FOR CHAPTER 7 129
D.1 Proof of Proposition 7.3.1 129
D.2 Proof of Proposition 7.3.2 129
D.3 Proof of Proposition 7.3.3 130

REFERENCES 131

VITA 139

LIST OF TABLES

Table 6.1 Overall coding rates of different spectral precoding schemes. 97

Table 7.1 Probabilistic information in resource allocation 115

LIST OF FIGURES

Figure 1.1 Framework of efficient spectrum sensing and utilization. 3

Figure 2.1 Frame structure for periodic spectrum sensing. 15

Figure 2.2 Overall average detection probability curves of different spectrum sensing schemes. 23

Figure 2.3 Conditional CDF curves of m for different idle duration distributions. . 23

Figure 2.4 Effect of uncertainties in the idle duration distribution. 26

Figure 2.5 Curves of $f(x)$ under different SNR levels. 30

Figure 2.6 Stable average detection probability curves of the conventional and probability-based energy detection schemes. 33

Figure 2.7 Stable conditional CDF curves of m under different SNR levels when the probability-based energy detection scheme is applied. 34

Figure 2.8 Convergence of $x(n)$ under different SNR levels. 34

Figure 3.1 Optimal silent block length versus state transition rate. 41

Figure 3.2 Normalized average transmission rate and interference power versus data block length. 46

Figure 3.3 Optimal data block length versus state transition rate. 47

Figure 3.4 Transmission rate increment and interference power decrease versus average receive SNR. 48

Figure 4.1 Combining model for cooperative spectrum sensing. 51

Figure 4.2 Optimal combination structure for cooperative spectrum sensing. . . . 54

Figure 4.3 Performance comparison of different cooperative spectrum sensing schemes. 55

Figure 5.1 Reporting in cooperative spectrum sensing. 60

Figure 5.2 Performance curves under Gaussian reporting channel with different relative reporting SNRs. 71

Figure 5.3 Bayesian cost under Gaussian reporting channel with different numbers of samples collected in local spectrum sensing. 72

Figure 5.4 Performance curves under fading reporting channel with different relative reporting SNRs. 74

Figure 5.5 Bayesian cost under fading reporting channel with different sensing SNRs. 75

Figure 5.6 Complementary ROC curves under fading reporting channel with different reporting schemes. 75

Figure 6.1 Opportunistic spectrum utilization with guard bands. 80

Figure 6.2 System diagram of spectrally precoded OFDM. 80

Figure 6.3 Subcarriers of the OFDM symbol with the proposed spectrum shaping scheme. 81

Figure 6.4 PSD curves of spectral precoded OFDM signals. 86

Figure 6.5 BER curves of spectral precoded OFDM signals. 87

Figure 6.6 PSD curves of the proposed spectral precoded OFDM signals. 88

Figure 6.7 PSD curves of user signals with the proposed spectral precoder. 95

Figure 6.8 User BER curves under different spectrum shaping schemes. 96

Figure 6.9 PSD curves of user signals with the proposed spectral precoder and notched frequency selection. 96

Figure 7.1 The conventional approach versus the proposed approach for resource allocation in CR networks. 102

Figure 7.2 Overall data rates with respect to different noise powers with a single CR user. 114

Figure 7.3 Weighted sum data rates with respect to different noise powers with 2 CR users in Case 1. 116

Figure 7.4 Weighted sum data rates with respect to different noise powers with 2 CR users in Case 2. 116

Figure 7.5 Received interference power in Channel 15 with respect to different noise powers in Case 1. 117

Figure 7.6 Weighted sum data rates with respect to different noise powers with 8 CR users. 118

Figure 7.7 Evolution of weighted sum data rate in probabilistic resource allocation. 118

Figure A.1 Illustrative curve of $\phi = h(x)$ 125

SUMMARY

Cognitive radio (CR) technology has recently been introduced to opportunistically exploit the spectrum. CR users are allowed to utilize licensed spectrum bands as long as they do not cause unacceptable interference with licensed users. Such flexibility alleviates the crowding issue in particular spectrum bands and greatly enhances the efficiency of spectrum utilization. However, such improvement relies on a robust and cost-effective design involving identification and reuse of spectrum opportunities changing over time, frequency, and space. In this dissertation, we focus on efficient spectrum sensing and utilization techniques for high-performance *opportunistic spectrum access* (OSA). We emphasize the importance of exploring probabilistic information unique for CR and develop novel techniques playing critical roles in CR systems.

One enabling technique for CR is spectrum sensing, which aims at monitoring the usage of licensed spectrum. We first propose probability-based periodic spectrum sensing by utilizing the statistical characteristics of licensed channel occupancy, which achieves nearly optimal performance with relatively low complexity. For the first time, the possibility that a licensed user appears in the middle of a sensing block is taken into account. Based on the statistical model of licensed channel occupancy, we then propose periodic spectrum sensing scheduling to determine the optimal inter-sensing duration. The statistical information of licensed channel activity is also used to vary the transmit power at each data sample to enhance throughput and reduce interference. As cooperative spectrum sensing can further improve the detection reliability with the introduced spatial diversity, we develop a probability-based scheme for combination of local sensing information collected from cooperative CR users, which enables combination of both synchronous and asynchronous sensing information. To satisfy the stringent bandwidth constraint for reporting, we also propose to simultaneously send local sensing data to a combining node through the same

narrowband channel. The optimal local processing functions at the CR users and final decision rule at the combining node are discussed when the reporting channel is Gaussian and experiences fading, respectively. Calculation of probabilistic information involved is given as well. In the proposed approach, the bandwidth required for reporting does not change with the number of cooperative users. With proper preprocessing at individual users, such a design still maintains reasonable detection performance.

After determining the availability of certain licensed spectrum bands, CR users must select appropriate transmission parameters to better utilize these bands and avoid possible interference, which includes spectrum shaping and resource allocation. We propose a low-complexity spectrum shaping scheme for *orthogonal frequency-division multiplexing* (OFDM) based CR systems by mapping antipodal symbol pairs onto adjacent subcarriers at the edges of the utilized subbands. Sidelobe suppression and system throughput can be well balanced by adjusting the coding rate of the corresponding spectral precoder while power control on different sets of subcarriers is introduced to further lower the sidelobes. We also propose a spectral precoding scheme for multiple OFDM-based CR users to enhance spectral compactness. By constructing individual precoders to render selected spectrum nulls, our scheme ensures user independence and provides sufficient *out-of-band* (OOB) radiation suppression without *bit-error rate* (BER) performance loss. We consider the selection of notched frequencies to further increase the bandwidth efficiency. The proposed schemes enable efficient spectrum sharing between CR and licensed users and exhibit the advantages of both simplicity and flexibility. Then we provide a new resource allocation approach for OSA based on the probabilities of licensed channel availability obtained from spectrum sensing. Different from conventional approaches, the probabilistic approach exploits the flexibility of OSA to ensure efficient spectrum usage and protect licensed users from unacceptable interference at the same time. It also supports diverse *quality-of-service* (QoS) requirements in multi-user networks and can be implemented in a distributed manner.

CHAPTER 1

INTRODUCTION

1.1 Motivation

Static spectrum allocation and exclusive access through licensing lead to significant radio spectrum underutilization [1, 2]. To improve spectrum efficiency, *cognitive radio* (CR) technology has recently been introduced to opportunistically exploit the spectrum [3,4,5,6, 7,8,9]. Different from conventional wireless radios, a CR is able to monitor and analyze the spectrum usage and then determine its operating parameters to better adapt to the varying radio environment. CR users are allowed to utilize licensed spectrum bands as long as they do not cause unacceptable interference with licensed users. Such flexibility alleviates the crowding issue in particular spectrum bands and greatly enhances the efficiency of spectrum utilization. Consequently, CR technology has gained increasing attention and been highlighted by both standards and regulatory bodies [10, 11, 12].

One enabling technique for CR is spectrum sensing [13, 14], which aims at monitoring the usage of licensed spectrum. Before attempting to use a licensed spectrum band, CR users need to identify whether the band is occupied by any licensed user. During the use of a licensed spectrum band, CR users also need to recognize whether any licensed user become active in the band. To ensure that CR users utilize licensed spectrum on a non-interfering basis, it is critical to reliably detect the presence of licensed users. There are two types of detection error: false alarm, the presence of licensed users is claimed when the licensed users are absent, which may result in the loss of spectrum opportunities, and mis-detection, the absence of licensed users is claimed when the licensed users are present, which may result in the interference with licensed users. The probabilities of false alarm and mis-detection need to be well balanced for efficient spectrum use. Due to the inherent natures of wireless channels, it is sometimes difficult for a single CR user to achieve satisfactory spectrum sensing performance, in which case cooperation among multiple CR

users is necessary [15]. User cooperation takes advantage of spatial diversity at the expense of additional processing and feedback. Efficient spectrum sensing will not only enhance potential spectrum utilization but also minimize system overhead.

After determining the availability of certain licensed spectrum bands, CR users must select appropriate transmission parameters to better utilize these bands [7]. Meanwhile, possible interference with licensed users should be kept minimum [16]. The spectrum shape of transmitted CR signal is one of the most important aspects for efficient spectrum use. As there may be other licensed users in the spectrum bands adjacent to the operating bands of CR users, it is necessary to control the *out-of-band* (OOB) emission of transmitted CR signal in the adjacent bands. Otherwise, a lot of bandwidth may be spent on guard bands to protect licensed users. With efficient spectrum shaping, proper signal reception at the CR receivers should also be guaranteed. When there are multiple CR users in a CR network utilizing multiple licensed channels, resource allocation, which includes both channel and power allocations, is another important aspect affecting spectrum utilization and interference suppression. Through resource allocation, CR users should maximize performance metrics of their own, such as system throughput, and maintain interference within the tolerance of licensed users. Since spectrum sensing is not always accurate and spectrum environment is varying in practice, efficient spectrum utilization schemes for CR need to be developed.

The improvement of spectrum efficiency through CR technology relies on a robust and cost-effective design involving identification and reuse of spectrum opportunities changing over time, frequency, and space. We focus on efficient spectrum sensing and utilization techniques for high-performance *opportunistic spectrum access* (OSA). Although CR users are capable of monitoring the radio environment, there is always some uncertainty. Therefore, we will emphasize the importance of exploring probabilistic information unique for CR and develop novel techniques playing critical roles in CR systems.

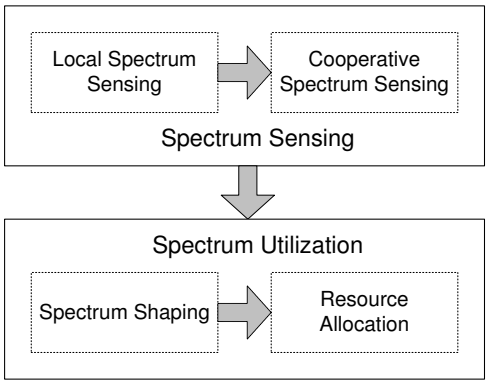

Figure 1.1. Framework of efficient spectrum sensing and utilization.

1.2 Literature Review

In this section, we review state-of-the-art spectrum sensing and utilization techniques for CR to improve spectrum efficiency on a non-interfering basis, including local spectrum sensing and scheduling, cooperative spectrum sensing and reporting, spectrum shaping, and resource allocation, the relationship among which is shown in Figure 1.1.

1.2.1 Spectrum Sensing for Cognitive Radio

As secondary users of the spectrum band, CR users are allowed to utilize the spectral resources only when they do not interfere with the licensed users. Spectrum sensing, which aims at monitoring the usage and characteristics of the spectrum band of interest, is thus required for CR users both before and during the use of the licensed spectrum band [13]. It involves deciding whether the licensed user signal is present or not from the observation and can be formulated as a binary hypothesis testing problem.

1.2.1.1 Local Spectrum Sensing and Scheduling

The goal of spectrum sensing is to decide between the two hypotheses, corresponding to the absence and presence of the licensed user signal, respectively. Various detection techniques, including matched filter detection, energy detection, feature detection, wavelet-based detection, and covariance-based detection, have been proposed for local spectrum sensing at a single CR user to identify the licensed user signal within a certain spectrum

band [13, 17, 18, 19, 20, 21, 22, 23, 24, 25, 26]. The optimal way for detection of a known signal under *additive white Gaussian noise* (AWGN) is the matched filter detection [13] that maximizes the received *signal-to-noise ratio* (SNR). It can be applied when pilots of licensed users are known to CR users. Energy detection [17] is, in contrast, the simplest spectrum sensing technique, which decides on the presence or absence of the licensed user signal based on the energy of the observed signal. It does not require a priori knowledge of the licensed user signal but is susceptible to the uncertainty of noise power. Feature detection is realized by analyzing the cyclic autocorrelation function [18, 19, 20, 21, 22] of the received signal. It is capable of differentiating the licensed user signal from the interference and noise and even works in very low SNR regions. In [23], a wavelet-based approach has been developed to identify and locate the spectrum holes by analyzing the irregularities in the estimated *power spectral density* (PSD) with wavelet transform. It can be used for wide-band spectrum sensing to estimate the number of subbands and the corresponding frequency boundaries. Covariance-based detection [24, 25] utilizes the property that the licensed user signal received at the CR user is usually correlated because of the dispersive channels, the utility of multiple receive antennas, or even oversampling, and differentiates the licensed user signal from white noise. It has been implied in the literature that the licensed user signal is present or absent within the entire sensing block.

Periodic spectrum sensing is usually applied to avoid interfering with licensed users that may appear during secondary communication. The efficiency of opportunistic spectrum utilization relies not only on the spectrum sensing technique but also on the scheduling of spectrum sensing activities [27, 28]. On one hand, if sensing activities are scheduled too often, CR users may spend too much time on sensing. On the other hand, if sensing activities are seldom scheduled, spectrum usage status may not be quickly discovered. In a typical periodic spectrum sensing framework, each frame consists of a sensing block and an inter-sensing block [29], the ratio of the sensing block length to the inter-sensing block length represents how frequently sensing activities are scheduled, and therefore is a key

parameter for spectrum sensing scheduling. Recently, optimization of spectrum sensing scheduling has been intensively studied [30, 31, 32, 33]. Sensing block length optimization has been investigated in [30] and [31] to improve the bandwidth efficiency of a CR user utilizing a single and multiple licensed channels, respectively. However, reappearance of licensed users or possible detection error has not been taken into account. The optimized inter-sensing block length has been found in [32] to maximize the throughput of a CR user. Without incorporating the collision probability constraint into the optimization problem, it fails to provide sufficient protection for licensed users. In [33], optimization of both sensing and inter-sensing block lengths has been investigated. Although the protection of licensed users is considered, the estimation of interference duration is inaccurate. Meanwhile, the transmit power of a CR user at different samples of one inter-sensing is usually assumed constant in the literature, which is not optimal.

1.2.1.2 Cooperative Spectrum Sensing and Reporting

The capability of spectrum sensing is critical to enable CR features and enhance spectrum utilization. Local spectrum sensing techniques do not always guarantee a satisfactory performance due to noise uncertainty and channel fading. For example, a CR user cannot detect the signal from a licensed transmitter shadowed by a high building, and it may access the licensed channel and interfere with the licensed receivers. With multiple users collaborating in spectrum sensing, the detection error possibilities will be reduced by the introduced spatial diversity [15, 34, 35, 36]. It has been shown in recent studies that cooperative spectrum sensing can improve the possibility of detection in fading channels [15]. The required detection time at any individual CR user may also decrease [37, 38].

In cooperative spectrum sensing, CR users first independently perform local spectrum sensing. Then each user reports either a binary decision or sensing data to a combining node. Finally, the combining node makes a decision on the presence or absence of the licensed user signal based on its received information. A straightforward form of cooperative spectrum sensing is to transmit and combine the samples received by all the CR users in the

local spectrum sensing phase. In [39], a combining scheme is proposed to process all the samples using tools from random matrix theory. Combining schemes using all the samples require significant bandwidth to report the data from the individual users to the combining node, which is usually implemented over a wired high-speed backbone. It is usually not the case for the CR users, and we have to consider communication constraints during reporting. A natural idea is that each CR user reports a summary statistic. A commonly used statistic is the observed energy acquired during energy detection. In [40], different cooperative energy detection schemes with low complexity have been investigated, where the final decision is based on a weighted summation. In the case that the communication constraints are more strict, hard combination schemes have been proposed in [15] and [40]. In these schemes, CR users transmit quantized sensing information to the combining node. The simplest form for combining is the counting scheme, in which each CR user makes a binary decision based on its observation, e.g., the threshold test in energy detection, and forwards the one-bit information to the combining node [41]. If there are at least K_0 out of K CR users inferring the presence of licensed activity, the licensed user signal will be declared present [42, 43, 44, 45]. Although K_0 is generally a design parameter, it is shown in [46] that 1-out-of-K rule has the best detection performance under most practical cases. In [40], one-bit combination is also extended to two-bit combination, in which three thresholds are used to divide the observed energy into four regions. Each CR user reports two-bit information to indicate the region of its observed energy. Then the combining node calculates a weighted summation of the numbers of CR users falling in different regions. The optimal partition of the regions and weight allocation have been given in [40] and its performance is shown to be comparable with equal-gain combination of the observed energies. However, it is implied in these schemes that local sensing data from different users are transmitted through orthogonal channels, i.e., separated in different time slots, frequency bands, or codes. As the number of cooperative users increases, the bandwidth required for

reporting also increases as implied and the stringent bandwidth constraint may not be satisfied. Therefore, bandwidth-efficient design with the required reporting bandwidth being independent of the number of cooperative users is desired.

Censoring [47, 48] is one of the approaches to bandwidth-efficient reporting, in which only the most informative data are reported. But selecting a fixed amount of local sensing data with the reporting bandwidth being independent of the number of cooperative users is difficult and the coordination among users is inevitable, which also consumes the limited bandwidth resource. Another approach is based on type-based distributed detection as proposed in [49]. However, this approach essentially requires transmitting multiple waveforms simultaneously to map different observations, so the bandwidth consumption will increase when the number of quantization regions for local observations increases.

Moreover, local observations of cooperative CR users may be obtained at different times due to individual sensing schedules and sent to the combining node with different delays, which affects the performance of the above combination schemes assuming synchronous sensing. In such a case, the combination approach should take the possibility of asynchronous sensing into account. To mitigate the performance loss with the assumption of synchronous sensing, a sliding-window algorithm has been proposed in [50] to make use of only the latest reports within an observation window for asynchronous cooperative sensing, while SNR diversity has been exploited in [51] to allow the final decision to be made without the information from the CR users with low SNRs in such a situation.

1.2.2 Spectrum Utilization for Cognitive Radio

After determining the absence of licensed user signal in a given spectrum band through spectrum sensing [13, 52], CR users are allowed to operate in this band as long as they adjust transmission parameters to avoid unacceptable interference with licensed users while ensuring proper signal reception [52]. The performance of the CR users and the interference with the licensed users need to be well balanced in spectrum utilization.

1.2.2.1 Spectrum Shaping

Orthogonal frequency-division multiplexing (OFDM) is an attractive transmission technique for CR [53] because it allows turning off tones to flexibly avoid licensed users and supports adaptation to radio environment and available resources. Meanwhile, with *orthogonal frequency-division multiple access* (OFDMA) as the multiple access technique, CR users can use non-adjacent sub-bands by dynamic spectrum aggregation to support higher data rate [54]. However, due to OOB leakage of OFDM signal, the interference to licensed users operating in adjacent bands cannot be completely eliminated [55]. Therefore, guard bands are usually required to separate the CR and licensed systems. To narrow the guard bands and enhance bandwidth efficiency, spectrum shaping that suppresses the OOB radiation in the adjacent bands becomes necessary.

Existing spectrum shaping approaches can be divided into time-domain and frequency-domain approaches. It is well known that a raised cosine window can be applied to the time-domain signal to suppress OOB radiation [55]. But system throughput is reduced in the windowing method because extension of symbol duration is needed to prevent *inter-symbol interference* (ISI). Another time-domain method at the expense of throughput reduction is adaptive symbol transition that inserts extensions between OFDM symbols [56]. In the frequency domain, a simple tone-nulling scheme [53] deactivates OFDM subcarriers at the edges of the utilized frequency band with the most significant impact on the OOB emission in adjacent bands. Moreover, active interference cancellation has been proposed in [57] by inserting cancelling tones adaptively at the edges. It enables deeper spectrum notches but is computational intensive at the transmitter. Similarly, subcarrier weighting [58], multiple-choice sequence [59], and selected mapping [60] have been proposed to suppress OOB radiation based on transmitted data.

In the multi-user case, it is undesirable to apply the above approaches where user dependence will be introduced. Recently, spectral precoding has been proposed [61, 62, 63] and is capable of reducing OOB emission significantly. The precoding matrix is constructed

from delicately designed basis sets [61] or determined to render time continuity of adjacent OFDM symbols or spectrum nulls at notched frequencies [62, 63]. With a block diagonal precoding matrix, it is possible to ensure user independence. However, existing spectral precoders degrade *bit-error rate* (BER) performance remarkably. Meanwhile, the coding block is required to be relatively long, so it is difficult to apply these precoders to users utilizing only a few subcarriers within the available frequency band.

1.2.2.2 Resource Allocation

After determining the availability of licensed spectrum bands, CR users adjust their transmission parameters through resource allocation to achieve certain performance requirements and realize effective interference management. Due to the existence of licensed users and possible mutual interference between two classes of users, the problem of resource allocation for opportunistic spectrum utilization in CR networks is no longer the same as that in conventional wireless networks. Generally, a CR user can transmit as long as the interference caused to the licensed receiver is below a threshold. The most common constraints to protect the licensed users are peak and average interference power constraints [64]. Moreover, the transmit power constraints of the CR users should be taken into account.

In a multi-channel environment where the available licensed spectrum band is divided into several non-overlapping frequency channels, resource allocation usually includes channel and power allocations among CR users. We may either allocate each channel to one user exclusively [65, 66], or allow each channel to be shared among multiple users [67]. Since interference management in the second approach is very difficult, the first approach is preferred. In such a case, the problem of channel and power allocations turns to be an NP-hard combinational optimization problem [68]. There are several efficient resource allocation schemes developed for OFDMA systems to reduce the computational complexity in solving this problem [69, 70], based on which most of the existing work on resource allocation in CR networks makes use of the hard decisions on the availability of licensed channels so

that channel and power allocations are carried out only among the decided available channels and is then similar to that in OFDMA systems [71,72,73,74,75,76,77,78,79,80]. Since decision errors from spectrum sensing are inevitable in practice, these resource allocation algorithms inherit the imprecise information in the hard decisions, which may introduce unacceptable interference to licensed users and lose the flexibility of OSA.

1.3 Our Approaches and Thesis Outline

The major goal of this research is to investigate novel spectrum sensing and utilization schemes to improve the performance of CR users and limit their interference with licensed users. Depending on the specific scenario, bandwidth or energy efficiency will be considered. Probabilistic information unique for CR will be explored extensively for both single-user and multi-user cases. With these schemes, spectrum opportunities brought by CR technology will be better captured and reused.

As the first step, we consider local spectrum sensing based on energy detection with a single CR user in Chapter 2. One major issue is the possibility that a licensed user appears in the middle of a sensing block. We establish a probability model regarding the appearance of the licensed user at any sample of a frame by utilizing the statistical characteristics of licensed channel occupancy. While conventional spectrum sensing schemes allocate the same weight to each sample, we vary the weight for each sample based on the probability of the presence of the licensed user at the corresponding sample. Such a probability-based spectrum sensing scheme has nearly optimal performance. Based on the assumption that the idle duration of the licensed channel is exponentially distributed, we further investigate how the probability model on the licensed user appearance varies from frame to frame in periodic spectrum sensing and show that both the conventional fixed weight and the probability-based dynamic weight energy detection schemes converge to their respective stable detection probabilities.

In periodic spectrum sensing, the scheduling of spectrum sensing is as important as the

spectrum sensing scheme itself. We further apply probability-based strategies to the optimization of inter-sensing duration and power control in Chapter 3. With utilization of the statistical characteristics of licensed channel occupancy, appropriate inter-sensing duration is determined to capture the recurrence of spectrum opportunity in time when the licensed user signal is detected, or to achieve the maximum spectrum efficiency under a certain level of interference with licensed communication when the licensed user signal is declared absent. Transmit power is varied dynamically according to the non-interfering probability at each sample so as to increase the transmission rate and decrease the interference power.

Cooperative spectrum sensing provides better performance in identification of spectrum opportunities. To ensure the performance enhancement, in Chapter 4, we develop a probability-based scheme for combination of spectrum sensing information collected from several CR users. Different from conventional cooperative spectrum sensing schemes that assume synchronous local sensing information, our scheme enables combination of both synchronous and asynchronous sensing information by utilizing the statistical characteristics of licensed channel occupancy. With our scheme, the amount of information from each CR user is flexible and a simplified implementation is feasible under a symmetrical case.

Another important aspect of cooperative spectrum sensing is how the local sensing information is reported to the combining node. In Chapter 5, we investigate bandwidth-efficient reporting of spectrum sensing information. To satisfy the stringent bandwidth constraint of the common control channel, we design a general approach that CR users are allowed to simultaneously send local sensing data to a combining node through the same narrowband channel. We develop both local processing at the CR users and final decision rule at the combining node under Bayesian criterion. Through proper preprocessing at individual users, the proposed approach requires fixed bandwidth regardless of the number of cooperative users while maintaining reasonable performance.

Based on spectrum sensing, efficient spectrum utilization can be realized. In Chapter 6, we first design a simple spectrum shaping scheme for OFDM-based CR users to enhance

spectral compactness. By mapping antipodal symbol pairs onto adjacent subcarriers at the edges of the utilized subbands, our scheme enables fast decaying of the sidelobes of OFDM signals without bringing much extra complexity. Moreover, the proposed scheme can flexibly balance sidelobe suppression and system throughput while power control on different sets of subcarriers can further lower the sidelobes. Then we develop an alternative spectral precoding scheme for multiple OFDM-based CR users to reduce OOB emission and enhance spectrum compactness. By constructing individual precoders to render selected spectrum nulls, our scheme suppresses the overall OOB radiation without sacrificing the bit-error rate performance of CR users. The proposed scheme ensures user independence with low encoding and decoding complexity. We also study the selection of notched frequencies to further increase the bandwidth efficiency and implementation flexibility.

Effective resource allocation is essential for efficient spectrum utilization and interference management. In Chapter 7, we study a probabilistic resource allocation approach to further exploit the flexibility of OSA. Based on the probabilities of channel availability obtained from spectrum sensing, the proposed approach optimizes channel and power allocations in a multi-channel environment. The developed algorithm maximizes the overall utility of a CR network and ensures sufficient protection of licensed users from unacceptable interference, which also supports diverse *quality-of-service* (QoS) requirements in multi-user networks and enables a distributed implementation. We demonstrate the effectiveness of this approach as well as its advantage over conventional approaches that rely upon the hard decisions on channel availability.

CHAPTER 2

PROBABILITY-BASED PERIODIC SPECTRUM SENSING

CR users can only access licensed channels when they do not cause unacceptable interference to licensed users. When a licensed user appear in the middle of a sensing block, spectrum sensing may become inaccurate and mis-detection is likely to occur. However, statistical characteristics of the licensed channel occupancy, including the distributions of the idle and busy durations of the licensed channel, can be utilized to improve the performance of spectrum sensing.

In this chapter, we are concerned with the case that the licensed user may appear at anytime within a sensing block. Based on the statistical characteristics of the licensed channel occupancy, we establish a probability model regarding the appearance of a licensed user at each sample of a CR user frame consisting of a sensing block and a data block. According to the Neyman-Pearson criterion, we obtain an optimal spectrum sensing scheme under this probability model that maximizes the detection probability for a given false alarm probability. While the conventional spectrum sensing scheme always allocates the same weight to each sample, we exploit the probability model on the licensed user appearance and further develop a suboptimal probability-based energy detection scheme, in which the weight for each sample is based on the probability of the presence of licensed user at the corresponding sample. Analytical and numerical results indicate that the probability-based energy detection scheme achieves almost the same performance with the optimal detection scheme with a relatively low complexity. By assuming that the idle duration of the licensed channel is exponentially distributed, we further investigate how the probability model on the licensed user appearance varies from frame to frame in periodic spectrum sensing, and show that both the conventional and the probability-based energy detection schemes converge to their respective stable average detection probabilities.

The rest of this chapter is organized as follows. In Section 2.1, we formulate the problem of licensed user signal detection and establish the probability model on the appearance of the licensed user at each sample. In Section 2.2, we develop a probability-based energy detection scheme and analyze its instantaneous detection performance within a single frame in comparison with the conventional one. In Section 2.3, we analyze the stable detection performance of the conventional and the probability-based energy detection schemes in periodic spectrum sensing. Finally we conclude this chapter in Section 2.4.

2.1 System Model

Spectrum sensing in CR involves deciding whether the licensed user is active or not from the observed signals at the CR user. It can be formulated as the following two hypotheses,

$$r_i = \begin{cases} n_i, & \mathcal{H}_I, \\ s_i + n_i, & \mathcal{H}_B, \end{cases} \tag{2.1}$$

where i denotes the time index, r_i denotes the received signal at the CR user, and s_i and n_i denote the received licensed user signal and white noise, respectively. In (2.1), $\mathcal{H}_I$ and $\mathcal{H}_B$ denote the hypotheses corresponding to the absence (idle state) and presence (busy state) of the licensed user, respectively.

2.1.1 Licensed User Signal Model

Throughout this chapter, we assume that s_i's are *independently and identically distributed* (i.i.d.) complex Gaussian random variables with zero mean and variance γ. While such a Gaussian licensed user signal assumption has been made in the literature [81] to facilitate analysis, it is also reasonable if there is no *line-of-sight* (LOS) path between the CR user and the licensed transmitter since, in this case, the received licensed user signal is a superposition of several *non-line-of-sight* (NLOS) signals and approximates Gaussian according to the *central limit theorem*. Without loss of generality, we further assume that the noise at each sample is complex Gaussian with zero mean and unit variance, independent of the licensed user signal under $\mathcal{H}_B$. Thus the variance of s_i's, γ, also denotes the average SNR.

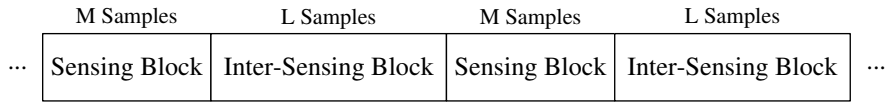

Figure 2.1. Frame structure for periodic spectrum sensing.

2.1.2 General Frame Structure for Periodic Spectrum Sensing

For spectrum sensing in CR, two different scenarios are involved: firstly, before any secondary data link is established, spectrum sensing needs to be performed to search for unoccupied channels for future secondary usage; secondly, after a secondary data link has been established over an idle licensed channel, periodic spectrum sensing is required to avoid interfering with the licensed user that may reappear. In this chapter, we focus on the latter scenario since it determines the protection level provided to licensed users and therefore is critical to any practical CR networks.

Figure 2.1 shows a general frame structure for periodic spectrum sensing. As indicated, the frame consists of an inter-sensing (silent or data depending on whether the licensed channel is identified as busy or idle) block of L samples and a sensing block of M samples. With this frame structure, spectrum sensing can be performed periodically during secondary communication, and once the licensed user signal is detected, CR users will vacate the licensed channel immediately.

2.1.3 Probability Model on Licensed User Appearance

We consider a licensed network where the licensed channel occupancy changes frequently so that the possible appearance of licensed users in the middle of a data or sensing block must be taken into account for the design and performance analysis of spectrum sensing schemes. Denote t_I as the idle duration of the licensed channel with the *cumulative distribution function* (CDF) $F_{t_I}(t_I)$. Suppose that a licensed user appears at the mth ($1 \leq m \leq M$) sample of the current sensing block, and then the *probability mass function* (PMF) of m, $p(m)$, can be obtained from $F_{t_I}(t_I)$. As an example, suppose that the licensed channel switches from the busy to the idle state at the beginning of the current CR frame, and then

the PMF of m can be obtained as

$$p(m)=\begin{cases} F_{t_I}((L+1)\tau), & m=1, \\ F_{t_I}((L+m)\tau)-F_{t_I}((L+m-1)\tau), & 2\le m\le M, \end{cases} \tag{2.2}$$

where L and M are the data and sensing block lengths, respectively, and τ denotes the sampling interval. Further denote $f_{t_I}(t_I)$ as the *probability density function* (PDF) of t_I, and then the average interference duration that the licensed system experiences in the current CR frame is given by

$$\overline{t_I} = \int_0^{L\tau} (L\tau - t) f_{t_I}(t) dt. \tag{2.3}$$

Apparently $\overline{t_I}$ is an increasing function of L. Thus Equation (2.3) can be used to determine L according to the maximum tolerable average interference duration of the licensed system.

Throughout this chapter, we assume that once a licensed user appears during secondary communication, it remains active during the whole spectrum sensing process. This assumption is reasonable since the licensed user has a higher priority than CR users and will keep trying to retrieve the licensed channel for data transmission until the CR user detects its presence and vacates the licensed channel.[1]

2.2 Spectrum Sensing within One Single Frame

In this section, the probability model on licensed user appearance during secondary communication will be utilized to investigate the instantaneous detection performance of different spectrum sensing schemes within one single frame. In particular, it should be noted that the analysis throughout this section applies to an arbitrary idle duration distribution.

Different from the existing work where the busy hypothesis, $\mathcal{H}_B$, corresponds to only one case that the licensed user appears at the beginning of the sensing block, $\mathcal{H}_B$ in this chapter is actually a composite hypothesis and consists of M different cases corresponding to the appearance of the licensed user at M different samples within the sensing block.

[1]Here we assume that the transmission duration of the licensed user is longer than the sensing block length of the CR system. Therefore, the licensed user can not transmit successfully until the CR user detects its presence and vacates the licensed channel.

Denote $\mathcal{H}_m$ as the sub-hypothesis that the licensed user appears at the mth ($1 \leq m \leq M$) sample of the current sensing block, and then the probability of $\mathcal{H}_m$ is given by $p(m)$ defined in (2.2) and the received signal under $\mathcal{H}_m$ can be expressed as

$$r_{\mathcal{H}_m,i} = \begin{cases} n_i, & 1 \leq i \leq m-1, \\ s_i + n_i, & m \leq i \leq M, \end{cases} \tag{2.4}$$

where s_i's and n_i's are i.i.d. complex Gaussian random variables with zero mean and variances γ and 1, respectively.

2.2.1 Optimal Detection Scheme

Here we adopt the Neyman-Pearson criterion [82] to obtain the optimal detection scheme for the binary hypothesis testing between $\mathcal{H}_I$ and $\mathcal{H}_B$ since it maximizes the detection probability for a given false alarm probability. Let $\mathbf{R} = (r_1, r_2, \cdots, r_M)$ be the received signal vector, and then, according to the Neyman-Pearson criterion, the decision is made by the following *likelihood ratio test* (LRT) [83],

$$LR(\mathbf{R}) = \frac{P(\mathbf{R}|\mathcal{H}_B)}{P(\mathbf{R}|\mathcal{H}_I)} \underset{\mathcal{H}_I}{\overset{\mathcal{H}_B}{\gtrless}} \zeta, \tag{2.5}$$

where ζ is the decision threshold determined by the given false alarm probability. According to the distribution of m, $LR(\mathbf{R})$ can be rewritten as

$$LR(\mathbf{R}) = \frac{\sum_{m=1}^{M} p'(m) P(\mathbf{R}|\mathcal{H}_m)}{P(\mathbf{R}|\mathcal{H}_I)} = \sum_{m=1}^{M} p'(m) LR(\mathbf{R}, \mathcal{H}_m), \tag{2.6}$$

where $p'(m) = \frac{p(m)}{\sum_{i=1}^{M} p(i)}$ is the conditional probability of $\mathcal{H}_m$ and $LR(\mathbf{R}, \mathcal{H}_m) = \frac{P(\mathbf{R}|\mathcal{H}_m)}{P(\mathbf{R}|\mathcal{H}_I)}$ is the likelihood ratio between $\mathcal{H}_m$ and $\mathcal{H}_I$. Since s_i's and n_i's are i.i.d. complex Gaussian random variables with zero mean and variances γ and 1, respectively, $LR(\mathbf{R}, \mathcal{H}_m)$ can be expressed as

$$\begin{aligned} LR(\mathbf{R}, \mathcal{H}_m) &= \frac{\prod_{i=1}^{m-1} \frac{1}{\pi} e^{-|r_i|^2} \cdot \prod_{i=m}^{M} \frac{1}{\pi(1+\gamma)} e^{-\frac{|r_i|^2}{1+\gamma}}}{\prod_{i=1}^{M} \frac{1}{\pi} e^{-|r_i|^2}} \\ &= \left(\frac{1}{1+\gamma}\right)^{M-m+1} \exp\left(\frac{\gamma}{1+\gamma} \sum_{i=m}^{M} |r_i|^2\right). \end{aligned} \tag{2.7}$$

Substitute (2.7) in (2.6), and then $LR(\mathbf{R})$ can be rewritten as

$$LR(\mathbf{R}) = \sum_{m=1}^{M} p'(m) \left(\frac{1}{1+\gamma} \right)^{M-m+1} \exp\left(\frac{\gamma}{1+\gamma} \sum_{i=m}^{M} |r_i|^2 \right). \tag{2.8}$$

Thus the test statistics of the optimal detection scheme for the binary hypothesis testing between $\mathcal{H}_I$ and $\mathcal{H}_B$ is $T_O(\mathbf{R}) = LR(\mathbf{R})$. Although this scheme is optimal in the sense that it maximizes the detection probability for a given false alarm probability, its test statistics, $T_O(\mathbf{R})$, depends on the SNR level, γ, which is usually unknown in practice. Moreover, the PDF of $T_O(\mathbf{R})$ is difficult to obtain. As a result, closed-form detection and false alarm probabilities are unavailable and the decision threshold for a given false alarm probability under a certain SNR level has to be found experimentally.

2.2.2 Probability-based Energy Detection Scheme

Equation (2.7) indicates that the test statistics for the binary hypothesis testing between $\mathcal{H}_I$ and $\mathcal{H}_m$ is given by $T_{\mathcal{H}_m}(\mathbf{R}) = \sum_{i=m}^{M} |r_i|^2$. That is, to decide between $\mathcal{H}_I$ and $\mathcal{H}_m$, the optimal detection scheme is simple energy detection with the following weight for each sample,

$$w_{\mathcal{H}_m,i} = \begin{cases} 0, & 1 \le i \le m-1, \\ 1, & m \le i \le M. \end{cases} \tag{2.9}$$

Since m is an unknown random variable, we can not apply such a weighted energy detector directly. Instead, we utilize the distribution of m and propose a probability-based weighted energy detector for the binary hypothesis testing between $\mathcal{H}_I$ and $\mathcal{H}_B$. The test statistics of this detector is given by

$$T_P(\mathbf{R}) = \sum_{i=1}^{M} w_i |r_i|^2, \tag{2.10}$$

where the weight for the ith sample, w_i, is obtained by averaging $w_{\mathcal{H}_m,i}$ *with respect to* (w.r.t.) m, i.e.,

$$w_i = E_m\{w_{\mathcal{H}_m,i}\} = \frac{\sum_{m=1}^{i} p(m)}{\sum_{m=1}^{M} p(m)} = P(m \le i | \mathcal{H}_B), \tag{2.11}$$

in which and subsequent equations of this chapter $E_m\{\cdot\}$ denotes expectation w.r.t. m conditioned on $\mathcal{H}_B$. Equation (2.11) indicates that the weight allocated to the ith sample is the

conditional CDF of m at that sample, namely the conditional probability of the presence of the licensed user at that sample. In Appendix A, we have proved the following proposition.

Proposition 2.2.1 *The optimal detection scheme reduces to the probability-based energy detection scheme in low SNR region.*

To analyze the performance of the probability-based energy detection scheme, we first get its detection probability under H_m, $P_D(m)$, and then obtain its overall average detection probability under H_B, $\overline{P}_D = E_m\{P_D(m)\}$. Since s_i's and n_i's are i.i.d. complex Gaussian random variables with zero mean and variances γ and 1, respectively, the observed energy in the probability-based scheme is given by

$$\begin{aligned} T_p &= \begin{cases} \sum_{i=1}^{m-1} w_i|n_i|^2 + \sum_{i=m}^{M} w_i|s_i+n_i|^2, & \mathcal{H}_m, \\ \sum_{i=1}^{M} w_i|n_i|^2, & \mathcal{H}_I, \end{cases} \\ &= \begin{cases} \sum_{i=1}^{M} w'_{m,i}E_i, & \mathcal{H}_m, \\ \sum_{i=1}^{M} w_iE_i, & \mathcal{H}_I, \end{cases} \end{aligned} \tag{2.12}$$

where

$$w'_{m,i} = \begin{cases} w_i, & 1 \le i \le m-1, \\ w_i(1+\gamma), & m \le i \le M, \end{cases} \tag{2.13}$$

and E_i's are powers of i.i.d. complex Gaussian random variables with zero mean and unit variance. Therefore, E_i's are i.i.d. exponential random variables with unit mean. Since T_p is a weighted summation of i.i.d. exponential random variables, its PDF can be obtained with the help of the characteristic function of the exponential distribution [84] as follows,[2]

$$f_{T_p}(T_p) = \begin{cases} \sum_{i=1}^{M} d'_i \cdot \frac{1}{w'_{m,i}} e^{-T_p/w'_{m,i}}, & \mathcal{H}_m, \\ \sum_{i=1}^{M} d_i \cdot \frac{1}{w_i} e^{-T_p/w_i}, & \mathcal{H}_I, \end{cases} \tag{2.14}$$

where

$$\begin{cases} d'_i = \prod_{j=1, j\neq i}^{M} \frac{1}{1-\frac{w'_{m,j}}{w'_{m,i}}}, \\ d_i = \prod_{j=1, j\neq i}^{M} \frac{1}{1-\frac{w_j}{w_i}}. \end{cases} \tag{2.15}$$

[2]Note that the characteristic function of w_iE_i is given by $\varphi(t) = \frac{1}{1-itw_i}$ and $\prod_{i=1}^{M} \frac{1}{1-itw_i} = \sum_{i=1}^{M} \frac{d_i}{1-itw_i}$ where $d_i = \prod_{j=1, j\neq i}^{M} \frac{1}{1-\frac{w_j}{w_i}}$.

Denote λ as the decision threshold, and then the detection probability under $\mathcal{H}_m$, $P_D(m) = P(T_p > \lambda|\mathcal{H}_m)$, and the false alarm probability, $P_F = P(T_p > \lambda|\mathcal{H}_I)$, can be obtained from (2.14) as

$$\begin{cases} P_D(m) = \sum_{i=1}^{M} d'_i e^{-\lambda/w'_{m,i}}, \\ P_F = \sum_{i=1}^{M} d_i e^{-\lambda/w_i}, \end{cases} \tag{2.16}$$

and the overall average detection probability of the probability-based scheme can be obtained by

$$\overline{P}_D = E_m\{P_D(m)\} = \frac{\sum_{m=1}^{M} p(m)P_D(m)}{\sum_{m=1}^{M} p(m)}. \tag{2.17}$$

2.2.3 Conventional Energy Detection Scheme

For comparison, we further investigate the performance of the conventional energy detection scheme for a given probability model on the licensed user appearance. In contrast with the probability-based energy detection scheme, the conventional one does not utilize the statistical distribution of m and always allocates the same weight to all of the samples. Without loss of generality, we let the common weight be 2, and then the observed energy in the conventional scheme is given by

$$T_c = \begin{cases} 2\left(\sum_{i=1}^{m-1} |n_i|^2 + \sum_{i=m}^{M} |s_i + n_i|^2\right), & \mathcal{H}_m, \\ 2\sum_{i=1}^{M} |n_i|^2, & \mathcal{H}_I. \end{cases} \tag{2.18}$$

Since n_i's are i.i.d. complex Gaussian random variables with zero mean and unit variance, T_c follows a central chi-square distribution with $2M$ degrees of freedom under $\mathcal{H}_I$, or follows a non-central chi-square distribution with $2M$ degrees of freedom and a non-central parameter $\mu = 2\sum_{i=m}^{M} |s_i|^2$ under $\mathcal{H}_m$, i.e.,

$$T_c \sim \begin{cases} \chi^2_{2M}(\mu), & \mathcal{H}_m, \\ \chi^2_{2M}, & \mathcal{H}_I. \end{cases} \tag{2.19}$$

Denote λ as the decision threshold, and then the false alarm probability can be obtained as [85]

$$P_F = P(T_c > \lambda|\mathcal{H}_I) = \frac{\Gamma(M, \frac{\lambda}{2})}{\Gamma(M)}, \tag{2.20}$$

where $\Gamma(M) = \int_0^\infty t^{M-1}e^{-t}dt$ denotes the gamma function and $\Gamma(M, \frac{\lambda}{2}) = \int_{\frac{\lambda}{2}}^\infty t^{M-1}e^{-t}dt$ denotes the upper incomplete gamma function.

Since s_i's are i.i.d. complex Gaussian random variables with zero mean and variance γ, the PDF of the non-central parameter, μ, can be obtained as

$$f_\mu(\mu) = \frac{1}{2\gamma(M-m)!}\left(\frac{\mu}{2\gamma}\right)^{M-m} e^{-\frac{\mu}{2\gamma}},\ \mu \geq 0. \tag{2.21}$$

Therefore, the detection probability under $\mathcal{H}_m$ is given by [85]

$$\begin{aligned} P_D(m) &= \int_0^{+\infty} P\left(T_c > \lambda | (\mathcal{H}_m, \mu)\right) f_\mu(\mu) d\mu \\ &= \int_0^{+\infty} Q_M(\sqrt{\mu}, \sqrt{\lambda}) f_\mu(\mu) d\mu, \end{aligned} \tag{2.22}$$

where $Q_M(\cdot,\cdot)$ is the generalized Marcum Q-function [86]. A general closed-form expression of this type of integrals like (2.22) has been derived in [85]. So we omit the derivation and give the final result as

$$\begin{aligned} P_D(m) = e^{-\frac{\lambda\beta}{2}}\Big(\beta^{M-m} L_{M-m}(-\omega) + (1-\beta)\sum_{i=0}^{M-m-1}\beta^i L_i(-\omega)\Big) \\ + \beta^{M-m+1} e^{-\frac{\lambda}{2}} \sum_{i=1}^{M-1} \frac{1}{i!}\Big(\frac{\lambda}{2}\Big)^i F(M-m+1; i+1; \omega), \end{aligned} \tag{2.23}$$

where $\beta = \frac{m}{m+(M-m+1)\gamma}$, $\omega = \frac{\lambda(1-\beta)}{2}$, $L_i(\cdot)$ is the Laguerre polynomial of degree i [87], and $F(\cdot;\cdot;\cdot)$ is the confluent hypergeometric function [87]. After getting $P_D(m)$ from (2.23), we can obtain the overall average detection probability of the conventional energy detection scheme similarly as in (2.17).

2.2.4 Numerical Results

In this subsection, we present numerical results to demonstrate the performance of different spectrum sensing schemes within one single frame under a given probability model of the licensed user appearance. While our analysis throughout this chapter is applicable to arbitrary data block and sensing block lengths, the presented numerical results are based on a licensed network where the licensed channel occupancy changes frequently so that the

data block length must be restricted to avoid interfering with licensed users that may appear within the data block. Specially, we let the mean idle duration of the licensed channel be 100 samples. To achieve an acceptable detection performance, we let the sensing block length be 6 ($M = 6$) samples; to reduce the probability of collision with licensed users, we let the data block length be also 6 ($L = 6$) samples. Without loss of generality, we assume that the licensed channel switches from the busy to the idle state at the beginning of the current CR frame. Therefore, the PMF of m, the location in the sensing block where the licensed user appears, is given by (2.2). To investigate the effect of the statistical distribution of the idle duration on the performance of different detection schemes, we consider three different idle duration distributions with the same mean of 100 samples. The first one is exponential distribution, which is actually a special gamma distribution [84] with a shape parameter of 1, i.e., $t_I \sim \Gamma(1, 100\tau)$; the second one is gamma distribution with a shape parameter of 2 ($k = 2$), i.e., $t_I \sim \Gamma(2, 50\tau)$; the third one is also gamma distribution but with a shape parameter of 10 ($k = 10$), i.e., $t_I \sim \Gamma(10, 10\tau)$. Experimental results presented in [88] have demonstrated that both the exponential and the gamma distributions are suitable for modeling the idle duration of the licensed channel.

Figure 2.2 shows the overall average detection probability curves of different spectrum sensing schemes when the given false alarm probability is $P_F = 10^{-1}$. Figure 2.3 gives the corresponding conditional CDF ($P(m \leq i|\mathcal{H}_B)$) curves of m, which, according to (2.11), also denote the corresponding weight sequences applied in the probability-based energy detection schemes. The decision thresholds of these schemes are set such that the given false alarm probability, P_F, is met exactly. While the overall average detection probabilities of the probability-based and the conventional energy detection schemes are calculated based on (2.16), (2.23), and (2.17), the counterpart of the optimal detection scheme is obtained experimentally.

Figure 2.2 indicates that the probability-based energy detection scheme has almost the same performance with the optimal detection scheme especially in low SNR region,

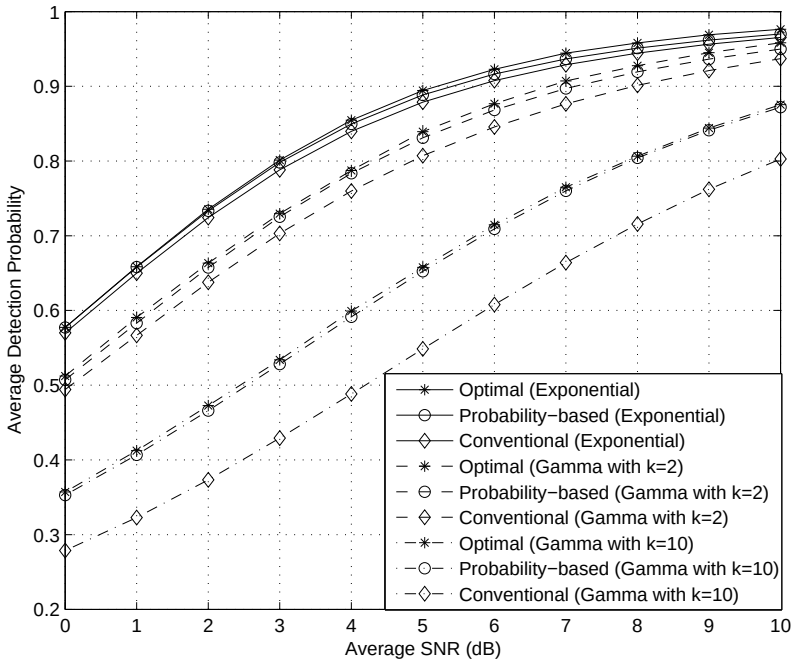

Figure 2.2. Overall average detection probability curves of different spectrum sensing schemes.

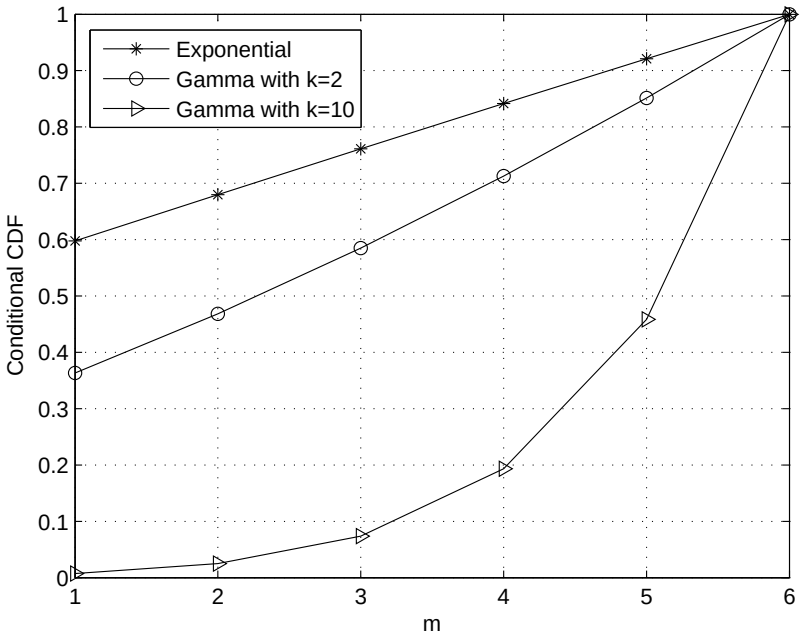

Figure 2.3. Conditional CDF curves of m for different idle duration distributions.

which verifies the earlier analysis. As mentioned, the optimal detection scheme requires the knowledge of the average SNR and thus may be infeasible under certain scenarios. In contrast, the probability-based energy detection scheme does not need the average SNR information and has relatively low complexity and nearly optimal performance. Therefore, it is an attractive spectrum sensing scheme when the statistics of the licensed channel occupancy is available. Figure 2.2 also indicates that the performance gain of the probability-based energy detection scheme over the conventional one depends on the idle duration distribution. In essence, this gain depends on the differences between the conditional probabilities of the presence of the licensed user at different samples. When all of the samples have the same CDF value, they are allocated the same weight and then the probability-based scheme reduces to the conventional one. Figure 2.3 indicates that the second gamma distribution with a shape parameter of 10 has the most different conditional CDF values at different samples. Therefore, the probability-based scheme achieves the largest gain over the conventional one when the idle duration follows the second gamma distribution. Furthermore, it can be also observed from Figure 2.2 that the average detection probabilities of all of the three schemes for an exponentially distributed idle duration are larger than that for gamma distributed idle durations. This can be explained by Figure 2.3 which indicates that an exponentially distributed idle duration, from a probabilistic point of view, means earlier licensed user appearance and greater licensed user signal energy in the sensing block, and thus a higher average detection probability than gamma distributed idle durations.

Figure 2.4 shows the effect of the uncertainties in the idle duration distribution on the performance of the probability-based energy detection scheme. We assume that the idle duration follows the gamma distribution with a shape parameter of 2, i.e., $t_I \sim \Gamma(2, 50\tau)$. Two different types of uncertainties in the idle duration distribution are considered: the first one, called *inaccurate mean*, corresponds to that the idle duration is conjectured as gamma distributed with an accurate shape parameter of 2 but an inaccurate mean of 50 samples, i.e., $t_I^{'} \sim \Gamma(2, 25\tau)$; the second one, called *inaccurate distribution*, corresponds to that the

idle duration is inaccurately conjectured as exponentially distributed with an accurate mean of 100 samples, i.e., $t_I'' \sim \Gamma(1, 100\tau)$. For comparison, we also show the overall average detection probability of the ideal probability-based scheme with accurate idle duration distribution. Figure 2.4 indicates that even though there is a nontrivial uncertainty in the idle duration distribution, the probability-based scheme still achieves a performance gain over the conventional one, which demonstrates its robustness to such uncertainties. Furthermore, we also observe that inaccurate distribution (or inaccurate conjecture of the shape parameter) has a more serious impact on the performance of the probability-based scheme than inaccurate mean.

As a final remark, the above numerical results are based on the assumption that the licensed channel state changes frequently so that the sensing and the data blocks have comparable lengths. If the licensed channel state changes sporadically, the probability that a licensed user appears in the middle of a data block is trivial and thus the data block can be significantly longer than the sensing block. In this case, the differences between the conditional CDF values at different sensing samples will be trivial and thus the probability-based energy detection scheme reduces to the conventional one.

2.3 Periodic Spectrum Sensing in Multiple Consecutive Frames

We have investigated the detection performance of different spectrum sensing schemes within one single frame. As indicated in (2.17), the overall average detection probability, $\overline{P}_D$, varies with the distribution of m, the location in the sensing block where the licensed user appears. Focusing on periodic spectrum sensing in multiple consecutive frames in this section, we will investigate how the distribution of m and thereby $\overline{P}_D$ vary from frame to frame when the conventional and the probability-based energy detection schemes are applied. As in the literature [32, 33], we assume throughout this section that the idle duration of the licensed channel is exponentially distributed since the memoryless property of the exponential distribution facilitates the performance analysis of periodic spectrum sensing

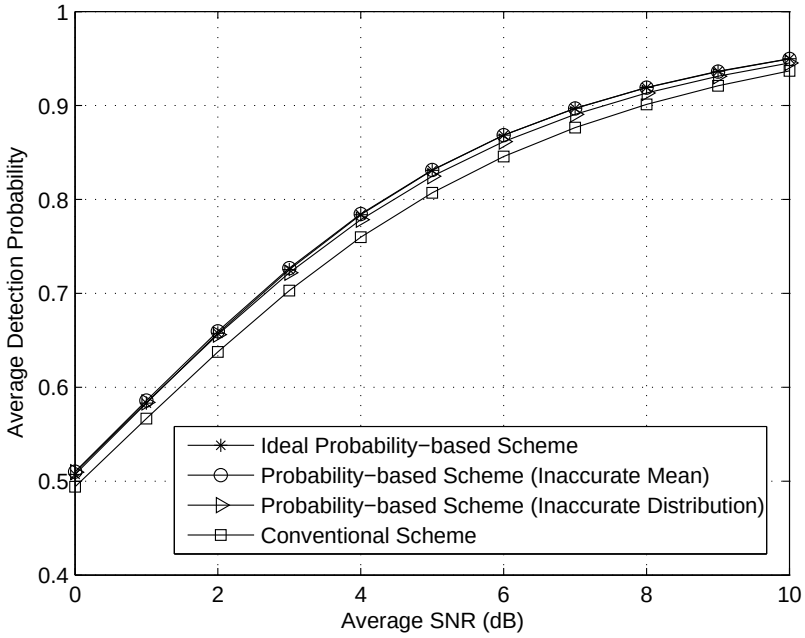

Figure 2.4. Effect of uncertainties in the idle duration distribution.

in multiple consecutive frames.

2.3.1 Probability Model in Multiple Consecutive Frames

As the first step, we investigate the probability model on the licensed user appearance in multiple consecutive frames. Throughout this section, the idle duration of the licensed channel is assumed to be exponentially distributed with an average of U samples. If we suppose that the licensed channel is idle at the beginning of the current frame and a licensed user appears at the mth sample of the sensing block, then, according to the memoryless property of the exponential distribution, the PMF of m, $p(m)$, can be obtained based on (2.2). For periodic spectrum sensing in multiple consecutive frames, however, there exists a chance that a licensed user is actually present at the beginning of the current frame but was not detected in the previous frames. Therefore, the probability model on the licensed user appearance needs to take this probability into account. Denote $x(n)$ as the probability that a licensed user is present at the beginning of the nth frame due to mis-detection in previous frames, and m as the location in the sensing block where a licensed user appears,

and then, from the memoryless property of the exponential distribution, we can obtain the PMF of m within the nth sensing block as

$$p_n(m) = \begin{cases} x(n) + [1 - x(n)]\, p(1), & m = 1, \\ [1 - x(n)]\, p(m), & 2 \le m \le M, \end{cases} \tag{2.24}$$

where $p(m)$ is given in (2.2). Obviously $p_n(m) = p(m)$ when $x(n) = 0$. Define $a = \sum_{m=1}^{M} p(m)$, and then the probabilities that the licensed channel is busy and idle within the nth sensing block are given by

$$P_{B,n} = \sum_{m=1}^{M} p_n(m) = x(n) + a\,[1 - x(n)]\,, \tag{2.25}$$

and

$$P_{I,n} = 1 - P_{B,n} = (1 - a)\,[1 - x(n)]\,, \tag{2.26}$$

respectively.

2.3.2 Evolution of Probability Sequence

Equation (2.24) indicates that, for a given $p(m)$, the distribution of m in the nth sensing block is uniquely determined by $x(n)$. Hence, we will investigate how the distribution of m varies from frame to frame by studying the evolution of $x(n)$.

Denote $P_{M,n}(m)$ as the mis-detection probability in the nth sensing block under $\mathcal{H}_m$. For the probability-based energy detection scheme that utilizes the PMF of m, $P_{M,n}(m)$ is a function of $x(n)$; for the conventional scheme that does not take the distribution of m into account, $P_{M,n}(m)$ is independent of $x(n)$.[3] The overall average mis-detection probability in the nth sensing block is given by

$$\overline{P}_M(n) = E_m\{P_{M,n}(m)\} = \frac{\sum_{m=1}^{M} p_n(m) P_{M,n}(m)}{\sum_{m=1}^{M} p_n(m)}. \tag{2.27}$$

The probability that the licensed channel is busy at the beginning of the $(n+1)$th frame can

[3]For notational consistency, we still use the denotation $P_{M,n}(m)$ instead of $P_M(m)$ for the conventional energy detection scheme.

be obtained by

$$\begin{aligned} y(n+1) &= P_{B,n} \cdot \overline{P}_M(n) \\ &= \sum_{m=1}^{M} p_n(m) P_{M,n}(m) \\ &= x(n) P_{M,n}(1) + [1 - x(n)] \sum_{m=1}^{M} p(m) P_{M,n}(m) \\ &= [b(n) - c(n)]\, x(n) + c(n), \end{aligned} \tag{2.28}$$

where $b(n) = P_{M,n}(1)$ and $c(n) = \sum_{m=1}^{M} p(m) P_{M,n}(m)$; the probability that the licensed channel is idle at the beginning of the $(n+1)$th frame is given by

$$z(n+1) = P_{I,n} \cdot (1 - P_F) = \varepsilon(1-a)\,[1 - x(n)]\,, \tag{2.29}$$

where P_F is the given false alarm probability and $\varepsilon = 1 - P_F$. Thus the conditional probability of the presence of a licensed user at the beginning of the $(n+1)$th frame, $x(n+1)$, can be obtained as a function of $x(n)$ given by

$$\begin{aligned} x(n+1) &= \frac{y(n+1)}{y(n+1) + z(n+1)} \\ &= \frac{[b(n) - c(n)]\, x(n) + c(n)}{[b(n) - c(n) - \varepsilon(1-a)]\, x(n) + c(n) + \varepsilon(1-a)}. \end{aligned} \tag{2.30}$$

2.3.3 Stable Detection Performance of Conventional Scheme

In this subsection, we investigate the stable detection performance of the conventional equal weight energy detection scheme; even so, the analysis throughout this subsection is actually applicable to a general fixed weight one.

Since $P_{M,n}(m)$ is independent of $x(n)$ for the conventional fixed wight energy detection scheme, $b(n)$ and $c(n)$ remain constant for different n's. Therefore, they are abbreviated as b and c in this subsection, respectively. Define

$$f(x) = \frac{(b-c)x + c}{[b - c - \varepsilon(1-a)]\, x + c + \varepsilon(1-a)}, 0 \le x \le 1, \tag{2.31}$$

and then, according to (2.30), $x(n+1) = f\,(x(n))$. In Appendix A, we have proved the following proposition.

Proposition 2.3.1 *For $0 \le x \le 1$, $f(x)$ is a convex and monotonically increasing function.*

2.3.3.1 Convergent Points of $x(n)$

Suppose that $x(n)$ converges at x^*, and then $f(x^*) = x^*$, i.e.,

$$f(x^*) - x^* = \frac{(1-x^*)\left(x^* - \frac{c}{c+\varepsilon(1-a)-b}\right)}{x^* - \frac{c+\varepsilon(1-a)}{c+\varepsilon(1-a)-b}} = 0,\ 0 \le x^* \le 1. \tag{2.32}$$

Since it has been shown that $c + \varepsilon(1-a) - b > 0$ in Appendix A, we have

$$x^* = \begin{cases} 1, & \text{if } \gamma \le \gamma_c^*, \\ 1 \text{ or } \frac{c}{c+\varepsilon(1-a)-b}, & \text{if } \gamma > \gamma_c^*, \end{cases} \tag{2.33}$$

where γ_c^* denotes the critical average SNR at which $b = \varepsilon(1-a)$, i.e.,

$$P_{M,n}(1)|_{\gamma=\gamma_c^*} = (1 - P_F)\left(1 - \sum_{m=1}^{M} p(m)\right). \tag{2.34}$$

Figure 2.5 shows the curves of $f(x)$ under different SNR levels when $U = 100$, $L = M = 6$, and $P_F = 10^{-1}$. The critical average SNR, γ_c^*, in this scenario can be found based on (2.23) and (2.34) as -7.55 dB. Figure 2.5 verifies that if $\gamma \le \gamma_c^*$, $f(x)$ intersects with $g(x) = x$ only at $x^* = 1$; otherwise, $f(x)$ intersects with $g(x)$ at both $x_1^* = \frac{c}{c+\varepsilon(1-a)-b}$ and $x_2^* = 1$.

Denote x_c^* as the leftmost intersection between $f(x)$ and $g(x) = x$, and then, according to (2.33),

$$x_c^* = \begin{cases} 1, & \text{if } \gamma \le \gamma_c^*, \\ \frac{c}{c+\varepsilon(1-a)-b}, & \text{if } \gamma > \gamma_c^*. \end{cases} \tag{2.35}$$

2.3.3.2 Convergence of $x(n)$ at x_c^*

For periodic spectrum sensing during secondary communication, it is reasonable to assume that $x(1) = 0$, i.e., the licensed channel is idle at the beginning of the first CR frame. In Appendix A, we have proved the following proposition.

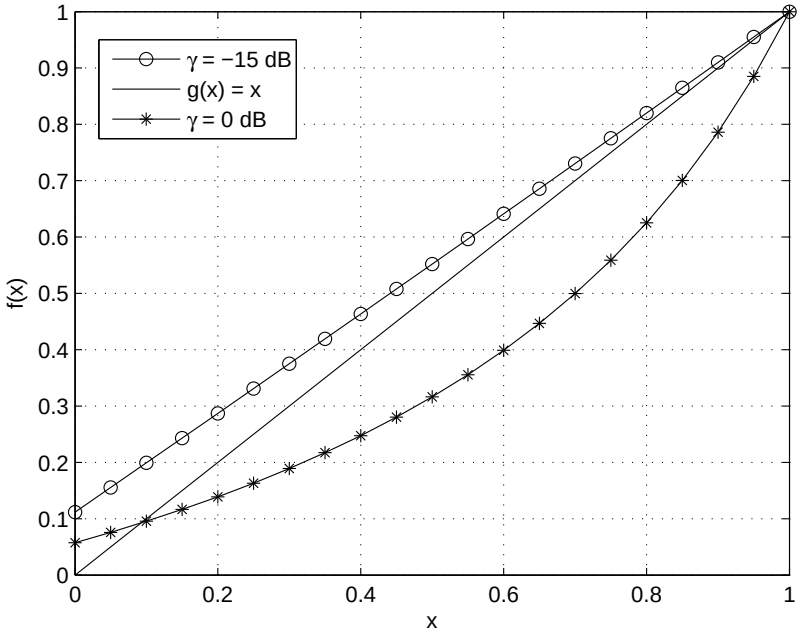

Figure 2.5. Curves of $f(x)$ under different SNR levels.

Proposition 2.3.2 *With $x(1) = 0$, $x(n)$ is an increasing sequence and converges at x_c^* linearly with the convergence ratio $f'(x_c^*) = \frac{df(x)}{dx}|_{x=x_c^*}$, i.e.,*

$$\lim_{n\to+\infty} x(n) = \begin{cases} 1, & \text{if } \gamma \le \gamma_c^*, \\ \frac{c}{c+\varepsilon(1-a)-b}, & \text{if } \gamma > \gamma_c^*. \end{cases} \tag{2.36}$$

According to (A.12), the convergence ratio, $f'(x_c^*)$, is an increasing function of γ when $\gamma \le \gamma_c^*$, and a decreasing function of γ when $\gamma > \gamma_c^*$. Therefore, in the nontrivial case that $\gamma > \gamma_c^*$, the convergence speed of $x(n)$ increases with the average SNR, γ. Moreover, Equation (2.36) indicates that when $\gamma \le \gamma_c^*$, the detection probability is so low that the licensed channel is certain to be busy at the beginning of the CR frame as time goes by. However, the critical average SNR, γ_c^*, can be reduced to a reasonable level by appropriately increasing the number of samples in the sensing block, M.

According to (2.24) and (2.27), as $x(n)$ converges at x_c^*, the $\overline{P}_M(n)$ sequence also converges at a stable average mis-detection probability given by

$$\overline{P}_{M,c}^* = \frac{(b-c)x_c^* + c}{(1-a)x_c^* + a}. \tag{2.37}$$

2.3.4 Stable Detection Performance of Probability-based Scheme

In this subsection, we investigate the convergence of $x(n)$ and $\overline{P}_M(n)$ when the probability-based energy detection scheme is applied. For the probability-based scheme, the weights allocated to different samples are based on the statistical distribution of m in the current sensing block. As a result, both $b(n)$ and $c(n)$ are functions of $x(n)$ and vary from frame to frame, which makes the convergence analysis of $x(n)$ different from that for the conventional scheme.

To investigate the convergence of $x(n)$, we define $\delta(n) = x(n+1) - x(n)$, and then, according to (2.30),

$$\delta(n) = \frac{[x(n) - \phi(n)]\,[x(n) - 1]}{\varphi(n) - x(n)}, \tag{2.38}$$

where

$$\phi(n) = \frac{c(n)}{c(n) + \varepsilon(1-a) - b(n)}, \tag{2.39}$$

and

$$\varphi(n) = \frac{c(n) + \varepsilon(1-a)}{c(n) + \varepsilon(1-a) - b(n)}. \tag{2.40}$$

Since we have proved that $c(n) + \varepsilon(1-a) - b(n) > 0$ in Appendix A, obviously $\phi(n) > 0$ and $\varphi(n) > 1$.

Assume that the licensed channel is idle at the beginning of the first CR frame, i.e., $x(1) = 0$. Denote γ_p^* as the critical average SNR below which $b(n) \geq \varepsilon(1-a)$ and thus $\phi(n) \geq 1$ for any n. If the average SNR is below γ_p^*, then, according to (2.38), $\delta(n) \geq 0$ for any n, where the equality holds if and only if $x(n) = 1$. In other words, $x(n)$ is an increasing sequence and converges at $x_p^* = 1$, which indicates that the detection performance is so poor that the licensed channel is certain to be busy during secondary communication as time goes by.

In the nontrivial case that $\gamma > \gamma_p^*$, $b(n) < \varepsilon(1-a)$ and thus $0 < \phi(n) < 1$. Assume $x(n) < 1$ for any n, and then, according to (2.38), $\delta(n) \propto [\phi(n) - x(n)]$. Since both $b(n)$ and

$c(n)$ are functions of $x(n)$, so is $\phi(n)$. Define $\phi(n) = h(x(n))$, and then we have proved the following proposition in Appendix A.

Proposition 2.3.3 *When $\gamma > \gamma_p^*$, the $x(n)$ sequence of the probability-based energy detection scheme converges at $x_p^* = h(x_p^*)$, i.e., $\lim_{n\to+\infty} x(n) = x_p^*$.*

To sum up, $x(n)$ converges at $x_p^* = 1$ if $\gamma \leq \gamma_p^*$ or otherwise converges at $x_p^* = h(x_p^*)$, the value of which can be obtained numerically. Suppose that as $x(n)$ converges at x_p^*, $b(n)$ and $c(n)$ converge at b^* and c^* accordingly, respectively, and then, according to (2.27), $\overline{P}_M(n)$ also converges at a stable average mis-detection probability given by

$$\overline{P}_{M,p}^* = \frac{(b^* - c^*)x_p^* + c^*}{(1-a)x_p^* + a}. \tag{2.41}$$

2.3.5 Numerical Results

Figure 2.6 shows the stable average detection probability curves of the conventional and the probability-based energy detection schemes when $P_F = 10^{-1}$, $U = 100$, and $L = M = 6$. Figure 2.7 shows the stable conditional CDF ($P^*(m \leq i|\mathcal{H}_B)$) curves of m under different SNR levels when the probability-based scheme is applied. These curves, according to (2.11), also denote the stable weight sequences applied in the probability-based scheme. While the stable average detection probability of the conventional scheme is calculated directly based on (2.37), the counterpart of the probability-based one is obtained by simulating the convergence process. For both schemes, only the nontrivial case that the average SNR is above the critical one is considered. Figure 2.6 indicates that the probability-based scheme exhibits a higher stable average detection probability than the conventional one. Also, it is observed that the higher the average SNR is, the larger the performance improvement of the probability-based scheme over the conventional one is. This is reasonable since a higher average SNR means a smaller average mis-detection probability, a smaller $x(n)$, and hence larger differences between the conditional CDF values at different m's, as demonstrated by Figure 2.7. Figure 2.8 shows the convergence process of $x(n)$ under different SNR levels. It can be observed that $x(n)$'s of the conventional and the probability-based

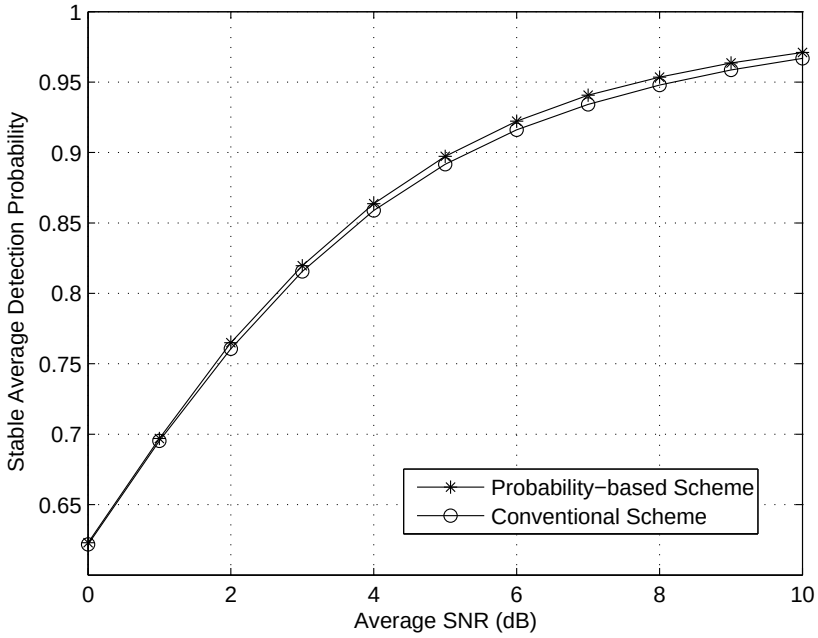

Figure 2.6. Stable average detection probability curves of the conventional and probability-based energy detection schemes.

energy detection schemes converge with almost the same speed. Figure 2.8 also indicates that the convergence speed of $x(n)$ increases with the average SNR, which verifies the earlier analysis. Furthermore, it can be observed that the probability-based scheme has a lower stable probability of the presence of the licensed user at the beginning of each CR frame than the conventional one, thus achieving a better stable detection performance.

2.4 Conclusion

By utilizing the statistical characteristics of the licensed channel occupancy, we have established a probability model on the appearance of a licensed user at each sample of a CR user frame. For the first time, the possibility that a licensed user appears in the middle of a sensing block has been taken into account for spectrum sensing scheme design in this chapter. While the conventional spectrum sensing scheme allocates the same weight to each sample, we have proposed a probability-based energy detection scheme in which the weight for each sample is based on the probability of the presence of a licensed user at the

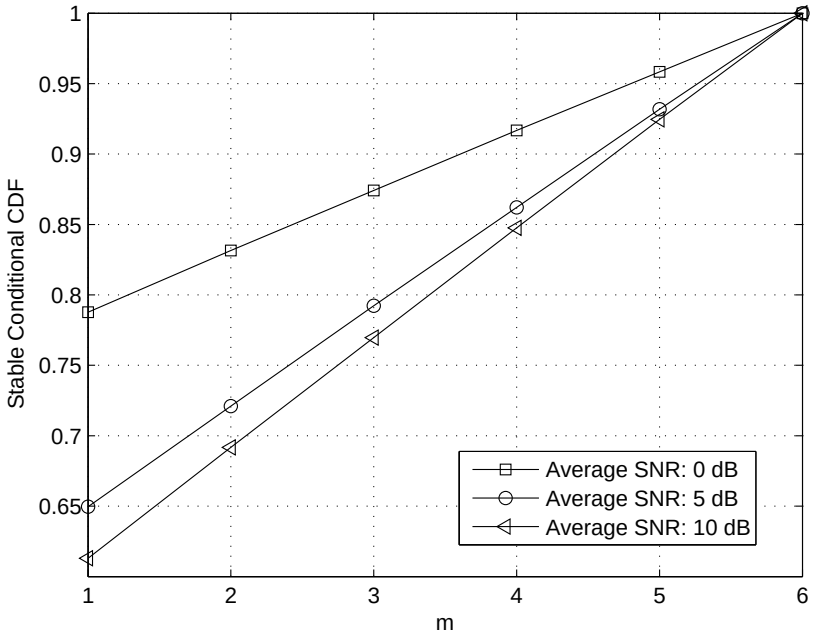

Figure 2.7. Stable conditional CDF curves of m under different SNR levels when the probability-based energy detection scheme is applied.

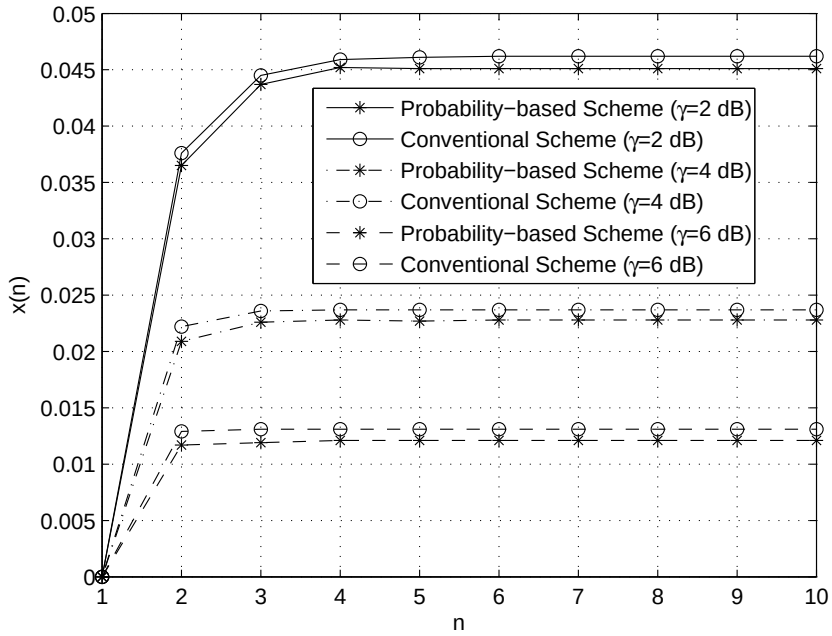

Figure 2.8. Convergence of $x(n)$ under different SNR levels.

corresponding sample. It has been demonstrated that this probability-based energy detection scheme achieves nearly optimal performance with relatively low complexity. Based on the assumption that the idle duration of the licensed channel is exponentially distributed, we have further analyzed the stable detection performance of the conventional and the probability-based energy detection schemes in periodic spectrum sensing and proved that both of them converge to their respective stable average detection probabilities.

CHAPTER 3

PROBABILITY-BASED OPTIMIZATION OF INTER-SENSING DURATION AND POWER CONTROL

The efficiency of opportunistic spectrum sharing relies not only on the spectrum sensing techniques applied but also on the scheduling of sensing activities. On one hand, if sensing activities are scheduled too often, CR users may waste too much time on sensing. On the other hand, if sensing activities are seldom scheduled, spectrum usage status may not be quickly discovered. In a periodic spectrum sensing framework where each frame consists of a sensing block and an inter-sensing block, the ratio of the sensing block length to the inter-sensing block length represents how frequently sensing activities are scheduled, and therefore is a key parameter in spectrum sensing scheduling. Meanwhile, the transmit power of a CR user at different samples of one frame may be varied in conjunction of spectrum sensing scheduling.

In this chapter, we study probability-based inter-sensing duration optimization schemes by utilizing the statistical characteristics of the licensed channel occupancy. Quick capture of spectrum opportunity is ensured when the licensed user signal is detected, and the spectrum efficiency is maximized under a given interference level when the licensed user signal is declared absent, in which case a power control scheme is further proposed to match the transmit power of each sample with the corresponding non-interfering probability to improve the performance.

The rest of this chapter is organized as follows. In Section 3.1, we describe the statistical model of the licensed channel occupancy and the frame structure of the CR system. In Section 3.2, we discuss silent block length optimization when the licensed user is detected. In Section 3.3, we discuss data block length optimization and transmit power control scheme when the licensed user is declared absent. Finally, we conclude this chapter in Section 3.4.

3.1 System Model

We consider a CR user pair, including a transmitter and a receiver, which opportunistically operates on a single frequency band assigned to the licensed users located in the same geographical region. The CR user determines the presence or absence of any licensed activity within the channel through spectrum sensing, and utilizes it if licensed activity is not detected.

The licensed channel is modeled as an alternating renewal source between busy and idle states [31, 89], where busy and idle denote that the channel is occupied and unoccupied by the licensed users, respectively. The busy and idle periods are random variables with PDFs $f_B(t)$ and $f_I(t)$, respectively. As indicated in [29, 88, 90], they can be assumed exponentially distributed with

$$f_B(t) = \alpha e^{-\alpha t} \tag{3.1}$$

and

$$f_I(t) = \beta e^{-\beta t}, \tag{3.2}$$

where α is the transition rate from busy to idle state, and β is the transition rate from idle to busy state [84], both of which can be estimated with statistical methods [31]. Therefore, we assume that they are already known to the CR user throughout this chapter. Accordingly, the average busy and idle periods are $1/\alpha$ and $1/\beta$, and the stationary probabilities for the channel to be busy and idle are

$$\bar{P}_B = \frac{\beta}{\alpha + \beta} \tag{3.3}$$

and

$$\bar{P}_I = \frac{\alpha}{\alpha + \beta}. \tag{3.4}$$

Denote the probability density functions of the remaining time that the channel stays in the current busy and idle states as $f_{BR}(t)$ and $f_{IR}(t)$, respectively, which are the same as $f_B(t)$ and $f_I(t)$ due to the memoryless property of the exponential distribution.

In our model, the activity of the CR user is periodic with the same frame structure introduced in the previous chapter. In each frame, the CR user first monitors the channel in the sensing block for M samples. Depending on whether the channel is identified as busy or idle, the CR user will either keep silent or start transmitting or receiving in the inter-sensing (silent or data) block for L samples. Since the channel may be reoccupied or released by the licensed users in the future, the CR user should restart a new frame beginning with the sensing block again following the previous inter-sensing block. Throughout this chapter, we assume that the CR user adopts a predetermined length of the sensing block for certain detection performance. In other words, M is fixed.

According to our model, if the channel is busy at the end of a sensing block, the conditional probability that it is still busy at the lth sample of the upcoming inter-sensing block is

$$P_{B_l|B} = \int_{l\tau}^{\infty} f_{BR}(t)dt = e^{-\alpha l\tau}, \tag{3.5}$$

where t is the remaining time in the current state from the last sample of the sensing block, and τ denotes the sampling interval. The conditional probability that it is idle at the lth sample of the upcoming inter-sensing block is $P_{I_l|B} = 1 - P_{B_l|B}$. Similarly, if the channel is idle at the end of the sensing block, the conditional idle and busy probabilities at the lth sample of the upcoming inter-sensing block are

$$P_{I_l|I} = \int_{l\tau}^{\infty} f_{IR}(t)dt = e^{-\beta l\tau} \tag{3.6}$$

and $P_{B_l|I} = 1 - P_{I_l|I}$, respectively.

3.2 Strategy within Silent Block

3.2.1 Silent Block Length Optimization

If a CR user detects the channel as busy within the sensing block, it will keep silent in the upcoming inter-sensing block of the current frame and initiate detection in the sensing block of the next frame. If the length of the silent block is larger, spectrum sensing actions will be taken less frequently, which saves energy. However, the spectrum opportunity may

not be quickly recognized and the latency of the CR user's packet may be increased. It is obvious that there is a tradeoff between energy efficiency and bandwidth efficiency when selecting the length of the silent block. To that end, we introduce the concept of *average spectrum opportunity loss*, which is defined as the expected number of idle samples within the upcoming inter-sensing block if the channel is detected as busy in the sensing block. From the definition, it can be expressed as

$$T_{I_L|\hat{B}} = \sum_{l=1}^{L} P_{I_l|\hat{B}}, \tag{3.7}$$

where $P_{I_l|\hat{B}}$ is the conditional idle probability at the lth sample of the upcoming inter-sensing block if the channel is detected as busy in the sensing block. With such a concept, we are able to estimate the throughput loss within the block, which is the product of the average spectrum opportunity loss and average transmission rate of the CR user for a given average transmit power.

There are two cases that the CR user may keep silent in the inter-sensing block: i) the sensing decision is busy while the channel is really busy at the end of the sensing block (correct detection), and ii) the sensing decision is busy while the channel is actually idle at the end of the sensing block (false alarm). Let P_B and P_I denote the busy and idle probabilities at the end of the sensing block, which can be substituted with the stationary probabilities $\bar{P}_B$ and $\bar{P}_I$, respectively. Since $P_B + P_I = 1$, we have

$$P_{I_l|\hat{B}} = P_{I_l|B} P_{B|\hat{B}} + P_{I_l|I} P_{I|\hat{B}}, \tag{3.8}$$

where $P_{I_l|B}$ and $P_{I_l|I}$ are the conditional idle probabilities with perfect sensing as we have introduced; $P_{B|\hat{B}}$ and $P_{I|\hat{B}}$ are the conditional busy and idle probabilities at the end of the sensing block if the channel is detected as busy in the sensing block, respectively. According to the Bayes' theorem, we have

$$P_{B|\hat{B}} = \frac{P_{\hat{B}|B} P_B}{P_{\hat{B}|B} P_B + P_{\hat{B}|I} P_I} \tag{3.9}$$

and

$$P_{I|\hat{B}} = \frac{P_{\hat{B}|I} P_I}{P_{\hat{B}|B} P_B + P_{\hat{B}|I} P_I}, \tag{3.10}$$

where $P_{\hat{B}|B}$ or $P_{\hat{B}|I}$ is the conditional probability that the channel is detected as busy if the channel is busy or idle at the end of the sensing block, which can be set equal to the average detection probability, P_D, or false alarm probability, P_F.

Accordingly, we find the relationship between the length of the silent block and the average spectrum opportunity loss for the case with exponentially distributed busy and idle states as

$$T_{I_L|\hat{B}} = (L - \frac{1 - e^{-\alpha\tau L}}{1 - e^{-\alpha\tau}} e^{-\alpha\tau}) P_{B|\hat{B}} + \frac{1 - e^{-\beta\tau L}}{1 - e^{-\beta\tau}} e^{-\beta\tau} P_{I|\hat{B}}. \tag{3.11}$$

To identify the spectrum opportunity quickly, it is usually required that L is small such that $\alpha\tau L$ and $\beta\tau L$ are close to 0. Therefore, the spectrum opportunity loss can be well approximated with partial Taylor polynomials as

$$T_{I_L|\hat{B}} = \frac{\alpha\tau L^2}{2} P_{B|\hat{B}} + (L - \frac{\beta\tau L^2}{2}) P_{I|\hat{B}}. \tag{3.12}$$

By taking the partial derivative with L, we find that it is an increasing function of L. So if it requires that the spectrum opportunity loss to be no larger than a predefined value, T_λ, which is set according to the speed requirement for emptying the queue of the CR user divided by its average transmission rate, the optimal length of the silent block is

$$L_{opt} = \left\lfloor \frac{\sqrt{P^2_{I|\hat{B}} + 2(P_{B|\hat{B}}\alpha\tau - P_{I|\hat{B}}\beta\tau)T_\lambda} - P_{I|\hat{B}}}{P_{B|\hat{B}}\alpha\tau - P_{I|\hat{B}}\beta\tau} \right\rfloor. \tag{3.13}$$

3.2.2 Numerical Results

Figure 3.1 shows the optimal length of the silent block with $T_\lambda = 100$ for different state transition rates. In this figure, $\tau = 0.0001$ sec, $M = 50$, $P_D = 0.95$, and $P_F = 0.1$. From the figure, as the transition rate from busy to idle state or from idle to busy state increases, the optimal length of the silent block becomes smaller or larger, respectively, which confirms our intuition.

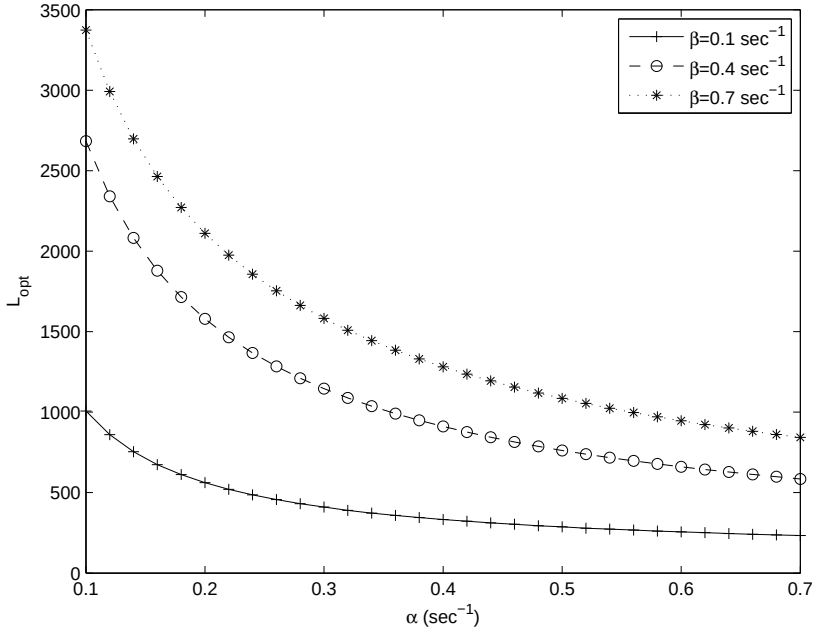

Figure 3.1. Optimal silent block length versus state transition rate.

3.3 Strategies within Data Block

3.3.1 Data Block Length Optimization

If a CR user detects the channel as idle within the sensing block, it will start transmitting or receiving data in the channel within the upcoming inter-sensing (data) block[1]. Intuitively, if the data block is too long, the licensed user is with high possibility to reoccupy the channel so that they may interfere with each other. If it is too short, the secondary communication may be interrupted too frequently for spectrum sensing and the CR user may lose the remaining spectrum opportunity within the idle channel, which results in low bandwidth efficiency. Therefore, there exist better strategies to determine the length of the data block, for the overall benefits of the licensed user and the CR user. We will first study how to choosing the optimal length of the data block. Here we use two metrics to characterize the system performance including average transmission rate and average interference power.

[1]Here we assume that the CR user always has data to send or receive after detecting an idle channel.

Average transmission rate, η, is defined as the expected average rate of the secondary communication within the whole frame. Mathematically,

$$\eta = \frac{\sum_{l=1}^{L} P_{I_l|\hat{I}} R_l}{M + L}, \tag{3.14}$$

where $P_{I_l|\hat{I}}$ is the conditional idle probability at the lth sample of the upcoming inter-sensing block if the channel is detected as idle in the sensing block, and R_l is the transmission rate of the CR user at the lth sample of the upcoming inter-sensing block, which is related to the transmit power S_l at the lth sample by [91]

$$R_l = \log_2(1 + \frac{S_l G}{\sigma^2}), \tag{3.15}$$

where G is the power gain from the CR transmitter to receiver and σ^2 is the noise variance at the CR receiver. G and σ^2 are both assumed to be constant during one data block, which can be obtained by channel and noise estimation methods. Similarly, *average interference power*, ε, is defined as the expected average interference power at the licensed receiver from secondary communication within the whole frame. Mathematically,

$$\varepsilon = \frac{\sum_{l=1}^{L} P_{B_l|\hat{I}} S_l G'}{M + L}, \tag{3.16}$$

where $P_{B_l|\hat{I}}$ is the conditional busy probability at the lth sample of the upcoming inter-sensing block if the channel is detected as idle in the sensing block, which is equal to $1 - P_{I_l|\hat{I}}$, and G' is the power gain from the CR transmitter to the licensed receiver. G' is also assumed to be constant during each data block. If the channel between the CR transmitter and the licensed receiver is reciprocal and the licensed communication is bi-directional, G' can be estimated through measuring the licensed user signal strength at the CR transmitter during spectrum sensing when the licensed receiver is transmitting.

The data block length optimization can be formulated as selecting the length of the data block so that

1. the average interference power in (3.16) is no more than a predefined threshold, and

2. the average transmission rate in (3.14) is maximized.

Similar to the previous discussion, denote $P_{B|\hat{I}}$ and $P_{I|\hat{I}}$ as the conditional busy and idle probabilities at the end of the sensing block if the channel is detected as idle in the sensing block, which can be represented as

$$P_{B|\hat{I}} = \frac{(1-P_D)\bar{P}_B}{(1-P_D)\bar{P}_B + (1-P_F)\bar{P}_I} \tag{3.17}$$

and

$$P_{I|\hat{I}} = \frac{(1-P_F)\bar{P}_I}{(1-P_D)\bar{P}_B + (1-P_F)\bar{P}_I}, \tag{3.18}$$

respectively, and set the transmit power of the CR user at each sample of the upcoming data block to be equal to S, we find the relationship between the length of the data block and the average transmission rate as

$$\eta = R\frac{\frac{\alpha\tau L^2}{2}P_{B|\hat{I}} + (L - \frac{\beta\tau L^2}{2})P_{I|\hat{I}}}{M+L} \tag{3.19}$$

and

$$\varepsilon = SG'\frac{(L - \frac{\alpha\tau L^2}{2})P_{B|\hat{I}} + \frac{\beta\tau L^2}{2}P_{I|\hat{I}}}{M+L}. \tag{3.20}$$

By taking the partial derivative with L, we find that the average transmission rate is initially increasing and then decreasing as the length of the data block increases, and the average interference power is an increasing function of the data block length. The maximum value of η is achieved at

$$L = L_{opt}^{(1)} = \left\lfloor \sqrt{M^2 + \frac{2P_{I|\hat{I}}M}{P_{I|\hat{I}}\beta\tau - P_{B|\hat{I}}\alpha\tau}} - M \right\rfloor. \tag{3.21}$$

To ensure $\frac{\varepsilon}{SG'} \leq \Gamma$, where Γ is the predefined threshold, we need

$$L \leq L_{opt}^{(2)} = \left\lfloor \frac{\sqrt{(P_{B|\hat{I}}-\Gamma)^2 + 2(P_{I|\hat{I}}\beta\tau - p_{B|\hat{I}}\alpha\tau)\Gamma L} - P_{B|\hat{I}} + \Gamma}{P_{I|\hat{I}}\beta\tau - P_{B|\hat{I}}\alpha\tau} \right\rfloor. \tag{3.22}$$

Therefore, the optimal length of the data block is

$$L_{opt} = \min(L_{opt}^{(1)}, L_{opt}^{(2)}). \tag{3.23}$$

3.3.2 Transmit Power Control

If the transmit power of the CR user in one data block can be varied, we can allocate the transmit power at each sample to further improve its performance.

Our objective is to maximize the average transmission rate of the CR user in (3.14) under its average transmit power constraint, $\bar{S}$, that is, to maximize

$$\eta = \frac{\sum_{l=1}^{L} P_{I_l|\hat{I}} \log_2(1 + S_l G/\sigma^2)}{M + L}, \tag{3.24}$$

subject to

$$\frac{1}{L}\sum_{l=1}^{L} S_l \leq \bar{S}. \tag{3.25}$$

This optimization problem can be solved via the Lagrangian methods [92]. Consider the Lagrangian

$$\mathcal{L}(\lambda, S_1, S_2, ..., S_L) = \sum_{l=1}^{L} P_{I_l|\hat{I}} \log_2(1 + S_l G/\sigma^2) - \lambda \sum_{l=1}^{L} S_l, \tag{3.26}$$

where λ is the Lagrange multiplier. The power allocation

$$S_l = \left(\frac{P_{I_l|\hat{I}}}{\mu} - \frac{\sigma^2}{G}\right)^+ \tag{3.27}$$

satisfies and is therefore optimal, where $(x)^+ = \max(x, 0)$ and μ is a parameter chosen such that the power constraint is met, that is,

$$\frac{1}{L}\sum_{l=1}^{L}\left(\frac{P_{I_l|\hat{I}}}{\mu} - \frac{\sigma^2}{G}\right)^+ = \bar{S}. \tag{3.28}$$

If σ^2/G is very small, which corresponds to the case of large signal to noise ratio at the CR receiver side, the transmit power is directly proportional to the conditional idle probability at each sample that $S_l = \frac{P_{I_l|\hat{I}}}{\bar{P}_{I_l|\hat{I}}}\bar{S}$ where $\bar{P}_{I_l|\hat{I}} = \frac{1}{L}\sum_{l=1}^{L} P_{I_l|\hat{I}}$. Note that the channel and noise information is not needed for implementation in this case. Compared with constant transmit power allocation within each data block, i.e., $S_l = \bar{S}$ for any l, our scheme

increases the average transmission rate of the CR user in (3.14) by

$$\begin{aligned}\Delta\eta &= \eta - \eta_0 \\ &= \frac{\sum_{l=1}^{L} P_{I_l|\hat{I}} \log_2(1+S_l G/\sigma^2)}{M+L} - \frac{\sum_{l=1}^{L} P_{I_l|\hat{I}} \log_2(1+\bar{S} G/\sigma^2)}{M+L} \\ &\approx \frac{\sum_{l=1}^{L} P_{I_l|\hat{I}} \log_2(\frac{P_{I_l|\hat{I}}}{\bar{P}_{I_l|\hat{I}}})}{M+L},\end{aligned} \tag{3.29}$$

where η_0 is the average transmission rate of the CR user under constant transmit power allocation. Note that the average interference power also decreases as

$$\begin{aligned}\Delta\varepsilon &= \varepsilon - \varepsilon_0 \\ &= \frac{\sum_{l=1}^{L} P_{B_l|\hat{I}} S_l G'}{M+L} - \frac{\sum_{l=1}^{L} P_{B_l|\hat{I}} \bar{S} G'}{M+L} \\ &= \frac{\bar{S} G' L}{\bar{P}_{I_l|\hat{I}}(M+L)} \left[\frac{1}{L} \sum_{l=1}^{L} P_{I_l|\hat{I}}(1-P_{I_l|\hat{I}}) - \bar{P}_{I_l|\hat{I}}(1-\bar{P}_{I_l|\hat{I}}) \right]\end{aligned} \tag{3.30}$$

is smaller than 0 by noting that $f(x) = x(1-x)$ is concave.

3.3.3 Numerical Results

Figure 3.2 shows the normalized average transmission rate, η/R, and interference power, ε/SG', with respect to the length of the data block, L, given the same parameters as in the previous section and $\alpha = \beta = 0.4$ sec^{-1}. It verifies that the average transmission rate is initially increasing and later decreasing with increased length of the data block while the average interference power is an increasing function of the data block length. In this figure, we also show how to find the corresponding optimal length of the data block given $\Gamma = 0.08SG'$. We find the maximum normalized average transmission rate and the corresponding length of the data block, $L_{opt}^{(1)}$, and find the interference power constraint and the corresponding length of the data block, $L_{opt}^{(2)}$. Then we select the optimal length of the data block, $L_{opt} = \min(L_{opt}^{(1)}, L_{opt}^{(2)})$.

Figure 3.3 shows the optimal length of the data block given $\Gamma = 0.08SG'$ for different state transition rates. When $\beta = 0.4$ sec^{-1}, the curve has an inflexion in the figure, the left and the right parts of which are determined by (3.22) and (3.21), respectively. The

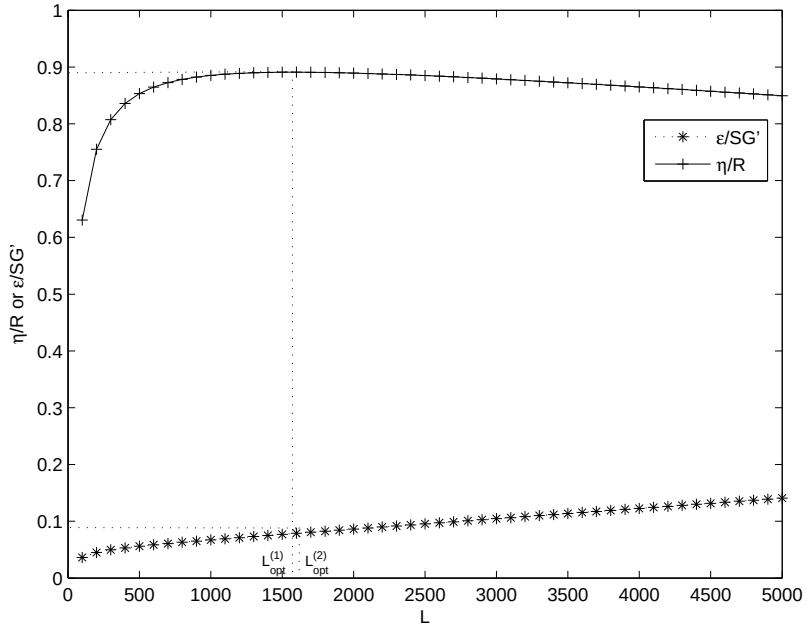

Figure 3.2. Normalized average transmission rate and interference power versus data block length.

whole curve is determined by (3.21) or (3.22) when $\beta = 0.1\ sec^{-1}$ or $\beta = 0.7\ sec^{-1}$. As the transition rate from busy to idle state, α, increases to a certain extent, the optimal length of the data block is not changing. This is because the length given by (3.21) equals $\left\lfloor \sqrt{M^2 + \frac{2(1-P_F)M}{\beta\tau(P_D-P_F)}} - M \right\rfloor$, which has nothing to do with α any more.

With transmit power control, the relative transmission rate increment, $\Delta\eta/\eta_0$, and interference power decrease, $-\Delta\varepsilon/\varepsilon_0$, for different values of the average receive SNR, γ, are shown in Figure 3.4. Note that our scheme exhibits greater performance gain at smaller average receive SNR. As the average receive SNR gets larger, our power control scheme is closer to the constant power allocation, which is similar to the trend of power allocation among parallel subchannels of OFDM systems.

3.4 Conclusion

Based on the statistical model of the licensed channel occupancy and the frame structure of the CR system, we have studied the strategies within the inter-sensing block for CR.

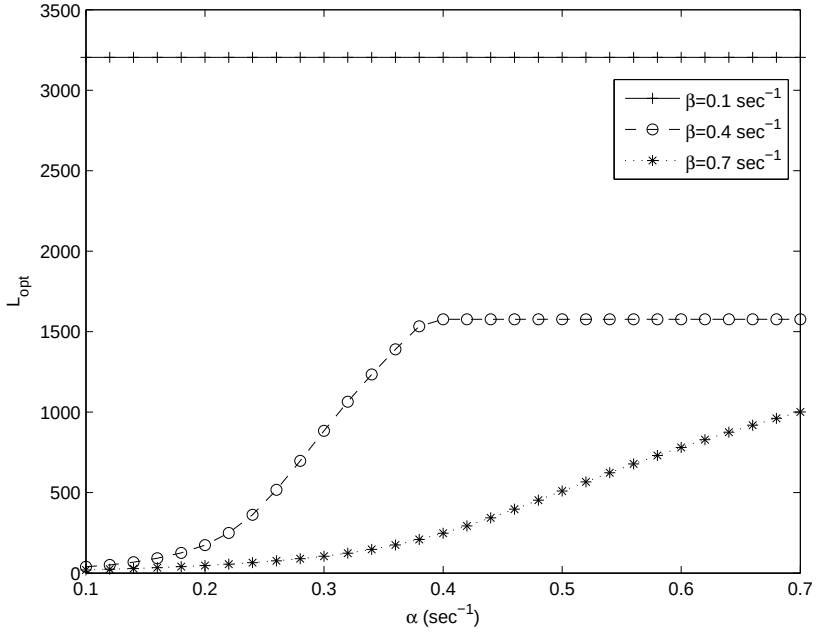

Figure 3.3. Optimal data block length versus state transition rate.

Our schemes utilize the statistical information of licensed channel activity to determine the optimal lengths of the silent and data blocks, or to vary the transmit power dynamically at each data sample. Numerical results have verified the performance improvement through our schemes.

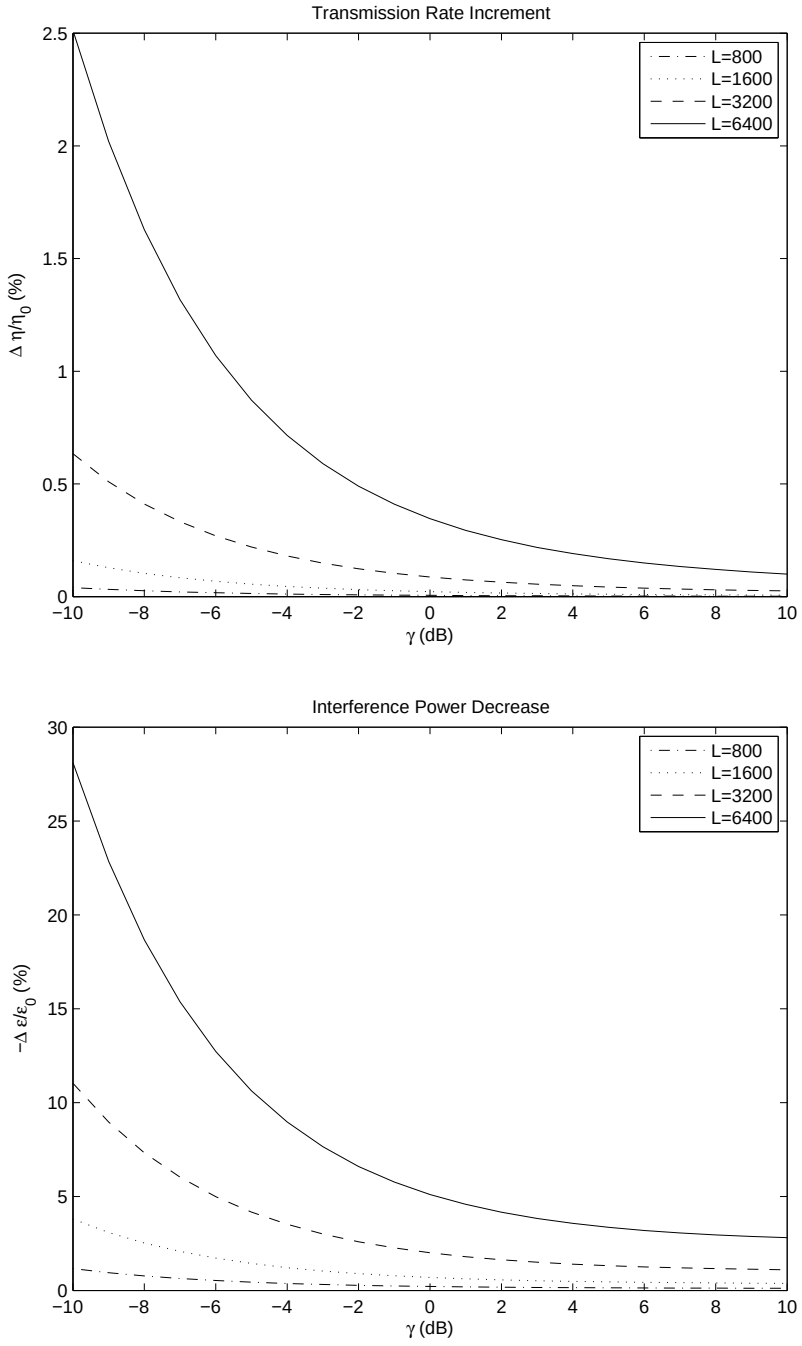

Figure 3.4. Transmission rate increment and interference power decrease versus average receive SNR.

CHAPTER 4

PROBABILITY-BASED COMBINATION FOR COOPERATIVE SPECTRUM SENSING

In cooperative spectrum sensing, each CR user sends its sensing information to the combining node, which makes a decision on the presence or absence of the licensed user signal. In practice, different CR users may have different sensing schedules and initiate spectrum sensing at different moments. In this case, any combination method assuming synchronous sensing would incur a performance loss and therefore needs to be modified for robust detection.

In this chapter, we propose a probability-based combination scheme for cooperative spectrum sensing, which, according to the Bayesian decision rule, is optimal in the sense that the average cost is minimized. Taking the time offsets among local sensing observations and final combination into account, our scheme enables combination of both synchronous and asynchronous sensing information from different CR users by utilizing statistical characteristics of the licensed channel occupancy.

The remainder of this chapter is organized as follows. In Section 4.1, we describe the statistical model of the licensed channel occupancy and formulate the detection problem in cooperative spectrum sensing. In Section 4.2, We present the probability-based combination scheme. Then we further develop a simplified implementation of our combination scheme under a symmetrical case in Section 4.3 and present simulation results in Section 4.4. Finally we conclude this chapter in Section 4.5.

4.1 System Model

As in the previous chapter, the occupancy of a licensed channel can be modeled as a renewal process which alternates between busy and idle states [31, 89], which correspond to that the channel is occupied and unoccupied by licensed users, respectively. The busy and

idle periods are random variables with PDFs denoted as $f_B(t)$ and $f_I(t)$, respectively, and assumed to be exponentially distributed with $f_B(t) = \alpha e^{-\alpha t}$ and $f_I(t) = \beta e^{-\beta t}$, respectively, where α is the transition rate from busy to idle state, and β is the transition rate from idle to busy state. While both α and β can be estimated from previous observations of the licensed channel utilization through continuous spectrum sensing, we assume that they are already known to the CR users throughout this chapter to facilitate analysis. Accordingly, the average busy and idle periods are $1/\alpha$ and $1/\beta$, respectively; the stationary probabilities for the channel to be busy and idle are $\bar{P}_B = \frac{\beta}{\alpha+\beta}$ and $\bar{P}_I = \frac{\alpha}{\alpha+\beta}$, respectively. It should be noted that although we assume exponentially distributed busy and idle periods in this chapter to get closed-form expressions, our analysis actually applies to any general PDFs of the two periods.

According to the renewal theory [89], we denote the PDF of the elapsed time that the channel has been staying in the current busy or idle state, i.e., age distribution, as $f_{BA}(t)$ or $f_{IA}(t)$. Due to the memoryless property of the exponential distribution, $f_{BA}(t) = \alpha e^{-\alpha t}$ and $f_{IA}(t) = \beta e^{-\beta t}$, which are the same as $f_B(t)$ and $f_I(t)$, respectively.

Spectrum sensing involves deciding whether the licensed user signal is present or not from the observed signal. It can be formulated as the binary hypothesis testing problem in (2.1). The goal of spectrum sensing is to decide between the two hypotheses, $\mathcal{H}_I$ and $\mathcal{H}_B$, corresponding to the absence and presence of the licensed user signal, from the observation.

4.2 Optimal Combination for Cooperative Spectrum Sensing

In cooperative spectrum sensing, CR users obtain local information of licensed channel activity and send it to a combining node through a dedicated control channel. Note that the local sensing information may be an individual decision on the absence or presence of the licensed user signal or preprocessed sensing data. According to the sensing information collected from different CR users, the combining node decides between the two hypotheses in (5.1). In the literature, it is usually assumed that the local observations of different users

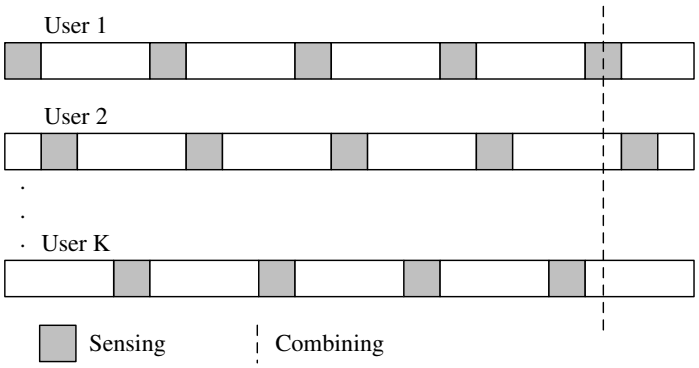

Figure 4.1. Combining model for cooperative spectrum sensing.

are obtained at the same time and sent to the combining node without delay, which does not always hold in reality. Therefore, cooperative spectrum sensing should take asynchronous sensing into account.

Figure 4.1 gives a general schematic representation for combination of sensing information in cooperative spectrum sensing. As shown in this figure, there are K cooperative users in the CR network and the kth ($k = 1, 2, ..., K$) CR user sends its sensing information u_k obtained at t_k to the combining node. After receiving the sensing information from individual CR users, the combining node makes the decision u on the absence or presence of the licensed user signal at t. Note that $t > t_k$ for $k = 1, 2, ..., K$. To facilitate analysis, here we assume the transmission of the local sensing information over the dedicated control channel is faultless.

As mentioned, the sensing information from the kth CR user, u_k, is either one-bit hard decision on the absence or presence of the licensed user signal, or multi-bit quantized data on its observation [40]. Specifically, User k divides the whole range of its measurement, such as the received signal energy within a predetermined interval, into L_k regions and reports to the combining node which region its observation falls in. Therefore, L_k is the number of distinct quantized sensing results from User k. Note that L_k's for different CR users are not necessarily the same. When $L_k = 1$, the sensing information from the kth user reduces to one-bit hard decision on the absence or presence of the licensed user signal;

when L_k goes to infinity, the sensing information of User k becomes its original measurement. Without loss of generality, we denote the L_k possible quantized sensing results of User k observed at t_k as $u_k(t_k) = l$ for $l = 0, 1, ..., L_k - 1$.

For optimal combination of local sensing information, here we apply the Bayesian decision rule [93] since it minimizes the average cost of false alarm and mis-detection. Consequently, the optimum decision is based on the following likelihood ratio,

$$Y = \frac{P(u_1, u_2, ..., u_K|\mathcal{H}_B)}{P(u_1, u_2, ..., u_K|\mathcal{H}_I)}, \tag{4.1}$$

where $\mathcal{H}_B$ and $\mathcal{H}_I$ denote the hypotheses corresponding to the presence and absence of the licensed user signal at t, respectively. Define the average cost as

$$R = C_F \Pr\{u = \mathcal{H}_B|\mathcal{H}_I\} P_I + C_M \Pr\{u = \mathcal{H}_I|\mathcal{H}_B\} P_B, \tag{4.2}$$

where P_B and P_I denote the prior probabilities of the presence and absence of the licensed user signal, which can be substituted with the stationary probabilities $\bar{P}_B$ and $\bar{P}_I$, respectively; C_F and C_M are the costs for false alarm (the decision is H_B while the licensed user signal is absent at t) and mis-detection (the decision is H_I while the licensed user signal is present at t), respectively. In practice, C_M is usually larger than C_F because, in the mis-detection case, the CR users are allowed to utilize the licensed channel and may generate interference to licensed users, which is more severe than possible loss of spectrum opportunities in the false alarm case.

To minimize the average cost, the optimum decision rule is given by [93] as

$$Y \underset{\mathcal{H}_I}{\overset{\mathcal{H}_B}{\gtrless}} \frac{P_I C_F}{P_B C_M}. \tag{4.3}$$

Since individual CR users are at different locations, we assume that their observations are statistically independent and therefore,

$$P(u_1, u_2, ..., u_K|\mathcal{H}_i) = \prod_{k=1}^{K} P(u_k|\mathcal{H}_i). \tag{4.4}$$

According to the Bayes' theorem [84],

$$P(u_k|\mathcal{H}_i) = P(u_k|B_k)P(B_k|\mathcal{H}_i) + P(u_k|I_k)P(I_k|\mathcal{H}_i), \tag{4.5}$$

where B_k and I_k denote that the licensed user signal is present and absent at t_k, respectively.

With the help of age distribution of a renewal process, we can obtain

$$P(B_k|\mathcal{H}_B) = \int_{t-t_k}^{\infty} f_{BA}(\tau)d\tau = e^{-\alpha(t-t_k)} \tag{4.6}$$

and

$$P(I_k|\mathcal{H}_I) = \int_{t-t_k}^{\infty} f_{IA}(\tau)d\tau = e^{-\beta(t-t_k)}. \tag{4.7}$$

Since $P(B_k|\mathcal{H}_i) + P(I_k|\mathcal{H}_i) = 1$ for $i = B, I$, $P(I_k|\mathcal{H}_B)$ and $P(B_k|\mathcal{H}_I)$ can be further obtained based on (4.6) and (4.7), respectively.

In (4.5), $P(u_k|B_k)$ and $P(u_k|I_k)$ are parameters reflecting the detection performance of the kth user. To be specific,

$$P(u_k = l|B_k) = \int_{\mathcal{R}_{k,l}} f_{B_k}(y_k)dy_k \tag{4.8}$$

and

$$P(u_k = l|I_k) = \int_{\mathcal{R}_{k,l}} f_{I_k}(y_k)dy_k, \tag{4.9}$$

where $\mathcal{R}_{k,l}$ is the lth quantization region of User k; $f_{B_k}(y_k)$ and $f_{I_k}(y_k)$ denote the PDFs of the measurement under B_k and I_k, respectively, which are given in [85] for energy detection. Note that in the one-bit hard decision case, $P(u_k = 1|B_k) = P_{D,k}$ is the local detection probability of User k, and $P(u_k = 1|I_k) = P_{F,k}$ is the local false alarm probability of User k.

From (4.4)–(4.9), we obtain the likelihood ratio in (4.3) as a function of detection error probabilities and time offsets between local observations and final decision. Therefore, we can present the structure of the optimal combination scheme for cooperative spectrum sensing in Figure 4.2.

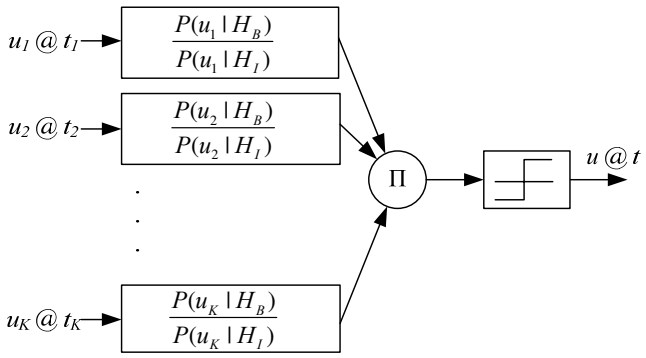

Figure 4.2. Optimal combination structure for cooperative spectrum sensing.

4.3 An Equivalent "K_0-Out-of-K" Scheme

K_0-*out-of-K* is a widely used rule for combination of one-bit hard decisions from individual users because of its simplicity. In this rule, the licensed user signal is declared present if and only if at least K_0 out of K users decide locally the presence of the licensed user signal [40]. Mathematically, its decision is given by

$$\sum_{k=1}^{K} u_k \underset{\mathcal{H}_1}{\overset{\mathcal{H}_B}{\gtrless}} K_0, \tag{4.10}$$

where $u_k = 0$ or 1 and K_0 is a design parameter chosen to achieve a target detection performance. The following proposition indicates the equivalence between the optimal combination scheme and the K_0-out-of-K scheme under certain scenarios, which has been proved in Appendix B.

Proposition 4.3.1 *The probability-based optimal combination of one-bit hard decisions reduces to the K_0-out-of-K scheme when all of the cooperative users have identical spectrum sensing operating points and obtain the sensing information at the same time.*

4.4 Simulation Results

In this section, we compare our scheme under the hard decision case with the conventional scheme presented in [93] that always assumes synchronous local observations as well as a simplified sliding-window scheme that maintains the sensing information within 1 sec before the final decision is made. We let 10 CR users take turns to perform spectrum

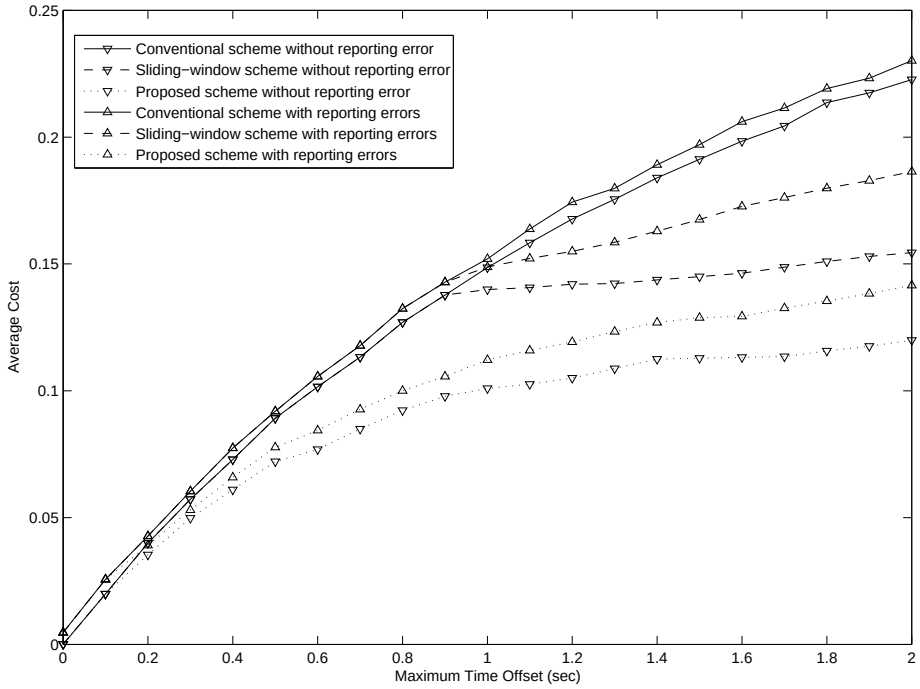

Figure 4.3. Performance comparison of different cooperative spectrum sensing schemes.

sensing and the time offsets between adjacent observations are the same. In our simulation, $\alpha = \beta = 0.5\ \text{sec}^{-1}$, $C_F = 1$, $C_M = 2$, $P_{D,k} = 0.95$, and $P_{F,k} = 0.1$ for $k = 0, 1, .., K$, all of which are assumed to be known at the combining node. The performance of the schemes with respect to different maximum offsets between the first observation and the final decision is shown in Figure 4.3. We also compare them under both faultless reporting channel and a *binary symmetric channel* (BSC) channel with crossover probability 0.1.

It is obvious that our scheme has lower average cost compared with both the conventional and the sliding-window schemes. The performance gap between them turns more and more obvious as the maximum offset between the first observation and the final decision increases, which demonstrates the effectiveness of our scheme in combining asynchronous sensing information. When there are reporting errors for the local information, our scheme remains superior.

4.5 Conclusion

In this chapter, we have proposed a probability-based combination scheme for cooperative spectrum sensing in CR networks. By utilizing the statistical characteristics of the licensed channel occupancy, this scheme achieves optimal combination of both synchronous and asynchronous sensing information. Compared with conventional combination schemes that always assume synchronous sensing in CR networks, our scheme improves the detection performance significantly under the asynchronous case.

CHAPTER 5

BANDWIDTH-EFFICIENT REPORTING FOR COOPERATIVE SPECTRUM SENSING

In cooperative spectrum sensing, CR users need to report individual sensing information to a combining node. Usually a common control channel is used for sending local sensing data. In the initial setup phase that the CR users are performing spectrum sensing, idle communication channels in the licensed spectrum have not been well identified so the bandwidth resource for the common control channel is quite limited. In bandwidth-efficient reporting schemes for cooperative spectrum sensing through quantization, it is implied that local sensing data from different users are transmitted through orthogonal channels, i.e., separated in different time slots, frequency bands, or codes. As the number of cooperative users increases, the bandwidth required for reporting also increases as implied and the stringent bandwidth constraint of the common control channel during spectrum sensing may not be satisfied. Therefore, bandwidth-efficient design with the required reporting bandwidth being independent of the number of cooperative users is desired.

We study in this chapter a general bandwidth-efficient reporting approach for cooperative spectrum sensing, in which different CR users are allowed to simultaneously send local sensing data to a combining node through the same narrowband channel using a common waveform. This approach saves the required reporting bandwidth, which is fixed regardless of the number of cooperative users, but results in the superposition of sensing data. Therefore, careful design of local information processing at the CR users and final decision rule at the combining node is required. Unlike the schemes that require user coordination to determine power scaling and instantaneous channel information to forward pre-equalized sensing measurement, our approach is based on local likelihood ratios and does not necessarily need such coordination or channel information. We build an optimal cooperative

spectrum sensing structure and consider the bandwidth-efficient design under Bayesian criterion and practical reporting channels. Calculation of probabilistic information involved in the design is also discussed. With proper preprocessing at individual users, the proposed schemes achieve reasonable performance despite the superposition of sensing data at the combining node.

The rest of this chapter is organized as follows. In Section 5.1, we briefly describe the system model of cooperative spectrum sensing in a multi-user CR network. In Section 5.2, we discuss the optimal bandwidth-efficient reporting scheme with Gaussian reporting channel. Then we develop the optimal bandwidth-efficient reporting scheme when the reporting channel experiences fading in Section 5.3. We present simulation results in Section 5.4 and finally conclude this chapter in Section 5.5.

5.1 System Model

In this chapter, we study cooperative spectrum sensing in a multi-user CR network consisting of several CR users and a combining node. Through local spectrum sensing, each CR user collects its observation on the spectrum band of interest, and then processes and sends the processed sensing data to the combining node via a common control channel [94]. Upon receiving the sensing data reported from different CR users, the combining node makes a decision on whether the licensed user is present or not.

5.1.1 Local Spectrum Sensing and Processing

We consider a CR network consisting of K cooperative users. In local spectrum sensing, each CR user collects M samples of its received signal. The nth sample of the kth CR user, $1 \leq n \leq M$, $1 \leq k \leq K$, is

$$r_{k,n} = \begin{cases} \tilde{w}_{k,n}, & \mathcal{H}_I, \\ s_{k,n} + \tilde{w}_{k,n}, & \mathcal{H}_B, \end{cases} \tag{5.1}$$

where $s_{k,n}$ denotes the received sample of licensed user signal and $\tilde{w}_{k,n}$ denotes the AWGN at the CR user; $\mathcal{H}_I$ and $\mathcal{H}_B$ denote the hypotheses corresponding to the absence and presence of the licensed user signal, respectively. Thus the received signal vector at the kth CR user can be denoted as $\mathbf{r}_k = [r_{k,1}, r_{k,2}, ..., r_{k,M}]^{\mathrm{T}}$.

CR users are not required to make local decisions in cooperative spectrum sensing since the combining node will finally make a decision. Therefore, the goal of local spectrum sensing at each CR user is generally to provide the combining node some indication on the likelihood between the two hypotheses, $\mathcal{H}_I$ and $\mathcal{H}_B$, from the observation. Sending the received signal vector, $\mathbf{r}_k$, without further processing is one basic option for the kth CR user to provide its local information. However, the common control channel for communication between CR users and the combining node is usually bandwidth constrained when idle communication channels in licensed spectrum have not been identified. Therefore, bandwidth-efficient transmission of local sensing data is desired.

Denote $Q_k(\cdot)$ as a general processing function at the kth CR user. The corresponding processed sensing data,

$$q_k = Q_k(\mathbf{r}_k), \tag{5.2}$$

will be sent by the user to the combining node, where q_k is in general a vector but we use the scalar version for bandwidth efficiency purpose throughout the chapter.

5.1.2 Combination for Cooperative Spectrum Sensing

In cooperative spectrum sensing, CR users report to the combining node through the common control channel. According to the sensing data collected from these users, the combining node decides between the two hypotheses in (5.1) based on its combination strategy. Figure 5.1 gives a general schematic representation for combination of sensing data in cooperative spectrum sensing. As shown in this figure, among the K cooperative CR users, the kth CR user, $1 \leq k \leq K$, independently obtains the signal vector, $\mathbf{r}_k$, and sends the processed sensing data, q_k, to the combining node through the common control channel.

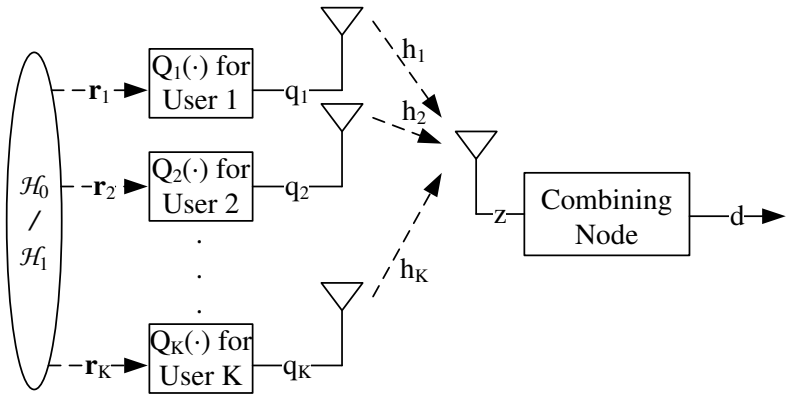

Figure 5.1. Reporting in cooperative spectrum sensing.

Upon receiving the combined sensing data, z, from all the CR users, the combining node makes a decision, d, on the absence or presence of the licensed user signal.

To separate the sensing data from different users, orthogonal channels, such as different time slots in *time division multiple access* (TDMA), frequency bands in *frequency division multiple access* (FDMA), and codes in *code division multiple access* (CDMA), are commonly used for reporting. Thus the received sensing data at the combining node can be expressed as

$$z = [h_1 q_1 + w_1, h_2 q_2 + w_2, ..., h_K q_K + w_K]^T, \tag{5.3}$$

where h_k is the reporting channel gain between the kth CR user and the combining node as shown in Figure 5.1, and w_k is the corresponding zero-mean AWGN at the combining node while reporting q_k. The total channel use is of $O(K)$, which, as the number of cooperative CR users increases, may not satisfy the stringent bandwidth constraint of the common control channel in this environment.

In this chapter, we focus on a novel approach that CR users simultaneously report the processed sensing data through the common control channel so that the combining node receives the superposition of all the data. Although such an approach is not preferred in general wireless communications, it intuitively works in cooperative spectrum sensing since the data from all the CR users are related to the same phenomenon, i.e., on the absence or presence of the licensed user signal. Under this approach, the received sensing data at

the combining node is

$$z = \sum_{k=1}^{K} h_k q_k + w, \tag{5.4}$$

where w is the zero-mean AWGN at the combining node. This approach is much more bandwidth-efficient because only one unit of bandwidth resource is required for reporting regardless of the number of cooperative users.

5.2 Optimal Design with Gaussian Reporting Channel

With the help of Bayesian criterion [93], we will design the local processing functions, $Q_k(\cdot)$, and the global decision rule so as to minimize the average Bayesian cost in (4.2).

5.2.1 General Principle

When the reporting channel is Gaussian, (5.4) can be rewritten as

$$z = \sum_{k=1}^{K} q_k + w, \tag{5.5}$$

where we let $h_k = 1$ for $1 \leq k \leq K$ without loss of generality.

Before considering the optimal design of the local processing functions and the global decision rule in this case, we first take a look at the situation if the combining node knows the received signal vectors at all the CR users. To minimize the average cost in (4.2), the optimal decision rule is given in [93] as

$$\frac{f(\mathbf{r}_1, \mathbf{r}_2, ..., \mathbf{r}_K|\mathcal{H}_B)}{f(\mathbf{r}_1, \mathbf{r}_2, ..., \mathbf{r}_K|\mathcal{H}_I)} \underset{\mathcal{H}_I}{\overset{\mathcal{H}_B}{\gtrless}} \frac{P_I C_F}{P_B C_M}, \tag{5.6}$$

where $f(\mathbf{r}_1, \mathbf{r}_2, ..., \mathbf{r}_K|\mathcal{H}_i)$ is the joint PDF of $\mathbf{r}_1, \mathbf{r}_2, ..., \mathbf{r}_K$ under hypothesis $\mathcal{H}_i$ for $i = 0, 1$. Since different CR users independently obtain the sensing data, we further assume

$$f(\mathbf{r}_1, \mathbf{r}_2, ..., \mathbf{r}_K|\mathcal{H}_i) = \prod_{k=1}^{K} f(\mathbf{r}_k|\mathcal{H}_i), \tag{5.7}$$

where $f(\mathbf{r}_k|\mathcal{H}_i)$ is the PDF of $\mathbf{r}_k$ under hypothesis $\mathcal{H}_i$.

Enlightened by the above, if we design the local processing function as

$$q_k = Q_k(\mathbf{r}_k) = \log \frac{f(\mathbf{r}_k|\mathcal{H}_B)}{f(\mathbf{r}_k|\mathcal{H}_I)}, \tag{5.8}$$

where q_k is a real-valued scalar, which will be sent by the kth CR user without quantization, the superposition of all the scalars, $\sum_{k=1}^{K} q_k$, will automatically become the logarithm of the test statistic in (5.6). Therefore, the global decision rule

$$d = \begin{cases} \mathcal{H}_I, & z < \log \frac{P_I C_F}{P_B C_M}, \\ \mathcal{H}_B, & z \geq \log \frac{P_I C_F}{P_B C_M} \end{cases} \tag{5.9}$$

is obviously optimal if there is no noise term in (5.5). If the channel noise exists, the unquantized transmission of q_k expressed in (5.8) is still asymptotically optimal under individual power constraint as has been proved in [95].

5.2.2 Probabilistic Information

The problem remaining is how each CR user computes its processed sensing data with its observation, i.e., to calculate $f(\mathbf{r}_k|\mathcal{H}_i)$ given $\mathbf{r}_k$. Note that although different CR users will send local sensing data at the same time, they may collect local observations at different moments since it is possible that they have different local spectrum sensing schedules. In other words, local observations from different users may reflect the status of the licensed spectrum band at different times prior to the combining moment.

We allow such reporting latencies and assume that the received signal vector of the kth CR user, $\mathbf{r}_k$, is acquired at t_k and the final combination is to be made at t. Therefore, $\mathcal{H}_I$ and $\mathcal{H}_B$ are, strictly speaking, the hypotheses corresponding to the absence and presence of the licensed user signal at the specific time t, respectively, as we have discussed in the previous chapter.

According to the Bayes' theorem [84], $f(\mathbf{r}_k|\mathcal{H}_i)$ can be expressed as

$$f(\mathbf{r}_k|\mathcal{H}_i) = f(\mathbf{r}_k|I_k)P(I_k|\mathcal{H}_i) + f(\mathbf{r}_k|B_k)P(B_k|\mathcal{H}_i), \tag{5.10}$$

where I_k and B_k denote that the licensed user signal is absent and present at t_k, and $P(I_k|\mathcal{H}_i)$ and $P(B_k|\mathcal{H}_i)$ are correspondingly the conditional probabilities that the licensed user signal is absent and present at t_k under $\mathcal{H}_i$, respectively.

We can model the occupancy of the licensed spectrum band as a renewal process alternating between busy and idle states [84, 31], which correspond to that the band is occupied and unoccupied by licensed users, respectively. We further assume the busy and idle periods to be exponentially distributed with PDFs $f_B(t) = \alpha e^{-\alpha t}$ and $f_I(t) = \beta e^{-\beta t}$ respectively, where α is the transition rate from busy to idle state, and β is the transition rate from idle to busy state, both of which can be estimated with statistical methods [31]. Therefore, the prior probabilities of the licensed spectrum band status can be obtained as $P_B = \frac{\beta}{\alpha+\beta}$ and $P_I = \frac{\alpha}{\alpha+\beta}$. With the help of age distribution of renewal process and memoryless property of exponential distribution, we obtain $P(B_k|\mathcal{H}_B)$ and $P(I_k|\mathcal{H}_I)$ in (4.6) and (4.7). And $P(B_k|\mathcal{H}_I)$ and $P(I_k|\mathcal{H}_B)$ can be further obtained.

Without prior knowledge on licensed user signal distribution, we assume that $s_{k,n}$ is Gaussian distributed with zero mean and variance σ_k^2. Meanwhile, we assume $\tilde{w}_{k,n}$ is with unit variance without loss of generality. According to (5.1),

$$r_{k,n} \sim \begin{cases} \mathcal{N}(0,1), & I_k, \\ \mathcal{N}(0,1+\sigma_k^2), & B_k. \end{cases} \tag{5.11}$$

Given that the samples of any CR user are independent, the conditional PDFs $f(\mathbf{r}_k|I_k)$ and $f(\mathbf{r}_k|B_k)$ in (5.10) are

$$\begin{aligned} f(\mathbf{r}_k|I_k) &= \prod_{n=1}^{M} \frac{1}{\sqrt{2\pi}} \exp\left(-\frac{r_{k,n}^2}{2}\right) \\ &= \left(\frac{1}{\sqrt{2\pi}}\right)^M \exp\left(-\frac{\sum_{n=1}^{M} r_{k,n}^2}{2}\right) \end{aligned} \tag{5.12}$$

and

$$\begin{aligned} f(\mathbf{r}_k|B_k) &= \prod_{n=1}^{M} \frac{1}{\sqrt{2\pi(1+\sigma_k^2)}} \exp\left(-\frac{r_{k,n}^2}{2(1+\sigma_k^2)}\right) \\ &= \left(\frac{1}{\sqrt{2\pi(1+\sigma_k^2)}}\right)^M \exp\left(-\frac{\sum_{n=1}^{M} r_{k,n}^2}{2(1+\sigma_k^2)}\right). \end{aligned} \tag{5.13}$$

Note that the observed energy of the kth CR user, y_k, can be calculated as the inner product

of its received signal vector, i.e.,

$$y_k = \mathbf{r}_k^{\mathrm{T}} \mathbf{r}_k = \sum_{n=1}^{M} r_{k,n}^2. \tag{5.14}$$

From (5.12) and (5.13), the observed energy is sufficient to compute those conditional PDFs. Therefore, energy detection [85] can be directly applied to the proposed approach in this case, which will also be used in another case subsequently.

With (5.10), (4.6), (4.7), (5.12), and (5.13), we can further obtain the likelihood ratio in (5.8) and the hypothesis test in (5.9) can be applied with a final decision on whether the licensed user signal is present or not.

5.2.3 Practical Considerations

It is obvious from (5.8) that each CR user is able to independently compute and send its processed sensing data without information exchange with other CR users. At the combining node, the global decision rule can be easily realized by directly comparing the received scalar with a predetermined threshold according to (5.9).

Although all the reporting channel gains are assumed to be 1, they can be compensated at individual users if known. Then the above scheme can be applied in the same way. These channel gains may be estimated over the reverse links if the combining node periodically feeds back its final decisions using the same control channel. However, if a certain channel gain is too small, the corresponding user may be required to report with very large power. In this case, the user should report nothing to save energy, which will not affect the decision process in (5.9).

5.3 Optimal Design with Fading Reporting Channel

When the reporting channel experiences fading and instant channel gains are unknown, the superposition of scalars in the above approach will no longer work as a proper test statistic due to unknown random phases of individual channel paths. Making the final decision at the combining node according to the received amplitude will be ineffective. However, we

may retain the bandwidth benefit with the proposed superposition approach by modifying the local processing functions and relating the global decision rule to the received power instead.

5.3.1 General Principle

We model the reporting channel between the kth CR user and the combining node to be Rayleigh fading with h_k being i.i.d. complex Gaussian with zero mean and unit variance.

Since a general optimal form of the local processing function, $Q_k(\cdot)$, is intractable, we consider specifying it as a quantizer with the following form:

$$q_k = Q_k(\mathbf{r}_k) = \begin{cases} A_0, & l_k < T_{k,1}, \\ A_1, & T_{k,1} \le l_k < T_{k,2}, \\ \vdots & \\ A_{L_k-1}, & l_k \ge T_{k,L_k-1}, \end{cases} \tag{5.15}$$

where

$$l_k = \frac{f(y_k|\mathcal{H}_B)}{f(y_k|\mathcal{H}_I)} \tag{5.16}$$

and q_k takes one of L_k possible values with the quantization regions divided by $L_k - 1$ thresholds, $T_{k,1}$, $T_{k,2}$, ..., and T_{k,L_k-1}, which can be further determined to achieve the optimal performance. Because of the one-to-one correspondence between the local likelihood ration l_k and the observed energy y_k, the quantization region for A_i can be transformed to $\{y_k : y_k \in R_{k,A_i}\}$.

As we have discussed, it is proper in this case to make the final decision based on the received power of z in (5.4). To be specific, the following threshold test is applied at the combining node,

$$d = \begin{cases} \mathcal{H}_I, & |z|^2 < \varsigma, \\ \mathcal{H}_B, & |z|^2 \ge \varsigma, \end{cases} \tag{5.17}$$

where the threshold ς can be further determined to achieve the optimal performance.

5.3.2 Threshold Optimization

In the following, we study how to determine the optimal thresholds for both the local processing functions in (5.15) and the final decision rule in (5.17) to minimize the average Bayesian cost defined in (4.2). According to the proof in the Appendix C, we can rewrite the cost as

$$C = \sum_{A_i} \int_{R_{j,A_i}} \left(K_{F_{j,A_i}} f(y_j|\mathcal{H}_I) + K_{M_{j,A_i}} f(y_j|\mathcal{H}_B) \right) dy_j, \tag{5.18}$$

where

$$K_{F_{j,A_i}} = \sum_{q_1,q_2,...,q_{j-1},q_{j+1},...,q_K} C_F \int_{\varsigma}^{\infty} f(|z|^2|q_1, q_2, ..., q_{j-1}, q_j = A_i, q_{j+1}, ..., q_K) d|z|^2 \cdot \prod_{k=1,k\neq j}^{K} \int_{R_{k,q_k}} f(y_k|\mathcal{H}_I) dy_k P_I \tag{5.19}$$

and

$$K_{M_{j,A_i}} = \sum_{q_1,q_2,...,q_{j-1},q_{j+1},...,q_K} C_M \int_{0}^{\varsigma} f(|z|^2|q_1, q_2, ..., q_{j-1}, q_j = A_i, q_{j+1}, ..., q_K) d|z|^2 \cdot \prod_{k=1,k\neq j}^{K} \int_{R_{k,q_k}} f(y_k|\mathcal{H}_B) dy_k P_B. \tag{5.20}$$

With the local processing functions of all the other users fixed, we can obtain the optimal quantization region for the jth CR user from the above as

$$R_{j,A_i} = \{y_j : K_{F_{j,A_i}} f(y_j|\mathcal{H}_I) + K_{M_{j,A_i}} f(y_j|\mathcal{H}_B) \leq K_{F_{j,A_{i'}}} f(y_j|\mathcal{H}_I) + K_{M_{j,A_{i'}}} f(y_j|\mathcal{H}_B), i' \neq i\}. \tag{5.21}$$

According to the connectivity of the quantization regions and using the method given in [96], we can find the optimal threshold for the jth CR user efficiently.

From [97], at the combining node, the optimal decision rule to minimize the average Bayesian cost is

$$\frac{f(|z|^2|\mathcal{H}_B)}{f(|z|^2|\mathcal{H}_I)} \underset{\mathcal{H}_I}{\overset{\mathcal{H}_B}{\gtrless}} \frac{P_I C_F}{P_B C_M}, \tag{5.22}$$

the threshold of which can be easily converted to ς with respect to $|z|^2$ in (5.17).

Therefore, we can optimize the thresholds for all the CR users and the combining node iteratively. Since we fix the local processing functions of all the other users and the final

decision rule to obtain the optimal processing function for the jth CR user, the optimality of any local processing function with the rest fixed is the necessary condition for the optimality of the system. Similarly, since we fix the local processing functions of all the users to obtain the final decision rule, the optimality of the final decision rule with all the local processing function fixed is the necessary condition for the optimality of the system. We design the following iterative algorithm to find the person-by-person optimal solution of the thresholds:

1. Initialize the quantization regions for all the local processing functions.
2. Find the optimal threshold with the decision rule in (5.22).
3. For $k = 1$ to K, find the optimal quantization regions for local processing function $Q_k(\cdot)$ according to (5.21) and using the method given in [96] with all the other local processing functions fixed.
4. Repeat from Step 2 until the Bayesian cost in (5.18) converges.

Note that the Bayesian cost decreases after each iteration and is bounded by zero. Thus the above algorithm always converges.

5.3.3 Probabilistic Information

To realize the above approach, each CR user needs to compute the involved probabilistic information, among which $f(y_k|\mathcal{H}_i)$ can be calculated using the same method introduced in the previous section allowing reporting latency with

$$f(y_k|\mathcal{H}_i) = f(y_k|I_k)P(I_k|\mathcal{H}_i) + f(y_k|B_k)P(B_k|\mathcal{H}_i). \tag{5.23}$$

Note that y_k is the observed energy of the kth CR user, which follows a central chi-square distribution with M degrees of freedom given I_k according to (5.11). Similarly, its value divided by $(1 + \sigma_k^2)$ follows the same distribution given B_k. To be specific,

$$f(y_k|I_k) = \frac{(\frac{1}{2})^{\frac{M}{2}}}{\Gamma(\frac{M}{2})} y_k^{\frac{M}{2}-1} e^{-\frac{1}{2}y_k} \tag{5.24}$$

and

$$f(y_k|B_k) = \frac{1}{1+\sigma_k^2}\frac{(\frac{1}{2})^{\frac{M}{2}}}{\Gamma(\frac{M}{2})}(\frac{y_k}{1+\sigma_k^2})^{\frac{M}{2}-1}e^{-\frac{1}{2}\frac{y_k}{1+\sigma_k^2}}, \tag{5.25}$$

where $\Gamma(\cdot)$ denotes the gamma function that $\Gamma(x) = \int_0^\infty t^{x-1}e^{-t}dt$.

Furthermore, we have

$$f(|z|^2|\mathcal{H}_i) = \sum_{q_1,q_2,...,q_K} f(|z|^2|q_1,q_2,...,q_K)P(q_1,q_2,...,q_K|\mathcal{H}_i). \tag{5.26}$$

According to our model, the conditional distribution of z in (5.4) given $q_1, q_2, ..., q_K$ is complex Gaussian with zero mean and variance $\sum_{k=1}^K q_k^2 + \sigma^2$, where σ^2 is the variance of w. Thus the conditional distribution of $|z|^2$ is exponential with PDF

$$f(|z|^2|q_1,q_2,...,q_K) = \frac{1}{\sum_{k=1}^K q_k^2+\sigma^2}\exp\left(\frac{-|z|^2}{\sum_{k=1}^K q_k^2+\sigma^2}\right). \tag{5.27}$$

Meanwhile,

$$P(q_1,q_2,...,q_K|\mathcal{H}_i) = \prod_{k=1}^K \int_{R_{k,q_k}} f(y_k|\mathcal{H}_i)dy_k \tag{5.28}$$

as we have already derived.

Based on these probabilities, we can obtain the local processing functions in (5.15) and the final decision rule in (5.17) with the optimal thresholds.

5.3.4 Performance Analysis

To obtain the detection performance of the above cooperative spectrum sensing scheme, we define the local probability of quantizer output A_m under $\mathcal{H}_B$ and $\mathcal{H}_I$ as

$$p_{1,k}^{(A_m)} = \int_{R_{k,A_m}} f(y_k|H_B)dy_k \tag{5.29}$$

and

$$p_{0,k}^{(A_m)} = \int_{R_{k,A_m}} f(y_k|H_I)dy_k, \tag{5.30}$$

respectively. The conditional PDF of $|z|^2$ can be easily determined and the overall detection error probabilities are

$$P_M = \Pr\{d=\mathcal{H}_I|\mathcal{H}_B\} = 1 - \sum_{q_1,q_2,...,q_K}\prod_{k=0}^K p_{1,k}^{(q_k)}\exp(-\frac{S}{\sum_{k=0}^K q_k^2+\sigma^2}) \tag{5.31}$$

and

$$P_F = \Pr\{d = \mathcal{H}_B | \mathcal{H}_I\} = \sum_{q_1, q_2, \ldots, q_K} \prod_{k=0}^{K} p_{0,k}^{(q_k)} \exp(-\frac{\varsigma}{\sum_{k=0}^{K} q_k^2 + \sigma^2}), \tag{5.32}$$

respectively. Then the Bayesian cost in (4.2) can be further determined.

If there are only two quantization levels, i.e., $L_k = 2$ in (5.15), the quantizer will simply be

$$q_k = Q_k(\mathbf{r}_k) = \begin{cases} 0, & l_k < T, \\ A, & l_k \geq T, \end{cases} \tag{5.33}$$

which is equivalent to one-bit hard decision made at the kth CR user. Note that we let $A_0 = 0$ and $A_1 = A$ so that the user will not send anything when l_k is below the local threshold T to save energy. Meanwhile, if each CR user is identical with the same error probabilities, denoted as $p_m = p_{m,k} = p_{1,k}^{(0)}$ and $p_f = p_{f,k} = p_{0,k}^{(A)}$ for $1 \leq k \leq K$, respectively, the detection error probabilities can be simplified as

$$P_M = 1 - \sum_{k=0}^{K} \binom{K}{k} (1 - p_m)^k (p_m)^{K-k} \exp(-\frac{\varsigma}{kA^2 + \sigma^2}) \tag{5.34}$$

and

$$P_F = \sum_{k=0}^{K} \binom{K}{k} (p_f)^k (1 - p_f)^{K-k} \exp(-\frac{\varsigma}{kA^2 + \sigma^2}). \tag{5.35}$$

Note that the symmetry allows a much simpler realization of optimal quantization at each user and decision making at the combining node. However, the performance will be affected if cooperative CR users are not identical as we have described due to different received licensed user signal powers at individual users or different local spectrum sensing schedules.

5.3.5 Practical Considerations

Although the proposed algorithm requires a certain number of iterations to reach the optimal thresholds for the local processing functions and the final decision rule, real time computation is not necessary since it is not based on the local observations. In other worlds, the thresholds can be predetermined and each CR user is able to independently compute and send the processed sensing data.

In practice, the output of each local processing function can be transmitted using a common waveform $v(t)$. Similarly, different pathloss factors can be compensated at individual users by properly scaling q_k.

5.4 Simulation Results

In this section, we present simulation results of the proposed approach, through which we assume independent observations across the CR users and let $C_F = 1$, $C_M = 2$, and $\alpha = \beta = 0.5$ sec^{-1}, i.e., $P_I = P_B = \frac{1}{2}$.

False alarm and mis-detection probabilities as well as Bayesian costs with respect to different relative reporting SNRs, defined as K/σ^2, where σ^2 is the noise variance at the combining node as we mentioned previously, with the reporting scheme proposed in Section 5.2 under Gaussian reporting channel are shown in Figure 5.2. In our simulation, $M = 10$, $\sigma_k^2 = 1$ for $1 \leq k \leq K$, and the latency between any individual observation and the final combination is uniformly distributed within [0 0.1] sec. The test threshold for making the final decision can be determined as $\frac{1}{2}$ according to (5.9). From the detection performance curves with different number of users, we can see clearly that cooperation greatly enhances the detection performance. We also notice that the detection performance does not change significantly once the relative reporting SNR exceeds 10 dB, which indicates that we can use the proposed reporting scheme as long as the CR users maintain proper received signal power at the combining node while reporting. The floor of the detection performance is mainly related to the number of samples collected in local spectrum sensing, M, and the reporting latency. Bayesian costs with respect to different number of samples collected in local spectrum sensing with and without reporting latency when the relative reporting SNR is 30 dB are shown in Figure 5.3, from which we observe that the floor of the Bayesian cost tends to be 0 as M increases when there is no latency between any individual observation and the final combination.

Bayesian costs with respect to different relative reporting SNRs at the combining node

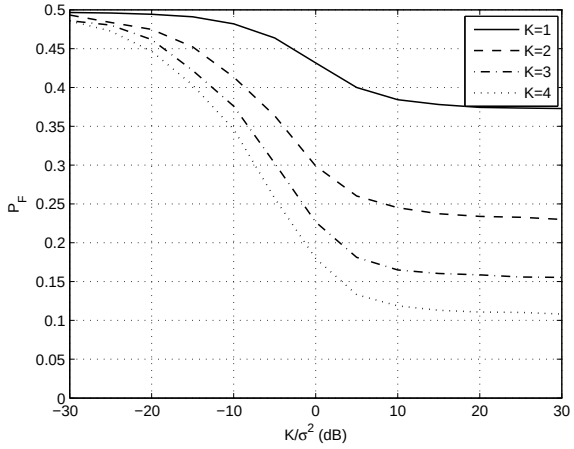

(a) False alarm

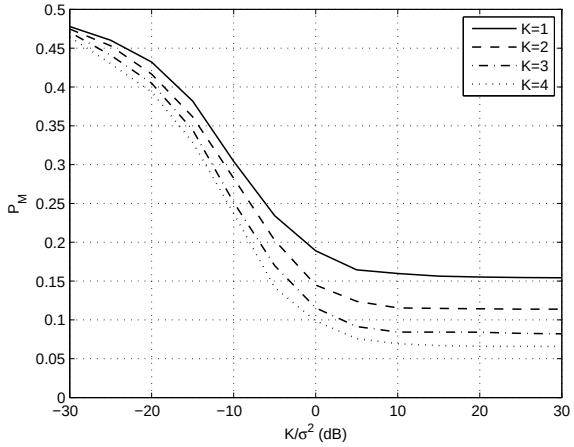

(b) Mis-detection

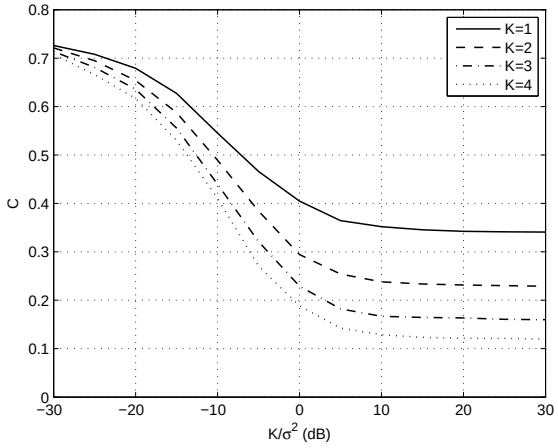

(c) Bayesian cost

Figure 5.2. Performance curves under Gaussian reporting channel with different relative reporting SNRs.

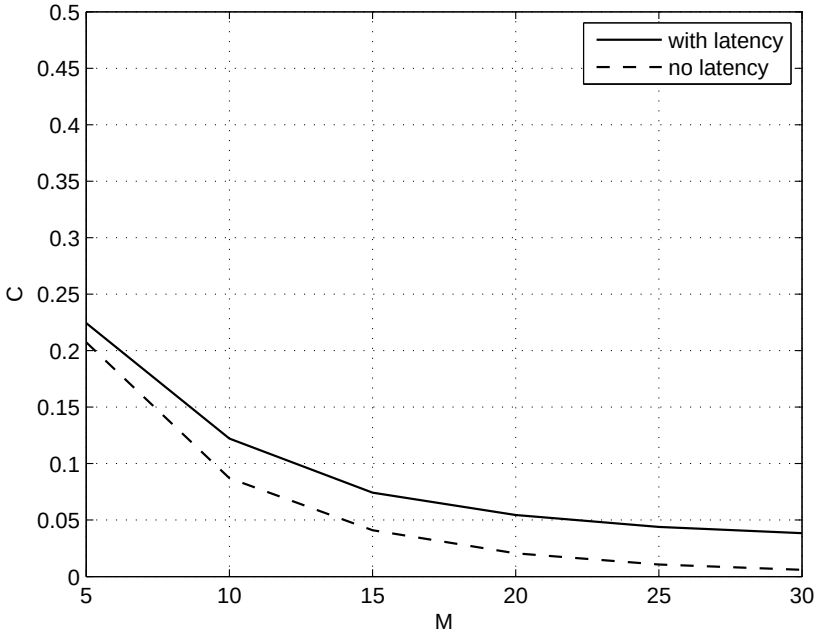

Figure 5.3. Bayesian cost under Gaussian reporting channel with different numbers of samples collected in local spectrum sensing.

with the reporting scheme proposed in Section 5.3 when the reporting channel experiences fading are shown in Figure 5.4. In our simulation, $M = 10$ and each CR user uses 4 quantization levels: $A_0 = 0$, $A_1 = 0.1$, $A_2 = 1$, and $A_3 = 10$. The latency between any individual observation and the final combination is 0. Optimal thresholds for quantization can be found with the proposed algorithm, which converges in less than 10 iterations in the simulation. We also observe that it may not always be optimal to use all the available quantization levels. From the detection performance curves with different number of users, we can see clearly that cooperation enhances the detection performance. The detection performance does not change significantly when the relative reporting SNR exceeds 10 dB, so proper transmit power is also necessary for reporting under fading channel as in the previous case under Gaussian reporting channel. By comparing the detection performance curves with different received licensed user signal powers at individual CR users, σ_k^2, we verify that cooperative spectrum sensing provides higher performance gain when

sensing SNRs, defined as σ_k^2 divided by the variance of Gaussian noise at the corresponding individual user, are low. In contrast, a few cooperative CR users would be enough to achieve similar detection performance as achieved by even more users when sensing SNRs at individual CR users are high. Bayesian costs with respect to different sensing SNRs and number of samples collected in local spectrum sensing when the relative reporting SNR is 30 dB in this case are given in Figure 5.5, from which we observe that the floor of the Bayesian cost tends to be 0 as σ_k^2 and M increase.

The complementary *receiver operating characteristic* (ROC) curves of the reporting scheme proposed in Section 5.3, the type-based distributed detection scheme [49] and the censoring scheme [47] when the reporting channel experiences fading are shown in Figure 5.6. In our simulation, there are 4 CR users, each with 2 quantization levels, $A_0 = 0$ and $A_1 = 1$, and $p_{m,1} = 0.05$, $p_{m,2} = 0.1$, $p_{m,3} = 0.15$, $p_{m,4} = 0.2$ with $p_{f,1} = p_{f,2} = p_{f,3} = p_{f,4} = 0.1$ for comparison purpose. The noise variance at the combining node is fixed at 0.2. In the type-based distributed detection scheme, two waveforms are needed to map the two quantization levels, which consumes twice the reporting bandwidth of the proposed scheme. In the censoring scheme, one waveform is used to map the result of the CR user with the highest received licensed user SNR, which requires the same reporting bandwidth but additional overhead for coordination. The overall transmit powers are set to be equal for different schemes. We can notice the performance improvement through the proposed scheme compared with the censoring scheme. Although the performance of the type-based scheme is slightly better than that of the proposed scheme, the former consumes more bandwidth resource and is not preferred in certain bandwidth constrained cases.

5.5 Conclusion

In this chapter, bandwidth-efficient reporting for cooperative spectrum sensing in a multi-user CR network is addressed. A general approach has been proposed that CR users simultaneously report individual sensing information to a combining node through the common

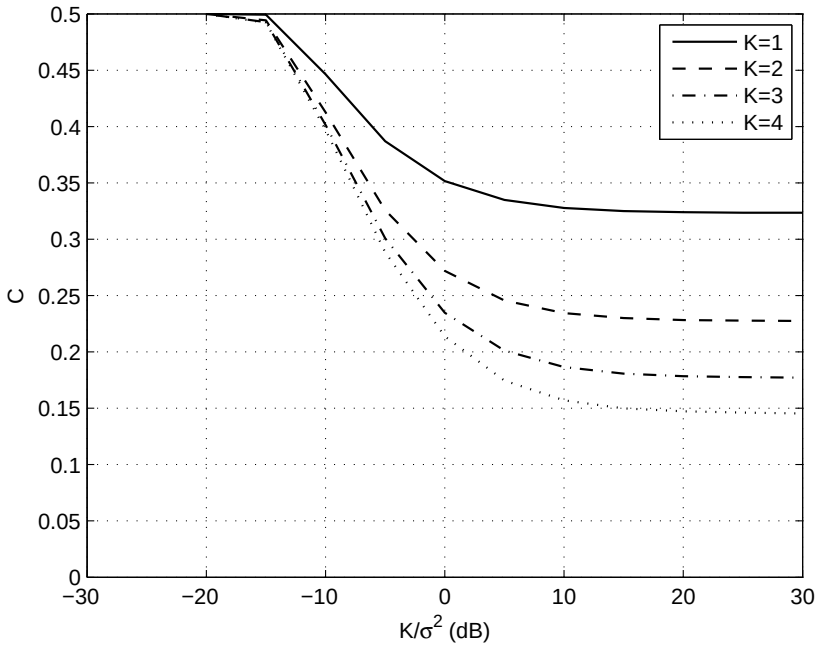

(a) Bayesian cost with $\sigma_k^2 = 1$ for $1 \leq k \leq K$

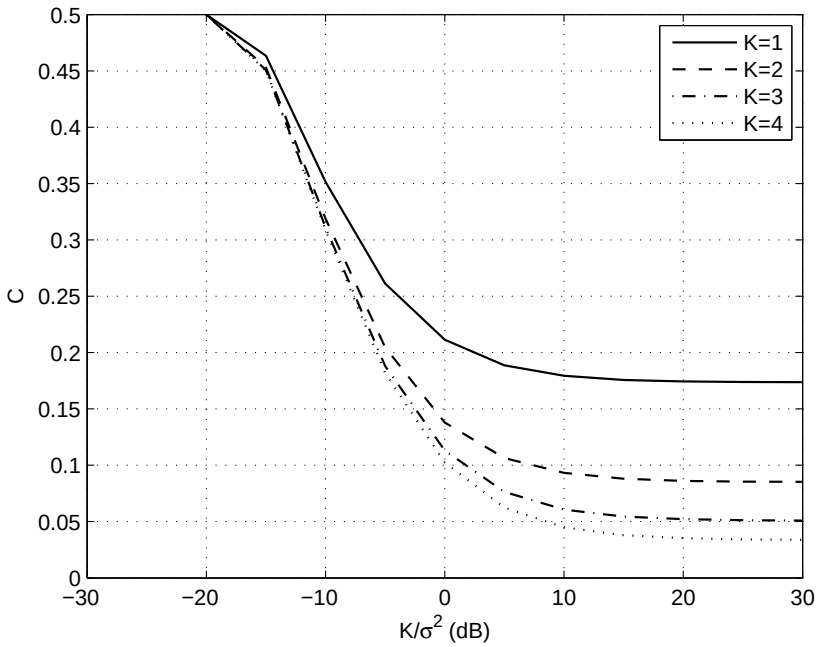

(b) Bayesian cost with $\sigma_k^2 = 2$ for $1 \leq k \leq K$

Figure 5.4. Performance curves under fading reporting channel with different relative reporting SNRs.

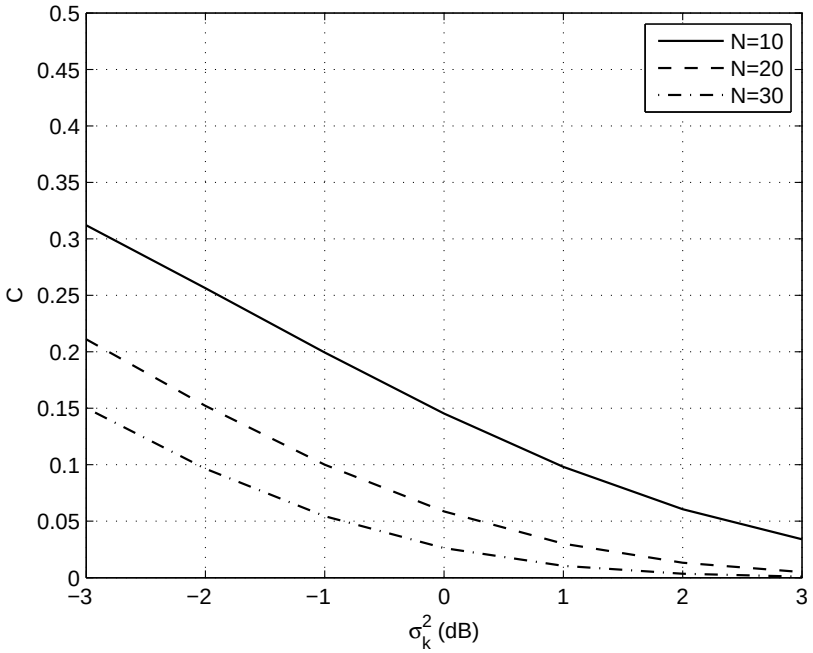

Figure 5.5. Bayesian cost under fading reporting channel with different sensing SNRs.

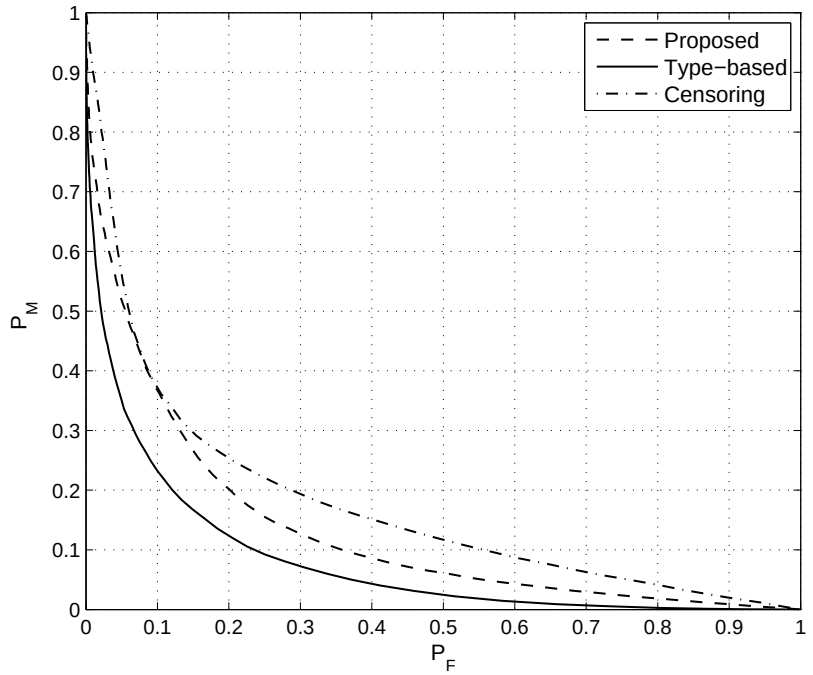

Figure 5.6. Complementary ROC curves under fading reporting channel with different reporting schemes.

control channel. The optimal design of local processing functions at the CR users and final decision rule at the combining node has been discussed based on Bayesian criterion when the reporting channel is Gaussian and experiences fading, respectively. Calculation of probabilistic information involved in our design has been given as well. In the proposed approach, the bandwidth required for reporting does not change with the number of cooperative users. Given proper preprocessing at individual users, our design maintains reasonable performance with the superposition of sensing data at the combining node. Simulation results have been shown to demonstrate the effectiveness of the proposed approach.

CHAPTER 6

SPECTRUM SHAPING FOR OFDM-BASED COGNITIVE RADIO SYSTEMS

In the previous chapters, we have focused on efficient spectrum sensing techniques for CR to determine the availability of licensed spectrum bands. After identifying the idle spectrum bands, CR users can utilize these bands for secondary communication. OFDM has been proposed as a candidate transmission technique for CR. By dividing a frequency band into orthogonal subcarriers, OFDM has its potential flexibility to fill spectrum gaps. With OFDMA, CR users are able to utilize non-adjacent spectrum bands of variable bandwidths with dynamic spectrum aggregation. However, OFDM signals exhibit relatively high power spectral sidelobes, which may bring severe OOB interference. Therefore, spectrum shaping that suppresses the OFDM signal sidelobes becomes necessary.

To enhance the bandwidth efficiency of OFDM-based CR systems and limit possible interference, we study in this chapter efficient spectrum shaping schemes based on spectral precoding. We first propose a low-complexity scheme that maps antipodal symbol pairs onto adjacent subcarriers at the edges of the utilized subbands. Sidelobe suppression and system throughput can be flexibly balanced. Moreover, power control on different sets of subcarriers further lowers the sidelobes. We also propose a spectral precoding scheme for multiple OFDM-based CR users to reduce OOB emission. By constructing individual precoders to render spectrum nulls, the proposed scheme ensures user independence and provides sufficient OOB radiation suppression with low complexity and no BER performance loss. To further increase the bandwidth efficiency, we also consider the selection of notched frequencies.

The rest of this chapter is organized as follows. In Section 6.1, we introduce the system model of OFDM spectral precoding. Then we present the proposed low-complexity spectrum shaping scheme and discuss its performance in Section 6.2. Next, in Section 6.3,

we develop the multi-user spectral precoding scheme and demonstrate its performance. Finally, we conclude this chapter in Section 6.4.

6.1 System Model

We consider an OFDM-based CR user utilizing a frequency band identified as unoccupied by any licensed user through spectrum sensing. The baseband OFDM signal during one symbol duration can be expressed as

$$s(t) = I(t) \sum_{n \in \mathcal{N}} d_n e^{j2\pi \frac{n}{T_s} t}, \tag{6.1}$$

where $\mathcal{N}$ is the set of the utilized subcarriers, either continuous or discontinuous in the frequency domain, with $|\mathcal{N}| = N_u$, d_n is the transmitted symbol over the nth subcarrier, T_s is the effective symbol duration, and $I(t)$ is an indicator function such that

$$I(t) = \begin{cases} 1, & -T_g \leq t \leq T_s, \\ 0, & \text{otherwise} \end{cases} \tag{6.2}$$

when a guard interval of cyclic prefix with length T_g is inserted.

The Fourier transform of $s(t)$ can be expressed as

$$S(f) = \sum_{n \in \mathcal{N}} d_n a_n(f) \tag{6.3}$$

with

$$a_n(f) = T e^{-j\pi(T_s - T_g)(f - \frac{n}{T_s})} \text{sinc}(\pi T(f - \frac{n}{T_s})), \tag{6.4}$$

where $T = T_s + T_g$ is the symbol duration and $\text{sinc}(x) = \sin(x)/x$.

The PSD of the OFDM signal is therefore

$$P(f) = \frac{1}{T} E\{|S(f)|^2\} = \frac{1}{T} \mathbf{a}^T(f) E\{\mathbf{d}\mathbf{d}^H\} \mathbf{a}^*(f), \tag{6.5}$$

where $\mathbf{a}(f) = (a_{n_0}(f), a_{n_1}(f), ..., a_{n_{N_u-1}}(f))^T$ and $\mathbf{d} = (d_{n_0}, d_{n_1}, ..., d_{n_{N_u-1}})^T$ with $n_i \in \mathcal{N}$ for $i \in \{0, 1, ..., N_u - 1\}$. The superscripts, T, $*$, and H, denote the transpose, conjugate transpose, and conjugate of a vector or a matrix, respectively.

To protect licensed users, guard bands may be required as shown in Figure 6.1 by deactivating subcarriers at the edges of the utilized subband [53]. In this way, the PSD of the CR signal will be under acceptable levels in the adjacent frequency bands. To further increase the bandwidth efficiency, a linear operation, which is called spectral precoding, can be applied prior to OFDM modulation instead of directly mapping information symbols onto the utilized subcarriers as shown in Figure 6.2 so that the sidelobes of the OFDM signal will roll off faster and the guard bands can be narrowed. Let $\mathbf{b} = (b_0, b_1, ..., b_{M_u-1})^T$ be a vector containing M_u information symbols that are assumed to be independent with zero mean and unit variance. In other words, $E\{\mathbf{b}\mathbf{b}^H\} = \mathbf{I}_{M_u}$, where $\mathbf{I}_{M_u}$ is an $M_u \times M_u$ identity matrix. Generally, spectral precoding can be expressed as

$$\mathbf{d} = \mathbf{G}\mathbf{b}, \tag{6.6}$$

where $\mathbf{G}$ denotes an $N_u \times M_u$ precoding matrix consisting of complex-valued precoding coefficients, $g_{n,m}$, $n \in \mathcal{N}$, $m \in \{0, 1, ..., M_u - 1\}$, lying in the nth row and the mth column. To ensure proper decoding, the utilized subcarriers is required to be no fewer than the information symbols, i.e., $N_u \geq M_u$. The coding rate of the spectral precoder is then defined as

$$\lambda_u = \frac{M_u}{N_u}. \tag{6.7}$$

Then we will have

$$P(f) = \frac{1}{T}\mathbf{a}^T(f)\mathbf{G}\mathbf{G}^H\mathbf{a}^*(f) = \frac{1}{T}\|\mathbf{G}^T\mathbf{a}(f)\|_2^2. \tag{6.8}$$

By choosing the precoding matrix, $\mathbf{G}$, carefully, we can change the shape of the PSD, $P(f)$, and therefore, reduce the power leakage to the adjacent bands that may be used by licensed users. Meanwhile, proper signal reception should be guaranteed with a decoder. Less extra complexity brought by the precoder at the transmitter and the decoder at the receiver is desired.

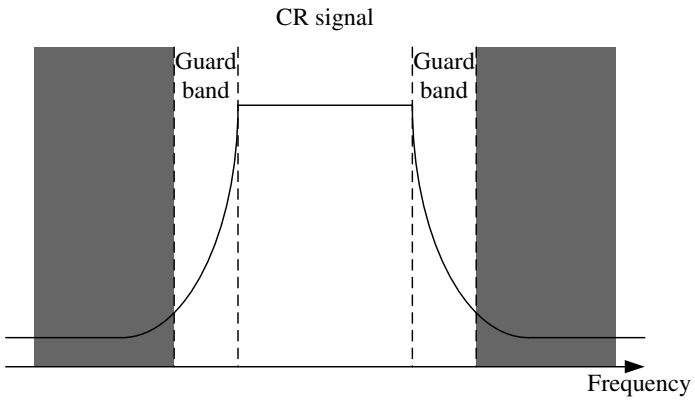

Figure 6.1. Opportunistic spectrum utilization with guard bands.

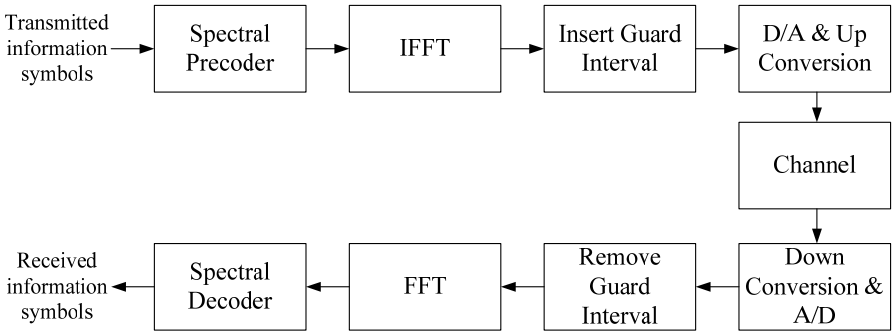

Figure 6.2. System diagram of spectrally precoded OFDM.

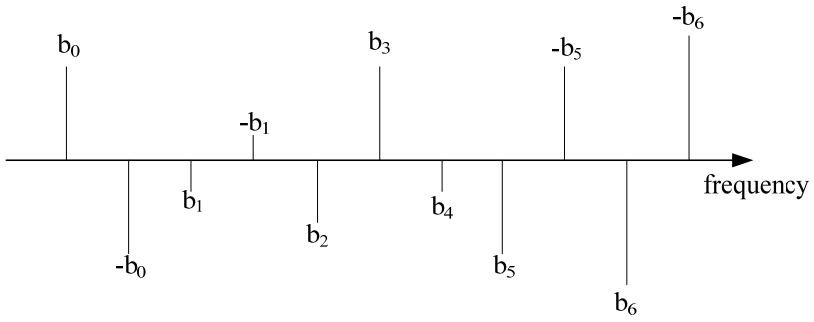

Figure 6.3. Subcarriers of the OFDM symbol with the proposed spectrum shaping scheme.

6.2 Low-Complexity Spectrum Shaping

Note that $a_n(f)$ in (6.4) may be viewed as the interference coefficient from the nth subcarrier to the frequency f. Adjacent subcarriers have similar impact factors on $S(f)$ in (6.5) at any specific frequency f as the values of the interference coefficients are close. Enlightened by the inter-carrier interference self-cancellation scheme in [65], we propose to map an antipodal symbol pair onto two adjacent subcarriers so that their contribution to the OOB interference of the OFDM signal will be mostly canceled. Meanwhile, as the subcarriers at the edges have higher impacts on $S(f)$ at the frequencies outside of the utilized subbands, it is preferable to apply such an antipodal coding scheme to the subcarriers at the edges.

6.2.1 Basic Approach

We consider one subband consisting of continuous subcarriers, i.e., $\mathcal{N} = \{0, 1, ..., N_u - 1\}$, and $N_u - M_u$ is assumed to be even. The spectrum shaping scheme can be performed as

$$d_n = \begin{cases} (-1)^n b_{\lfloor \frac{n}{2} \rfloor}, & 0 \le n \le N_u - M_u - 1, \\ b_{n - \frac{N_u - M_u}{2}}, & N_u - M_u \le n \le M_u - 1, \\ (-1)^{n - M_u} b_{\lfloor \frac{n - M_u}{2} \rfloor + \frac{3M_u - N_u}{2}}, & M_u \le n \le N_u - 1, \end{cases} \tag{6.9}$$

where $\lfloor x \rfloor$ denotes the largest integer less than or equal to x. Figure 6.3 demonstrates our spectrum shaping scheme when $M_u = 7$ and $N_u = 11$. Note that we will mainly focus on the case of $N_u \le 2M_u$ in the rest of the chapter since a relative large coding rate is preferred.

From (6.9), the corresponding precoding matrix of our scheme can be expressed as

$$\mathbf{G} = \begin{bmatrix} \mathbf{G}_e & \mathbf{0} & \mathbf{0} \\ \mathbf{0} & \mathbf{I}_{2M_u - N_u} & \mathbf{0} \\ \mathbf{0} & \mathbf{0} & \mathbf{G}_e \end{bmatrix}, \tag{6.10}$$

where

$$\mathbf{G}_e = \begin{bmatrix} 1 & & & & \\ -1 & & & & \\ & 1 & & & \\ & -1 & & & \\ & & \ddots & & \\ & & & 1 & \\ & & & -1 & \end{bmatrix}, \tag{6.11}$$

which is an $(N_u - M_u) \times (\frac{N_u - M_u}{2})$ matrix with zero entries omitted.

When the utilized subcarriers are discontinuous in the frequency domain and divided into several subbands of continuous subcarriers, the above procedure can be applied to each of the subbands. The coding rate for each subband can be different.

As will be demonstrated, the major advantage of our scheme is that it enables fast power spectral sidelobe rolling off near the edges of the utilized subbands. Therefore, the proposed spectrum shaping scheme enhances spectral compactness and ensures high bandwidth efficiency. The complexity of the precoder at the transmitter and its decoder at the receiver is very low because of the special structure, which will be discussed in detail later. After the utilized subcarriers are determined in the proposed scheme, the number of information symbols for each OFDM symbol, M_u, is a design parameter and can be adjusted to balance sidelobe suppression and system throughput. Meanwhile, there is no requirement for the number of the utilized subcarriers, N_u, to be a positive integer power of two or relatively large as in the existing spectral precoding schemes [61, 62, 63]. With both simplicity and flexibility, the proposed scheme is especially suitable for CR users opportunistically utilizing small spectrum segments.

6.2.2 Sidelobe Decaying Rate

In the following, we will analyze the power spectral sidelobe decaying rate of the OFDM signal with the proposed spectrum shaping scheme. Define $\mathcal{N}_c = \{N_u - M_u, N_u - M_u + 1, ..., M_u - 1\}$ as a set consisting of indices of subcarriers in the center of a utilized subband without antipodal coding, $\mathcal{N}_e = \{0, 1, ..., N_u - M_u - 1, M_u, M_u + 1, ..., N_u - 1\}$ as a set consisting of indices of subcarriers at the edges of the subband with antipodal coding, and $\mathcal{N}_e^{(0)} = \{0, 2, ..., N_u - M_u - 2, M_u, M_u + 2, ..., N_u - 2\}$. Then $S(f)$ in (6.3) can be expressed as

$$S(f) = \sum_{n\in\mathcal{N}_c} d_n a_n(f) + \sum_{n\in\mathcal{N}_e} d_n a_n(f) = \sum_{n\in\mathcal{N}_c} d_n a_n(f) + \sum_{n\in\mathcal{N}_e^{(0)}} d_n(a_n(f) - a_{n+1}(f)). \quad (6.12)$$

According to (6.5), the PSD of the OFDM signal can be obtained as

$$\begin{aligned} P(f) &= \frac{1}{T}E\{|S(f)|^2\} = \sum_{n\in\mathcal{N}_c} T\left[e^{-j\pi(T_s-T_g)(f-\frac{n}{T_s})}\mathrm{sinc}(\pi T(f-\frac{n}{T_s}))\right]^2 \\ &+ \sum_{n\in\mathcal{N}_e^{(0)}} T\left[e^{-j\pi(T_s-T_g)(f-\frac{n}{T_s})}\left(\mathrm{sinc}(\pi T(f-\frac{n}{T_s})) - e^{j\pi\frac{T_s-T_g}{T_s}}\mathrm{sinc}(\pi T(f-\frac{n+1}{T_s}))\right)\right]^2. \quad (6.13) \end{aligned}$$

If there is no guard interval, i.e., $T_g = 0$ and $T = T_s$, we will have

$$P(f) = \sum_{n\in\mathcal{N}_c} \frac{e^{-j2\pi T_s f}\sin^2(\pi T_s f)}{\pi^2 T_s\left(f-\frac{n}{T_s}\right)^2} + \sum_{n\in\mathcal{N}_e^{(0)}} \frac{e^{-j2\pi T_s f}\sin^2(\pi T_s f)}{\pi^2 T_s^3\left(f-\frac{n}{T_s}\right)^2\left(f-\frac{n+1}{T_s}\right)^2}, \quad (6.14)$$

in which the first and second parts roll off asymptotically as of f^{-2} and f^{-4}, respectively. An uncoded OFDM signal corresponds to $\mathcal{N}_e^{(0)} = \emptyset$. Consequently, the power spectral sidelobe of the uncoded OFDM signal without guard interval decay asymptotically as of f^{-2}, which is also indicated in [61]. On the other hand, if antipodal symbol pairs are mapped to all the subcarriers of the OFDM signal, i.e., $N_u = 2M_u$ and $\mathcal{N}_c = \emptyset$, the power spectral sidelobes of the OFDM signal without guard interval after the proposed scheme decay asymptotically as of f^{-4}. When antipodal symbol pairs are only mapped to the subcarriers at the edges of the utilized subbands or when a guard interval is inserted, the power spectral sidelobes after the proposed scheme may not roll off as fast. However, the sidelobe suppression gain still exists, especially near the edges of the utilized subbands, which will be demonstrated in the simulation.

6.2.3 Decoding

The precoding matrix in (6.10) consists of -1, 0, and 1 only, and therefore there is no need of general matrix multiplication for the precoder at the transmitter, which actually works in the way shown in (6.9). Similarly, due to the special structure of the spectral precoder, we do not need matrix inversion for decoding at the receiver, which is necessary for those schemes in [61, 62, 63]. The decoding can be simply performed as

$$b'_m = \begin{cases} \frac{d'_{2m} - d'_{2m+1}}{2}, & 0 \le m \le \frac{N_u - M_u}{2} - 1, \\ d'_{m+\frac{N_u - M_u}{2}}, & \frac{N_u - M_u}{2} \le m \le \frac{3M_u - N_u}{2} - 1, \\ \frac{d'_{2m-2M_u+N_u} - d'_{2m-2M_u+N_u+1}}{2}, & \frac{3M_u - N_u}{2} \le m \le M_u - 1, \end{cases} \tag{6.15}$$

where d'_n is the received symbol on the nth subcarrier and b'_m is the decoded mth information symbol. Therefore, the added complexity with the proposed precoder is $O(N_u)$ for either the CR transmitter or receiver, which is $O(N_u^2)$ for the existing precoders in [61,62,63]. Furthermore, in the multi-user case that user data are mapped to different subcarrier groups, the decoding for a specific user only requires the data from its own subcarrier group, which is impossible for the existing schemes in [62,63] where the transmitted symbol over each subcarrier is the weighted summation of the information symbols in all the subcarrier groups.

It can be noticed that there is an SNR gain for the information symbols at the edges of the utilized subband since the signal power is increased by 4 while the noise power is only increased by 2 after decoding when there is no power control. Therefore, the information symbols at the edges will be less vulnerable to the interference after precoding, where the interference level is usually higher than that in the center due to the proximity to the adjacent spectrum bands that may be occupied by other systems. It is also possible to use a higher modulation order to compensate the throughput loss due to precoding.

6.2.4 Two-Level Power Control

We have previously assumed unit power for the transmitted data symbol over each subcarrier of the OFDM signal. However, we may assign different power levels to different subcarriers based on different rules. For example, we may reduce the power of those coded

subcarriers at the edges, P_e, to half of that of the uncoded subcarriers in the center, P_c, so that each information symbol will have the same average power.

On the other hand, we may also consider a two-level power control scheme in the following to further deepen the power spectral sidelobes. As we have discussed, the power spectral sidelobes after the proposed precoder may not roll off as fast as f^{-4} like the ideal case. The PSD of the coded OFDM signal can be expressed as

$$P(f) = \frac{1}{T}\left(P_c A_c^2(f) + P_e A_e^2(f)\right), \tag{6.16}$$

where $A_c(f) = \sum_{n\in\mathcal{N}_c} a_n(f)$ and $A_e(f) = \sum_{n\in\mathcal{N}_e^{(0)}}(a_n(f) - a_{n+1}(f))$. Usually $A_c(f) > A_e(f)$ holds, so we may reduce P_c while increase P_e when the total transmit power, denoted as P_t, is fixed, i.e.,

$$(2M_u - N_u)P_c + 2(N_u - M_u)P_e = P_t. \tag{6.17}$$

Note that the power level of the subcarriers at the edges will be higher with such power control. So these subcarriers may be assigned to the users near the edge of a cell with *fractional frequency reuse* (FFR) [98] or mapped with data symbols of a higher modulation order to compensate the throughput loss due to precoding.

6.2.5 Simulation Results

In the following, we will present simulation results to illustrate the performance of the proposed spectrum shaping scheme. Existing schemes including tone nulling in [53], ν_L-coded OFDM in [61], continuous OFDM in [62], and frequency notching in [63] are also considered for comparison. In our simulation, $T_s = \frac{1}{15}$ ms, $T_g = \frac{1}{16}T_s$, and $N_u = 512$ unless otherwise stated.

Figure 6.4 shows the PSD of the OFDM signals with different spectral precoding schemes. All the N_u subcarriers are used in different schemes except that half subcarriers at the edges of the utilized spectrum band are deactivated in the tone nulling scheme. Here, we choose $M_u = \frac{3}{4}N_u$ in the proposed scheme, $L = 5$ in the ν_L-coded OFDM scheme, and ±3999 KHz and ±4000 KHz are notched in the frequency notching scheme. It is obvious that

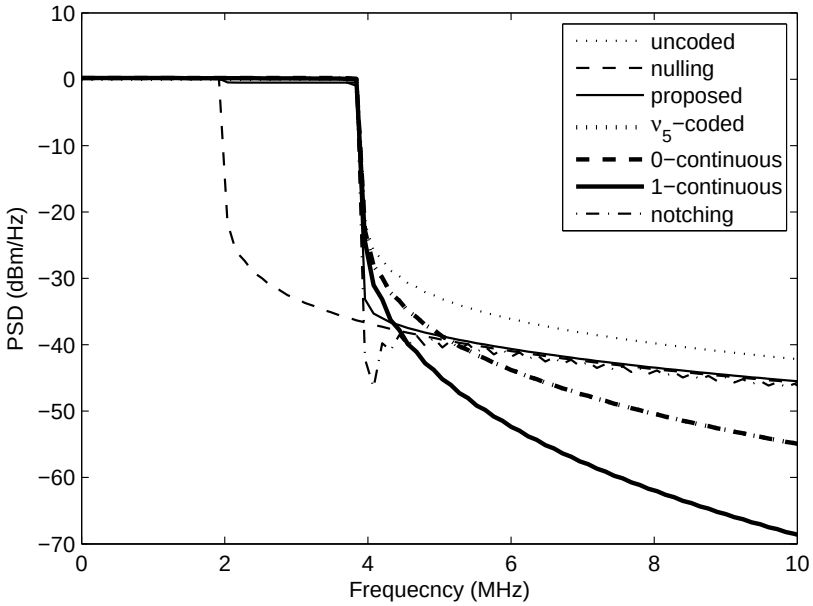

Figure 6.4. PSD curves of spectral precoded OFDM signals.

the uncoded OFDM signal exhibits the slowest power spectral sidelobe decaying, which is not desired. The tone nulling scheme exhibits a similar sidelobe level with the proposed scheme. However, the former does not utilize the subcarriers at the edges at all while the latter uses them to map antipodal symbol pairs and transmit more information symbols. Although the ν_5-coded, 0-continuous, and 1-continuous OFDM signals exhibit lower sidelobe levels, the frequency notching and proposed schemes exhibit the greatest decaying rate near the edges of the utilized spectrum band, whose sidelobe level reaches -30 dBm/Hz the earliest. Therefore, it is suitable to use the proposed scheme to achieve the narrowest guard band under a relatively loose spectral mask requirement when the transmit power level of the CR users is low [99].

Figure 6.5 illustrates the BER performance with different spectrum shaping schemes using 16QAM and no channel coding under AWGN. Here ±999 KHz and ±1000 KHz are notched in the frequency notching scheme when $N_u = 128$. We assign half power for those coded subcarriers at the edges in the proposed scheme so that each information symbol

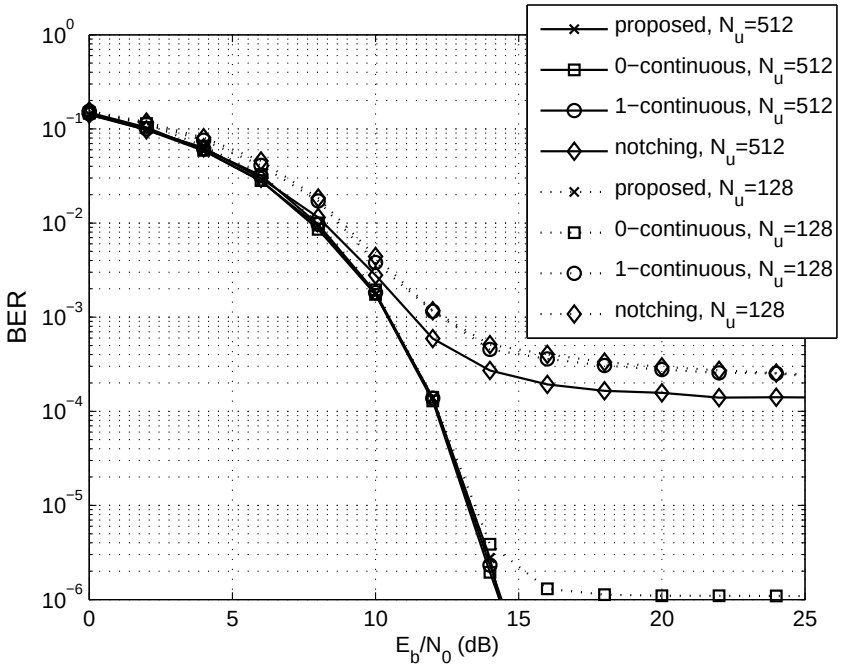

Figure 6.5. BER curves of spectral precoded OFDM signals.

will have the same average power. It can be seen that the proposed scheme never introduces any BER performance loss to the OFDM system. In contrast, the 0-continuous or 1-continuous OFDM scheme introduces notable BER performance loss especially when N_u is small. Therefore, our scheme is more appropriate to use when the utilized spectrum band is narrow, which is common in the CR environment. The frequency notching scheme introduces even greater BER performance loss despite its greatest decaying rate near the edges of the utilized spectrum band shown in Figure 6.4, which is not preferred. Our scheme is suitable for applications requiring guaranteed BER performance allowing moderate throughput loss.

Figure 6.6 shows the PSD of the OFDM signals with the proposed spectrum shaping scheme using different coding rates. When all the subcarriers are allocated the same power, i.e., $P_c = P_e = 1$, the proposed scheme always exhibits fast sidelobe decaying near the edges of the utilized spectrum band even with a higher coding rate, though different coding rates will have impacts on the sidelobe levels. We can flexibly select the coding rate, $\frac{M_u}{N_u}$,

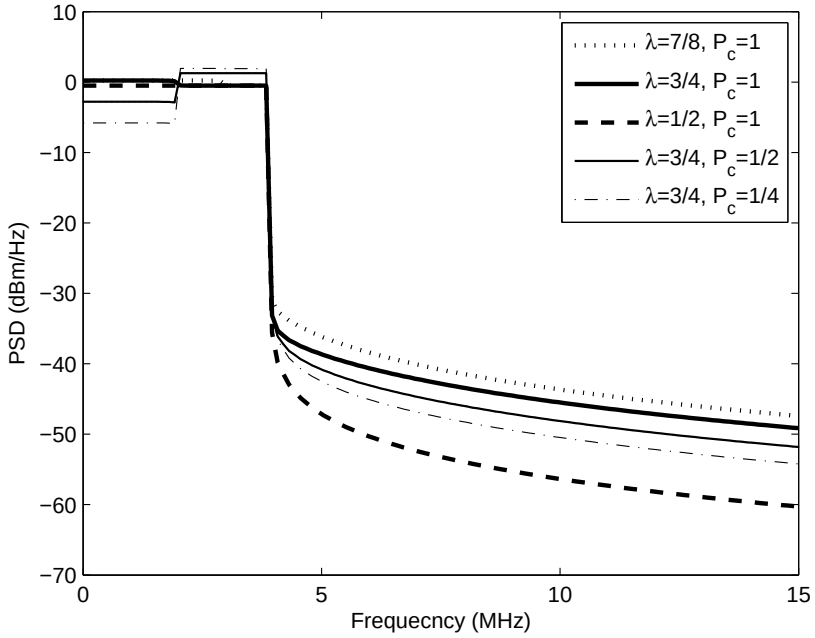

Figure 6.6. PSD curves of the proposed spectral precoded OFDM signals.

in our scheme to satisfy different spectral mask requirements in different scenarios. Figure 6.6 also demonstrates the advantage of using two-level power control. When we decrease the power of the subcarriers in the center of the utilized spectrum band, i.e., $P_c = 1/2$ and $P_c = 1/4$ with different P_e's satisfying $P_t = N_u$, the sidelobe level can be further lowered.

6.3 Multi-User Spectral Precoding

In the following, we consider K OFDM-based CR users utilizing the set of N_u subcarriers, $\mathcal{N}$, in a frequency band identified as unoccupied by licensed users through spectrum sensing. Let $\mathcal{N}_k$ denote the set of subcarriers, either continuous or discontinuous in frequency, utilized by the kth CR user with $|\mathcal{N}_k| = N_k$ for $0 \leq k \leq K-1$. To minimize inter-user interference, we assume that each subcarrier is used by at most one CR user at the same time, i.e., $\mathcal{N}_{k_1} \bigcap \mathcal{N}_{k_2} = \emptyset$ for $k_1 \neq k_2$ and $\bigcup_{k=0}^{K-1} \mathcal{N}_k = \mathcal{N}$.

A spectral mask is often used to define the maximum acceptable radiation level in the adjacent frequency bands [100]. To reduce the OOB radiation of the OFDM signal and meet the requirement of spectral mask with narrower guard bands, spectral precoding can

be applied. To remove the interdependency among individual CR users, spectral precoding is realized on a user basis, which can be expressed as

$$\mathbf{d}_k = \mathbf{G}_k \mathbf{b}_k \tag{6.18}$$

for the kth user, where $\mathbf{b}_k$ is a vector consisting of M_k information symbols and $\mathbf{G}_k$ denotes an $N_k \times M_k$ precoding matrix consisting of complex-valued precoding coefficients. To ensure proper decoding, the number of utilized subcarriers is usually no smaller than that of the information symbols for each user, i.e., $N_k \geq M_k$. The spectral coding rate for the kth user is defined as

$$\lambda_k = \frac{M_k}{N_k}. \tag{6.19}$$

The information symbols are assumed to be independent with zero mean and unit variance. In other words, $E\{\mathbf{b}_k \mathbf{b}_k^H\} = \mathbf{I}_{M_k}$, where $\mathbf{I}_{M_k}$ is an $M_k \times M_k$ identity matrix. Let $\mathbf{b}_O = \{\mathbf{b}_0^T, \mathbf{b}_1^T, ..., \mathbf{b}_{K-1}^T\}^T$. Then $E\{\mathbf{b}_O \mathbf{b}_O^H\} = \mathbf{I}_{\sum_{k=0}^{K-1} M_k}$. Meanwhile, let $\mathbf{d}_O = \{\mathbf{d}_0^T, \mathbf{d}_1^T, ..., \mathbf{d}_{K-1}^T\}^T$, which is the reordered $\mathbf{d}$ vector in (6.6). Then $\mathbf{a}(f)$ in (6.8) can be reordered as $\mathbf{a}_O(f) = \{\mathbf{a}_0^T, \mathbf{a}_1^T, ..., \mathbf{a}_{K-1}^T\}^T$ accordingly. Based on (6.8) and (6.18), we have

$$\begin{aligned} P(f) &= \frac{1}{T} \mathbf{a}_O^T(f) E\{\mathbf{G}_O \mathbf{b}_O (\mathbf{G}_O \mathbf{b}_O)^H\} \mathbf{a}_O^*(f) \\ &= \frac{1}{T} \mathbf{a}_O^T(f) \mathbf{G}_O \mathbf{G}_O^H \mathbf{a}_O^*(f) \\ &= \frac{1}{T} \|\mathbf{a}_O^T \mathbf{G}_O(f)\|_2^2, \end{aligned} \tag{6.20}$$

where

$$\mathbf{G}_O = \text{diag}\,(\mathbf{G}_0, \mathbf{G}_1, ..., \mathbf{G}_{K-1}) \tag{6.21}$$

is a block diagonal matrix.

By choosing the individual precoding matrices, $\mathbf{G}_k$'s, carefully, we can change the shape of the PSD in (6.20) and therefore, reduce the emission in the adjacent bands that may be used by licensed users. Meanwhile, proper signal reception must be guaranteed with a realizable decoder at each individual receiver.

6.3.1 Basic Approach

To suppress the OOB radiation in the adjacent bands, we should in general minimize the overall PSD level, $\int_{\mathcal{F}} P(f)df$, over an optimization frequency range $\mathcal{F}$ [59], which is usually difficult. Instead, we consider forcing the PSD in (6.20) to be zero at a few frequencies, f_l, $l = 0, 1, ..., L_f - 1$, selected in the adjacent bands. Then we have

$$\mathbf{A}_O\mathbf{G}_O = \mathbf{0}, \tag{6.22}$$

where the lth row of the matrix $\mathbf{A}_O$ is $\mathbf{a}_O^T(f_l)$. In this way, the PSD of the CR signal may be entirely under the spectral mask in the adjacent bands.

Constructing a matrix $\mathbf{A}_k$ whose columns are the $(\sum_{i=0}^{k-1} N_i)$th, $(\sum_{i=0}^{k-1} N_i+1)$th, ..., $(\sum_{i=0}^{k} N_i-1)$th columns of $\mathbf{A}_O$ for the kth user, we further have

$$\mathbf{A}_k\mathbf{G}_k = \mathbf{0} \tag{6.23}$$

for $k = 0, 1, ..., K - 1$, which indicates that we can design individual precoders independently.

The *singular value decomposition* (SVD) of $\mathbf{A}_k$ can be obtained as

$$\mathbf{A}_k = \mathbf{U}_k\mathbf{\Sigma}_k\mathbf{V}_k^H, \tag{6.24}$$

where $\mathbf{U}_k$ is an $L_f \times L_f$ matrix, $\mathbf{\Sigma}_k$ is an $L_f \times N_k$ matrix, and $\mathbf{V}_k$ is an $N_k \times N_k$ matrix. Note that the last $N_k - L_f$ columns of $\mathbf{V}_k$, denoted by $\mathbf{v}_k^{(L_f)}$, $\mathbf{v}_k^{(L_f+1)}$, ...,$\mathbf{v}_k^{(N_k-1)}$, constitute an orthogonal basis for the null space of $\mathbf{A}_k$. Therefore,

$$\mathbf{G}_k = [\mathbf{v}_k^{(L_f)}\ \mathbf{v}_k^{(L_f+1)}\ ...\ \mathbf{v}_k^{(N_k-1)}] \tag{6.25}$$

satisfies (6.23) and can be used as the precoding matrix for the kth user. Here $\mathbf{G}_k$ is an $N_k \times (N_k - L_f)$ matrix and $\mathbf{b}_k$ is an $M_k \times 1$ vector in (6.18). So we have $M_k = N_k - L_f$, i.e., the number of information symbols in an OFDM symbol of a CR user should be set equal to the difference between the number of its utilized subcarriers and the number of notched

frequencies. The spectral precoder should be prior to IFFT block as shown in Figure 6.2. The coding rate of the precoder for the kth user is

$$\lambda_k = 1 - \frac{L_f}{N_k}. \tag{6.26}$$

The overall coding rate for all the K users is therefore

$$\lambda_u = 1 - \frac{KL}{N_u}. \tag{6.27}$$

In other words, the system throughput reduces as the number of users increases in the proposed precoding scheme to guarantee user independence.

By choosing notched frequencies appropriately, our scheme ensures that the OOB radiation is under the spectral mask and the licensed users are well protected. Spectral compactness is enhanced and bandwidth efficiency is potentially improved with no or narrower guard bands. Unlike the existing spectral precoding schemes [61,62,63], there is no restriction on the number of utilized subcarriers in the proposed scheme. It is always possible for CR users to utilize small spectrum segments with a few subcarriers.

6.3.2 Decoding

After FFT and the frequency domain equalizer, the receiver of the kth user obtains $\tilde{\mathbf{d}}_k$. To recover the information symbols, a decoder is needed to revert the precoding operation. From the previous discussion, we know $\mathbf{G}_k^H \mathbf{G}_k = \mathbf{I}_{M_k}$. Therefore, the individual decoder can simply be realized as

$$\tilde{\mathbf{b}}_k = \mathbf{G}_k^H \tilde{\mathbf{d}}_k. \tag{6.28}$$

With the above operation, the information symbols can be perfectly recovered, i.e., $\tilde{\mathbf{b}}_k = \mathbf{b}_k$, if the channel and other system blocks are ideal.

We notice that both the coding and decoding operations are on a user basis so that the data of different users can be processed independently at both the transmitter and receiver. Especially, the individual receivers can avoid any further processing of data for other users after the FFT block. The computational complexity of the coding and decoding operations

is limited to $O(N_k^2)$ for the kth user instead of being fixed to $O(N_u^2)$ in some of the existing spectral precoding schemes. It is also possible to divide the subcarriers utilized by a user into groups and create several virtual users to further reduce the complexity with a smaller number of subcarriers for each virtual user.

As long as the individual transmitter and receiver know where the utilized subcarriers and notched frequencies are, they will be able to compute the precoder and decoder independently based on (6.4), (6.24), and (6.25). It is unnecessary for them to exchange the precoding matrix, which involves a lot of overhead. It is also possible to independently determine the notched frequencies based on the utilized subcarriers by following the same rule at the transmitter and receiver, the detail of which will be discussed in the following. With such flexibilities, our scheme is suitable in the scenario of dynamic spectrum sharing between CR and licensed users, where the utilized subcarriers keep on varying.

6.3.3 Selection of Notched Frequencies

From the previous discussion, the overall system throughput with the proposed precoding scheme will increase if the number of users, K, or the number of notched frequencies, L_f, decreases. We cannot change the number of users, but it is possible to reduce the number of notched frequencies to improve the bandwidth efficiency. We will see in the following that 1) a minimum number of notched frequencies can be determined to satisfy (6.22), and 2) the number of notched frequencies may be further reduced for different users so that the system throughput loss does not necessarily increase linearly with the number of users.

Generally, we need 2 pairs of notched frequencies in each adjacent band on one side. Each pair consists of 2 frequencies closely located to ensure effective suppression there. One pair should be placed near the edge of the adjacent band so that the OOB radiation will drop quickly under the spectral mask. Let D denotes the bandwidth of the entire available frequency band. Then the other pair should be placed D/Q away from the edge so that the OOB radiation will not climb up over the spectral mask, where Q is a design parameter. As the OOB radiation must be suppressed in adjacent bands on both sides, totally $L_f = 8$

notched frequencies are needed.

In practice, it is not necessary to enforce (6.22) strictly. The spectral precoding scheme is effective as long as the PSD is rendered under the spectral mask. We may consider relaxing the requirement as

$$\mathbf{A}_O\mathbf{G}_O \preceq \boldsymbol{\eta}, \tag{6.29}$$

where $\boldsymbol{\eta}$ is a vector representing spectrum mask requirement at the previously defined notched frequencies, and $\preceq$ stands for component-wise inequality. Consequently, (6.29) may also yield in an effective spectral precoder.

Enlightened by the above observation, we can further adjust the locations and number of notched frequencies to balance OOB radiation suppression and system throughput. Basically, if the part of frequency band utilized by a user is not close to the edge of an adjacent band, the OOB emission on that side may be not so significant and thus some of the notched frequencies may be unnecessary. Assume that the two pairs of notched frequencies are centered around f_{l_1}, which is near the edge, and f_{l_2}, which is D/Q away from the edge, respectively. We may use

$$P(f) = \frac{1}{T}\mathbf{a}_k^T(f)\mathbf{a}_k^*(f) \tag{6.30}$$

to evaluate the PSD of the user signal at $f = f_{l_1}$ and $f = f_{l_2}$ without spectral precoding. The pair of notched frequencies centered around $f_{l_i}, i = 1, 2$ is not required if $P(f_{l_i}) \leq \eta_{f_{l_i}}$, where $\eta_{f_{l_i}}$ is the element of $\boldsymbol{\eta}$ in (6.29) corresponding to f_{l_i} together with some margin.

Therefore, it is possible to have different sets of notched frequencies for users utilizing different portions of the detected available frequency band. In other words, L_f should be replaced with $L_{f,k}$ for the kth user. We have

$$\mathbf{A}_k'\mathbf{G}_k' = \mathbf{0}, \tag{6.31}$$

where $\mathbf{A}_k'$ is an $L_{f,k} \times N_k$ matrix by removing unnecessary rows of $\mathbf{A}_k$, and $\mathbf{G}_k'$ is an $N_k \times (N_k - L_{f,k})$ precoding matrix constructed by the last $N_k - L_{f,k}$ right singular vectors of $\mathbf{A}_k'$. The length of the information vector for the kth user is then $N_k - L_{f,k}$ and the coding rate is

correspondingly

$$\lambda_k' = 1 - \frac{L_{f,k}}{N_k}. \tag{6.32}$$

The overall coding rate is

$$\lambda_u' = 1 - \frac{\sum_{k=0}^{K-1} L_{f,k}}{N_u}. \tag{6.33}$$

Note that $\lambda_u' \geq \lambda_u$ as $L_{f,k} \leq L_f$ for $k = 0, 1, ..., K-1$.

Usually, the individual transmitter and receiver can independently determine the notched frequencies based on the utilized subcarriers. Let d and d' denote the bandwidth of the part of frequency band utilized by the user and the frequency distance between the edges of the utilized and adjacent frequency bands on one side, respectively. Then the second pair of notched frequencies D/Q away from the edge can be avoided when $d' \geq Bd$. And if $d' \geq Ad$ $(A > B)$, the first pair of notched frequencies near the edge can be avoided as well. Here B and A can be obtained by setting $P(Bd + D/Q) = P(Ad) = \eta$ in (6.30) with $T_s d$ subcarriers spanning from $f = -d$ to $f = 0$ and η as a rough spectrum mask requirement.

6.3.4 Simulation Results

In the following, we present simulation results to illustrate the performance of the proposed multi-user spectral precoding scheme. In our simulation, $T_s = \frac{1}{15}$ ms, $T_g = \frac{3}{640}$ ms, and $\mathcal{N} = \{-240, ..., -1, 1, ..., 240\}$.

In Figure 6.7, the PSD curves of the precoded OFDM signals of 4 users utilizing 4 equally divided portions of a frequency band are shown. There are totally 8 notched frequencies on two sides: {-6101,-6099,-4101,-4099,4099,4101,6099,6101} KHz. It can be seen that the resulted PSD curves are well below the spectral mask. Therefore, sufficient suppression of OOB radiation is achieved with the proposed scheme. If we apply the projection precoder in [63] to the individual users, the same PSD curves will be generated.

Figure 6.8 illustrates the BER performance of User 0 with different schemes using QPSK, 16QAM, and 64QAM without channel coding under AWGN. It can be noticed that the proposed spectral precoding scheme never introduces any BER performance loss to the

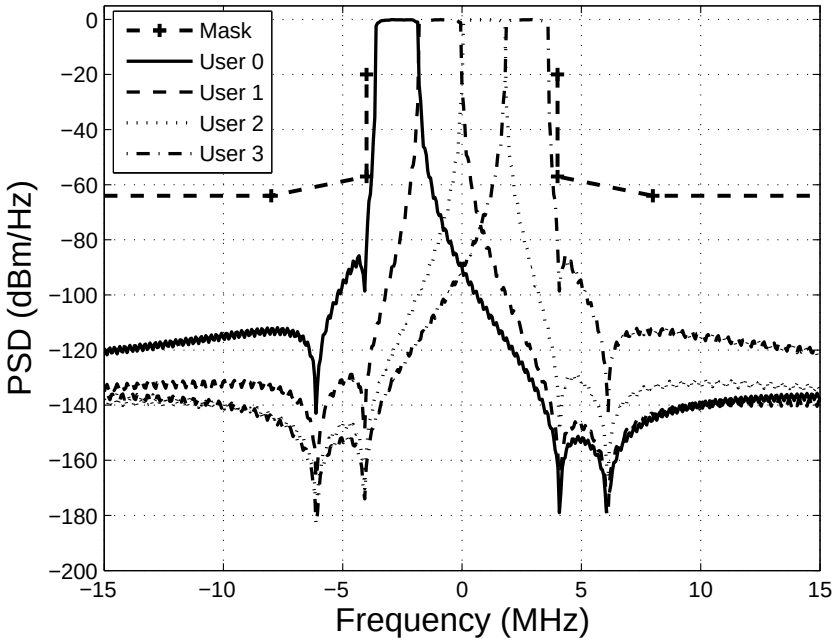

Figure 6.7. PSD curves of user signals with the proposed spectral precoder.

OFDM system. But the projection precoder [63] brings significant BER performance loss in such a case, which is undesired.

In Figure 6.9, the PSD curves of the precoded OFDM signals of 4 users with notched frequency selection are shown. Here, $Q = 4$, $A = 1$, and $B = 2.5$. For User 0 utilizing the left 1/4 of the subcarriers, $d = D/4$ with D being the entire available bandwidth. Note that $d' \approx 3D/4$ relative to the right edge. Since $d' \geq Bd$, no notched frequencies are needed near the right edge. Meanwhile, $d' \approx 0$ relative to the left edge. Since $d' < Ad$, 2 pairs of notched frequencies located at the left edge and $D/Q = D/4$ away from the left edge are needed to ensure sufficient suppression. We can similarly determine the notched frequencies for the other 3 users. In Table 6.1, we compare the overall coding rates of different precoding schemes in the simulation. We notice that, with proper notched frequency selection, the proposed scheme is with relatively low throughput performance loss, and such loss does not necessarily grow linearly with the number of users.

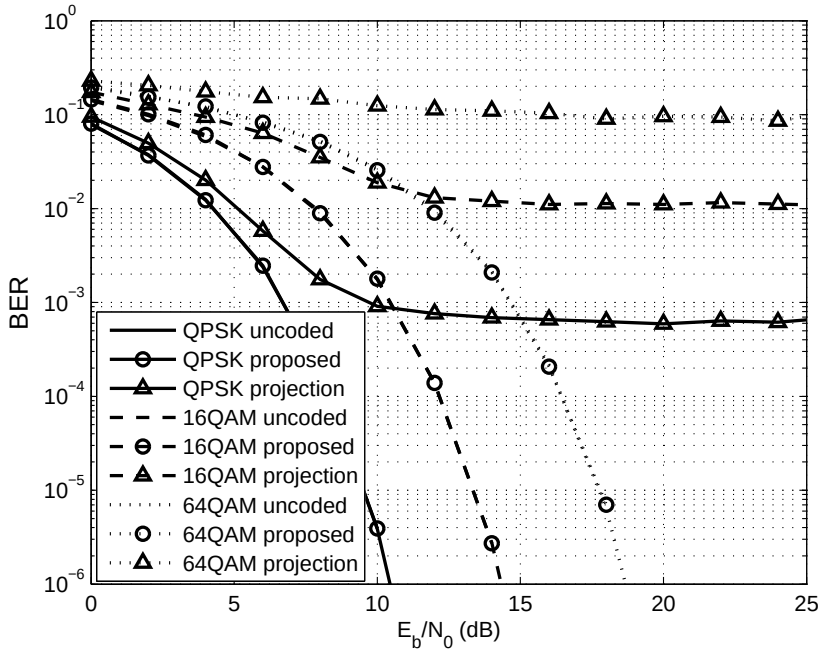

Figure 6.8. User BER curves under different spectrum shaping schemes.

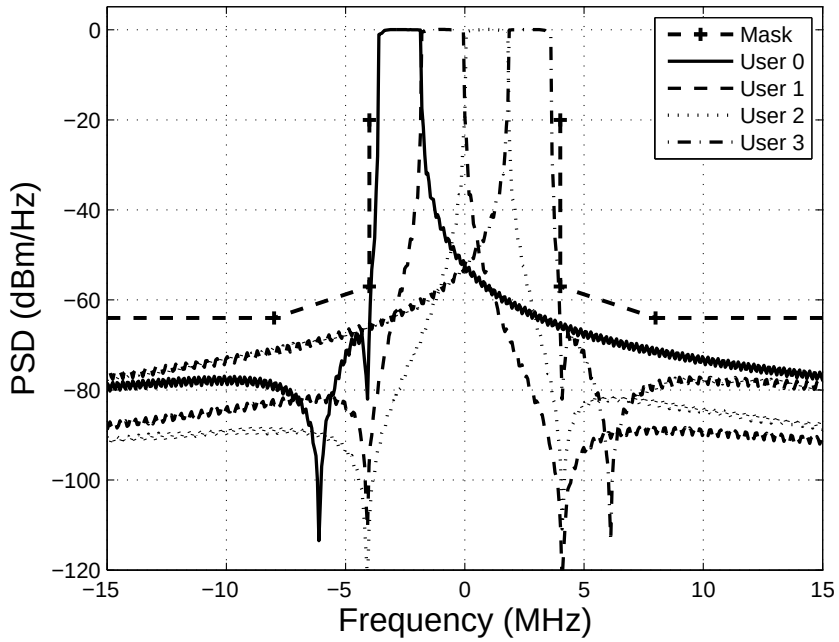

Figure 6.9. PSD curves of user signals with the proposed spectral precoder and notched frequency selection.

Table 6.1. Overall coding rates of different spectral precoding schemes.

Precoding Scheme	Coding Rate
Projection	1
Proposed w/o notched frequency selection	14/15
Proposed with notched frequency selection	29/30

6.4 Conclusion

In this chapter, we have proposed a low-complexity spectrum shaping scheme for OFDM-based CR systems by mapping antipodal symbol pairs onto adjacent subcarriers at the edges of the utilized subbands. Sidelobe suppression and system throughput can be well balanced by adjusting the coding rate of the corresponding spectral precoder while power control on different sets of subcarriers has been introduced to further lower the sidelobes. Meanwhile, we have also proposed a spectral precoding scheme for multiple OFDM-based CR users to enhance spectral compactness. By constructing individual precoders to render selected spectrum nulls, our scheme ensures user independence and provides sufficient OOB radiation suppression without BER performance loss. We have also considered the selection of notched frequencies to further increase the bandwidth efficiency. The proposed schemes enable efficient spectrum sharing between CR and licensed users and exhibit the advantages of both simplicity and flexibility.

CHAPTER 7

PROBABILISTIC RESOURCE ALLOCATION FOR OPPORTUNISTIC SPECTRUM ACCESS

In Chapter 6, we have proposed efficient spectrum shaping schemes for OFDM-based CR systems, which limit the interference with licensed users operating in the adjacent bands and ensure proper signal reception of secondary communication. However, possible interference with licensed users in the operating spectrum band should also be under control while the throughput performance of CR systems needs to be further enhanced. Resource allocation, which usually includes channel and power allocations, can be applied for such purposes. In a multi-channel environment where the available licensed spectrum band is divided into several non-overlapping frequency channels, we focus on the approach to allocate each channel to at most one user exclusively, which eases interference management. We note that decision errors from spectrum sensing are inevitable in practice and approaches relying on hard decisions only may introduce unacceptable interference to licensed users and lose the flexibility of OSA.

In this chapter, we use the probabilistic information of channel availability obtained from spectrum sensing to assist resource allocation in CR networks, which exploits the flexibility of OSA and has better performance compared with conventional approaches based on the hard decisions on channel availability. We study resource allocation in a multi-channel environment to maximize the overall utility of CR users accessing licensed channels and ensure the protection of licensed users from unacceptable interference. Our approach can also provide diverse QoS support for CR users with different minimum data rate requirements.

The rest of this chapter is organized as follows. In Section 7.1, we describe the system model. In Section 7.2, we introduce the basic idea in probabilistic resource allocation and the method to obtain the probabilities of channel availability from spectrum sensing.

Next, in Section 7.3, we address probabilistic resource allocation for the single-user case and discuss several properties of this approach. In Section 7.4, we extend the probabilistic resource allocation approach to the multi-user case and give the distributed implementation. Then we present simulation results in Section 7.5. Finally, we conclude this chapter in Section 7.6.

7.1 System Model

In this section, we introduce the system model of OSA in CR networks. Spectrum sensing procedures related to resource allocation in the multi-channel environment are briefly discussed as well.

7.1.1 Opportunistic Spectrum Access

Without loss of generality, we consider a CR network with K active users exploiting communication opportunities over a portion of licensed spectrum. Each CR user consists of a transmitter and an intended receiver. The total bandwidth of interest is equally divided into N non-overlapping channels, each with a bandwidth of B. OSA is realized by assigning different licensed channels to CR users and allocating transmit powers accordingly.

Each channel is exclusively assigned to at most one CR user at a time, so there will be no mutual interference among different users. Denote the transmit power of User k over Channel n as $p_{k,n}$. If $p_{k,n} > 0$, then $p_{k',n} = 0$ for any $k' \neq k$ in this case. The received SNR of User k over Channel n is

$$\gamma_{k,n} = \frac{p_{k,n} g_{k,n}}{\sigma^2}, \tag{7.1}$$

where $g_{k,n}$ is the power gain from the transmitter of User k to its receiver over Channel n, and σ^2 is the noise power, which is, without loss of generality, assumed to be the same for all the users over all the channels. If the licensed user signal is absent at the receiver of User k, the maximum data rate of the user over Channel n is accordingly

$$r_{k,n} = B \log_2 (1 + \gamma_{k,n}). \tag{7.2}$$

If a certain licensed user is simultaneously using Channel n, the transmitter of User k will generate interference to the licensed receiver with the power given by

$$I_{k,n} = p_{k,n} g'_{k,n}, \tag{7.3}$$

where $g'_{k,n}$ is the power gain from the transmitter of CR User k to the licensed receiver over Channel n.

Resource allocation in a CR network maximizes the overall system utility. The utility is usually a function of the received SNRs or data rates of all the CR users under a certain transmit power constraint of each CR user denoted as $\hat{P}_k$ for User k. To protect licensed communication, we post an allowable average interference level at the licensed receiver over Channel n denoted as $\hat{I}_n$. Therefore, we must limit the transmit powers from the CR network to meet the constraint, which is originated from the concept of interference temperature [101].

7.1.2 Multi-Channel Spectrum Sensing

Spectrum sensing, which decides whether the licensed user signal is present or not from the observed signal, must be performed by the CR network before resource allocation. Since any licensed channel may be either occupied or unoccupied by the licensed user at a certain time, it is commonly formulated as the following binary hypothesis testing problem in a multi-channel environment [15]

$$y_n(t) = \begin{cases} \tilde{n}_n(t), & \mathcal{H}_{I,n}, \\ s_n(t) + \tilde{n}_n(t), & \mathcal{H}_{B,n}, \end{cases} \tag{7.4}$$

where $y_n(t)$, $s_n(t)$, and $\tilde{n}_n(t)$ denote the received signal, the received licensed user signal, and the additive noise over the nth channel at the CR node performing spectrum sensing, respectively; $\mathcal{H}_{I,n}$ and $\mathcal{H}_{B,n}$ denote the hypotheses corresponding to the absence and presence of the licensed user signal in the nth channel, respectively. The goal of spectrum sensing is to decide between the two hypotheses, $\mathcal{H}_{I,n}$ and $\mathcal{H}_{B,n}$, from the observation, $y_n(t)$.

While the performance of local spectrum sensing at a single CR node is usually limited due to channel shadowing and fading, the reliability of spectrum sensing can be improved by taking advantage of spatial diversity with cooperative spectrum sensing [15], in which multiple CR nodes obtain local information of licensed channel availability and send it out through a dedicated control channel. Note that the local sensing information can be either one-bit hard decision on the absence or presence of the licensed user signal, or preprocessed sensing data on the observation. After collecting the sensing information from different CR nodes, the fusion node finally determines the availability of the licensed channel of interest.

7.2 Probabilistic Resource Allocation

In this section, we present the basic idea in probabilistic resource allocation and the method to obtain the probabilities of channel availability from spectrum sensing.

7.2.1 Metrics for Resource Allocation

The hard decisions on the availability of licensed channels are usually used in resource allocation and only the channels determined to be available by spectrum sensing will be utilized by CR users as shown in Figure 7.1. Since there are inevitably decision errors in spectrum sensing, this approach inherits the imprecise information within the hard decisions, which loses the flexibility of OSA and may generate unacceptable interference to licensed users. To improve both flexibility and performance, we propose the resource allocation approach that considers average utility for given sensing information.

Denote $U_{k,n}$ as the utility of User k accessing Channel n, which depends on the licensed channel status. The average utility within Channel n for CR User k is defined as

$$\bar{U}_{k,n} = \mathbf{E}[U_{k,n}], \tag{7.5}$$

where the expectation is taken under the conditional distribution of the utility related to the absence or presence of the licensed user signal at the CR receiver given the current sensing information. Even though other utility measures may be applied, we will focus on using

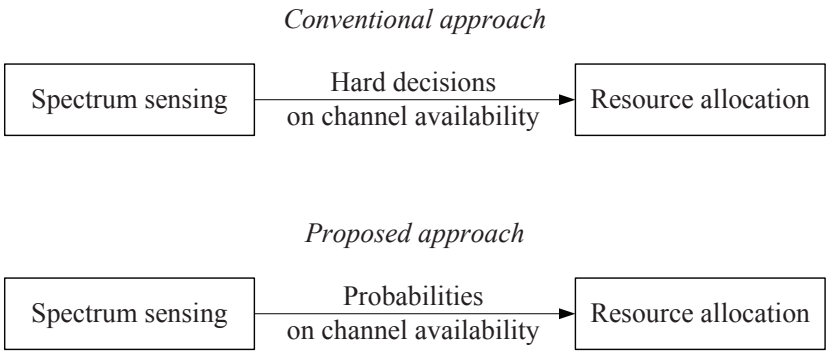

Figure 7.1. The conventional approach versus the proposed approach for resource allocation in CR networks.

the achievable data rate. Consequently,

$$U_{k,n} = \begin{cases} r_{k,n}, & \text{no licensed user signal at the CR receiver,} \\ 0, & \text{otherwise.} \end{cases} \tag{7.6}$$

Here we assume that if the licensed user signal is present at the CR receiver, the transmission of the CR user will fail. Therefore, the average data rate will be

$$\bar{r}_{k,n} = q^{(I)}_{R_k,n} r_{k,n}, \tag{7.7}$$

where $q^{(I)}_{R_k,n}$ is the conditional probability that the licensed user signal is absent in Channel n at the receiver of CR User k given the current sensing information.

Similarly, average interference to the licensed user must be considered when performing resource allocation. The average interference in Channel n from the transmitter of CR User k can be expressed as

$$\bar{I}_{k,n} = q^{(B)}_{T_k,n} I_{k,n}, \tag{7.8}$$

where $q^{(B)}_{T_k,n}$ is the conditional probability that the licensed user signal is present in Channel n at the transmitter of CR User k given the current sensing information. Note that the interference generated to the licensed user is from the CR transmitter; that is why we associate $q^{(B)}_{T_k,n}$ with the transmitter of User k. This is different from the discussion of $\bar{r}_{k,n}$, in which we associate $q^{(I)}_{R_k,n}$ with the receiver of User k since secondary communication will be affected when the licensed user signal is present at the CR receiver.

7.2.2 Probabilistic Information from Spectrum Sensing

The probabilistic information, i.e., $q_{T_k,n}^{(B)}$ and $q_{R_k,n}^{(I)}$, may be obtained through either local spectrum sensing by the transmitter and receiver of User k, respectively, or preferably, cooperative spectrum sensing [15, 102]. Note that the probabilities for the licensed user signal to be present or absent in a certain channel can be different among CR nodes due to their geographical differences relative to the licensed network. For example, a CR node with a large distance from a licensed user may determine the licensed channel to be available and utilize it while another CR node near the licensed user cannot claim the same. Therefore, the CR nodes with data to transmit or receive will work as fusion nodes and combine the local sensing information from only proper nearby CR nodes so that the combined information will be more accurate than that based on the sensing information from all the nodes including those far away.

Denote $\Omega_{T_k,n}$ and $\Omega_{R_k,n}$ as the vectors consisting of sensing information about the nth channel collected from nearby CR nodes by the kth CR transmitter and receiver, respectively. For example, the vector may look like $[1, 0, 1, ...]^T$ when local decisions are made at cooperative CR nodes, where 1 and 0 denote the local decisions that the licensed user signal is present and absent, respectively. According to the Bayesian theorem, we can obtain the conditional probabilities, $q_{T_k,n}^{(B)}$ and $q_{R_k,n}^{(I)}$. Note that the sum of $q_{T_k,n}^{(B)}$ and $q_{R_k,n}^{(I)}$ does not in general equal 1 because different sensing information at the CR transmitter and receiver may be collected. More specifically,

$$\begin{aligned} q_{T_k,n}^{(B)} &= P(\mathcal{H}_{B,n}|\Omega_{T_k,n}) \\ &= \frac{P(\Omega_{T_k,n}|\mathcal{H}_{B,n}) * P_{B,n}}{P(\Omega_{T_k,n}|\mathcal{H}_{B,n}) * P_{B,n} + P(\Omega_{T_k,n}|\mathcal{H}_{I,n}) * P_{I,n}} \end{aligned} \tag{7.9}$$

and

$$\begin{aligned} q_{R_k,n}^{(I)} &= P(\mathcal{H}_{I,n}|\Omega_{R_k,n}) \\ &= \frac{P(\Omega_{R_k,n}|\mathcal{H}_{I,n}) * P_{I,n}}{P(\Omega_{R_k,n}|\mathcal{H}_{B,n}) * P_{B,n} + P(\Omega_{R_k,n}|\mathcal{H}_{I,n}) * P_{I,n}}, \end{aligned} \tag{7.10}$$

where $P_{B,n}$ and $P_{I,n}$ are the stable probabilities that the licensed user signal is present and

absent; $P(\Omega_{T_k,n}|\mathcal{H}_{B,n})$ and $P(\Omega_{T_k,n}|\mathcal{H}_{I,n})$, or $P(\Omega_{R_k,n}|\mathcal{H}_{B,n})$ and $P(\Omega_{R_k,n}|\mathcal{H}_{I,n})$, are the conditional probabilities that the sensing information is $\Omega_{T_k,n}$ or $\Omega_{R_k,n}$ given that the licensed user signal is present and absent, respectively. $P_{B,n}$ and $P_{I,n}$ can be obtained through successive spectrum sensing on the licensed activity; $P(\Omega_{T_k,n}|\mathcal{H}_{B,n})$ and $P(\Omega_{T_k,n}|\mathcal{H}_{I,n})$, or $P(\Omega_{R_k,n}|\mathcal{H}_{B,n})$ and $P(\Omega_{R_k,n}|\mathcal{H}_{I,n})$ can be obtained from the collected sensing information based on the conditional distributions of local measurements using the method detailed in Chapter 4.

7.3 Resource Allocation for One Single Cognitive Radio User

In this section, we consider the case when there is a single CR user exploiting communication opportunities among all the candidate licensed channels, in which resource allocation reduces to power allocation that determines the transmit power in each channel. Without loss of generality, we let the index of the CR user, k, to be 1.

According to the discussion in the previous section, if the overall data rate, $\sum_{n=1}^{N} \bar{r}_{1,n}$, is used as the utility, resource allocation for a single CR user can be formulated as the following optimization problem

$$\begin{aligned} \max_{\mathbf{p}} \quad & \sum_{n=1}^{N} \bar{r}_{1,n} \\ \text{subject to} \quad & \sum_{n=1}^{N} p_{1,n} \le \hat{P}_1, p_{1,n} \ge 0, \forall n, \\ & q^{(B)}_{T_1,n} g'_{1,n} p_{1,n} \le \hat{I}_n, \forall n, \end{aligned} \tag{7.11}$$

where $\mathbf{p} = [p_{1,1}, p_{1,2}, ..., p_{1,N}]^T$ and $\bar{r}_{1,n} = q^{(I)}_{R_1,n} r_{1,n} = q^{(I)}_{R_1,n} B \log_2\left(1 + \frac{p_{1,n} g_{1,n}}{\sigma^2}\right)$.

The Lagrangian function of the problem is given by

$$\begin{aligned} L(\mathbf{p}, \lambda_0, \boldsymbol{\mu}) &= \sum_{n=1}^{N} \bar{r}_{1,n} + \lambda_0 \left(\hat{P}_1 - \sum_{n=1}^{N} p_{1,n} \right) \\ &+ \sum_{n=1}^{N} \mu_n \left(\hat{I}_n - q^{(B)}_{T_1,n} g'_{1,n} p_{1,n} \right), \end{aligned} \tag{7.12}$$

where λ_0 and μ_n are introduced Lagrange multipliers and $\boldsymbol{\mu} = [\mu_1, \mu_2, ..., \mu_N]^T$. By taking the partial derivative of L with $p_{1,n}$, λ_0 and μ_n, the *Karush-Kuhn-Tucker* (KKT) [103] condition

can be obtained as that there exists $\lambda_0 \geq 0$ and $\mu_n \geq 0, \forall n$, such that

$$\frac{\partial \bar{r}_{1,n}}{\partial p_{1,n}} - \lambda_0 - \mu_n q^{(B)}_{T_1,n} g'_{1,n} = 0, \forall n, \tag{7.13}$$

$$\lambda_0 \left(\hat{P}_1 - \sum_{n=1}^{N} p_{1,n} \right) = 0, \tag{7.14}$$

$$\mu_n \left(\hat{I}_n - q^{(B)}_{T_1,n} g'_{1,n} p_{1,n} \right) = 0, \forall n. \tag{7.15}$$

From (7.13), the power allocation can be determined in a water-filling fashion as

$$p_{1,n} = \left[\frac{q^{(I)}_{R_1,n} B}{(\lambda_0 + \mu_n q^{(B)}_{T_1,n} g'_{1,n}) \ln 2} - \frac{\sigma^2}{g_{1,n}} \right]^+, \tag{7.16}$$

where $[x]^+ = \max(x, 0)$. Using the iterative algorithm, $p_{1,n}$ is updated according to (7.16) while the multipliers can be found with the subgradient method [104] in each step such that

$$\lambda_0^{(i+1)} = \left[\lambda_0^{(i)} - s^{(i)} \left(\hat{P}_1 - \sum_{n=1}^{N} p^{(i)}_{1,n} \right) \right]^+, \tag{7.17}$$

$$\mu_n^{(i+1)} = \left[\mu_n^{(i)} - s^{(i)} \left(\hat{I}_n - q^{(B)}_{T_1,n} g'_{1,n} p^{(i)}_{1,n} \right) \right]^+, \tag{7.18}$$

where $s^{(i)}$ is a small positive step size for the ith iteration.

To better understand our approach, we compare it with two conventional approaches relying upon the hard decisions on channel availability instead of the probabilistic information.

7.3.0.1 Decision-based Aggressive Resource Allocation

This is a most commonly used approach that resource allocation is based on the decision in spectrum sensing [71, 72, 73, 74]. In this approach, resource is allocated within all determined available channels assuming spectrum sensing decision is perfect. Therefore, possible interference due to detection errors, especially mis-detection, is ignored. Without loss of generality, assume that the indices of decided available channels in spectrum sensing are $1, 2, ..., N_0 (\leq N)$. In the single-user case, decision-based aggressive resource

allocation can be formulated as the following optimization problem

$$\begin{aligned} \max_{\mathbf{p}} \quad & \sum_{n=1}^{N_0} r_{1,n} \\ \text{subject to} \quad & \sum_{n=1}^{N_0} p_{1,n} \le \hat{P}_1, p_{1,n} \ge 0, \forall n. \end{aligned} \tag{7.19}$$

Compare the probabilistic and decision-based aggressive approaches, and we notice that (7.11) will be equivalent to (7.19) by changing N to N_0 and setting $q^{(I)}_{R_1,n} = 1$ and $q^{(B)}_{T_1,n} = 0$ for all $n \le N_0$ in (7.11). This approach is called decision-based aggressive resource allocation because it assumes that spectrum sensing decision represents actual channel status. In other words, all decided available channels are assumed absent of licensed communication and all decided unavailable channels are assumed present of licensed communication.

7.3.0.2 Decision-based Conservative Resource Allocation

This is another commonly used approach especially in *ultra wideband* (UWB) systems [7]. In this approach, resource is allocated within all decided available channels while possible interference is not allowed to exceed the interference constraint. In the single-user case, it can be formulated as the following optimization problem

$$\begin{aligned} \max_{\mathbf{p}} \quad & \sum_{n=1}^{N_0} r_{1,n} \\ \text{subject to} \quad & \sum_{n=1}^{N_0} p_{1,n} \le \hat{P}_1, p_{1,n} \ge 0, \forall n, \\ & g'_{1,n} p_{1,n} \le \hat{I}_n, \forall n. \end{aligned} \tag{7.20}$$

Compare the probabilistic and decision-based conservative approaches, and we notice that (7.11) will be equivalent to (7.20) by changing N to N_0 and setting $q^{(I)}_{R_1,n} = q^{(B)}_{T_1,n} = 1$ for all $n \le N_0$ in (7.11). This approach is called decision-based conservative resource allocation because it ensures that the CR signal power at any mis-detected licensed receiver is always below a certain threshold.

The following properties indicate the optimality of the proposed probabilistic resource allocation approach in the single-user case, which have been proved in Appendix D.

Proposition 7.3.1 *The average interference of the decision-based aggressive resource allocation is not guaranteed to be within the acceptable level even when the maximum transmit power is low.*

Proposition 7.3.2 *The average data rate of the decision-based aggressive resource allocation is no more than that of the probabilistic resource allocation if the interference constraints are inactive.*

Proposition 7.3.3 *The average data rate of the decision-based conservative resource allocation is no more than that of the probabilistic resource allocation if the maximum power constraint is inactive for both.*

Note that for any optimization problem, an inequality constraint that does not hold with equality is defined as an inactive constraint.

Property 1 indicates that the decision-based aggressive approach cannot control the interference level, which is due to the fact that it assumes perfect spectrum sensing decision and thus sets no interference constraint. Property 2 indicates that the decision-based aggressive approach does not work as well as the probabilistic approach when the maximum power constraint is the primary limitation in the system. This is because channel availability is determined by thresholding the probabilities in the former. Property 3 indicates that the decision-based conservative approach does not work as well as the probabilistic approach when the interference constraints are the primary limitation in the system. This is because strict interference limit is applied in the former. Overall, the probabilistic approach best exploits the flexibility of OSA thus can achieve the most satisfactory performance.

7.4 Resource Allocation for Multiple Cognitive Radio Users

In the previous section, we have considered the case when there is a single CR user in the network and given several properties of the proposed approach. If there are more than one CR user accessing several licensed channels, resource allocation will become more complicated because the coordination among different users is inevitable. In this section, we

will generalize the probabilistic resource allocation to multi-user case in which the licensed channels are used exclusively in the network. Emphasis will be put mainly on the differences between the single-user and multi-user cases as well as practical implementation considerations.

Here we use the weighted sum data rate of the CR network as the utility measure, where weights take the priorities of different CR users into consideration. For example, queue-weighted sum data rate can be used for stability and throughput optimality [98]. It is obvious that the weighted sum data rate turns into sum data rate when every weight is 1.

We assume that each channel can be at most allocated to one CR user and each CR user may be allocated more channels so that mutual interference among CR users is avoided. Therefore, channel allocation will be considered in addition to power allocation. Furthermore, each CR user should guarantee a minimum average data rate [105].

Let $\rho_{k,n}$ be the channel allocation indicator defined as

$$\rho_{k,n} = \begin{cases} 1, & \text{Channel n is allocated to User k,} \\ 0, & \text{otherwise,} \end{cases} \tag{7.21}$$

w_k be the weight for the data rate of the kth CR user, and $\check{R}_k$ be the minimum data rate requirement for User k. Meanwhile, let $\boldsymbol{\rho} = [\rho_{k,n}], 1 \leq k \leq K, 1 \leq n \leq N$ and $\mathbf{p} = [p_{k,n}], 1 \leq k \leq K, 1 \leq n \leq N$ be the allocation indicator and transmit power matrix, respectively. Based on the probabilistic information on channel availability, we can formulate resource

allocation among multiple CR users as the following optimization problem

$$\begin{aligned}
\max_{\boldsymbol{\rho},\mathbf{p}} \quad & \sum_{k=1}^{K} w_k \sum_{n=1}^{N} \rho_{k,n} \bar{r}_{k,n} \\
\text{subject to} \quad & \sum_{k=1}^{K} \rho_{k,n} \leq 1, \forall n, \rho_{k,n} \in \{0,1\}, \forall k, n, \\
& \sum_{n=1}^{N} \rho_{k,n} p_{k,n} \leq \hat{P}_k, \forall k, p_{k,n} \geq 0, \forall k, n, \\
& \sum_{k=1}^{K} q^{(B)}_{T_k,n} g'_{k,n} \rho_{k,n} p_{k,n} \leq \hat{I}_n, \forall n, \\
& \sum_{n=1}^{N} \rho_{k,n} \bar{r}_{k,n} \geq \check{R}_k, \forall k,
\end{aligned} \tag{7.22}$$

where the objective function and constraints reflect all the aspects in the previous discussion, i.e., to maximize the weighted sum data rate with exclusive licensed channel usage and to satisfy the user power and channel interference constraints as well as the minimum user data rate requirements.

In order to make the resource allocation algorithm practical, we consider using the dual decomposition approach [104] and form the dual problem of (7.22) as

$$\begin{aligned}
\min_{\boldsymbol{\lambda_1},\boldsymbol{\lambda_2},\boldsymbol{\lambda_3},\boldsymbol{\lambda_4}} \max_{\boldsymbol{\rho},\mathbf{p}} \quad & \sum_{k=1}^{K} w_k \sum_{n=1}^{N} \rho_{k,n} \bar{r}_{k,n} \\
& + \sum_{n=1}^{N} \lambda_{1,n} \left(1 - \sum_{k=1}^{K} \rho_{k,n} \right) \\
& + \sum_{k=1}^{K} \lambda_{2,k} \left(\hat{P}_k - \sum_{n=1}^{N} \rho_{k,n} p_{k,n} \right) \\
& + \sum_{n=1}^{N} \lambda_{3,n} \left(\hat{I}_n - \sum_{k=1}^{K} q^{(B)}_{T_k,n} g'_{k,n} \rho_{k,n} p_{k,n} \right) \\
& + \sum_{k=1}^{K} \lambda_{4,k} \left(\sum_{n=1}^{N} \rho_{k,n} \bar{r}_{k,n} - \check{R}_k \right) \\
\text{subject to} \quad & \rho_{k,n} \in \{0,1\}, p_{k,n} \geq 0, \forall k, n, \\
& \lambda_{1,n} \geq 0, \lambda_{3,n} \geq 0, \forall n, \\
& \lambda_{2,k} \geq 0, \lambda_{4,k} \geq 0, \forall k,
\end{aligned} \tag{7.23}$$

where $\lambda_{1,n}$, $\lambda_{2,k}$, $\lambda_{3,n}$, and $\lambda_{4,k}$ are the introduced Lagrange multipliers, and the vectors $\boldsymbol{\lambda_1} = [\lambda_{1,1}, \lambda_{1,2}, ..., \lambda_{1,N}]^T$, $\boldsymbol{\lambda_2} = [\lambda_{2,1}, \lambda_{2,2}, ..., \lambda_{2,K}]^T$, $\boldsymbol{\lambda_3} = [\lambda_{3,1}, \lambda_{3,2}, ..., \lambda_{3,N}]^T$, and $\boldsymbol{\lambda_4} = [\lambda_{4,1}, \lambda_{4,2}, ..., \lambda_{4,K}]^T$, respectively.

Such a problem can be decomposed into two layers of subproblems. In the lower layer, we have K subproblems:

$$\begin{aligned} \max_{\boldsymbol{\rho}, \mathbf{p}} \quad & \sum_{n=1}^{N} \rho_{k,n} v_{k,n} \\ \text{subject to} \quad & \rho_{k,n} \in \{0, 1\}, p_{k,n} \geq 0, \forall k, n, \end{aligned} \tag{7.24}$$

where

$$v_{k,n} = (w_k + \lambda_{4,k}) \bar{r}_{k,n} - \lambda_{1,n} - \left(\lambda_{2,k} + \lambda_{3,n} q^{(B)}_{T_k,n} g'_{k,n}\right) p_{k,n}. \tag{7.25}$$

Let $\tilde{U}_k$ be the maximum value of the objective function in the lower layer; the master problem in the upper layer is

$$\begin{aligned} \min_{\boldsymbol{\lambda_1}, \boldsymbol{\lambda_2}, \boldsymbol{\lambda_3}, \boldsymbol{\lambda_4}} \quad & \sum_{k=1}^{K} \tilde{U}_k + \sum_{n=1}^{N} \lambda_{1,n} + \sum_{k=1}^{K} \lambda_{2,k} \hat{P}_k \\ & + \sum_{n=1}^{N} \lambda_{3,n} \hat{I}_n - \sum_{k=1}^{K} \lambda_{4,k} \check{R}_k \\ \text{subject to} \quad & \lambda_{1,n} \geq 0, \lambda_{3,n} \geq 0, \forall n, \\ & \lambda_{2,k} \geq 0, \lambda_{4,k} \geq 0, \forall k. \end{aligned} \tag{7.26}$$

In the lower layer, if $\rho_{k,n} = 1$, the power allocation can be determined in a water-filling fashion such that

$$p_{k,n} = \left[\frac{(w_k + \lambda_{4,k}) q^{(I)}_{R_k,n} B}{(\lambda_{2,k} + \lambda_{3,n} q^{(B)}_{T_k,n} g'_{k,n}) \ln 2} - \frac{\sigma^2}{g_{k,n}} \right]^+. \tag{7.27}$$

Then for any n, $\rho_{k,n}$ is chosen to be 1 for the largest $v_{k,n}$ defined in (7.25) substituting $p_{k,n}$ obtained through (7.27), and 0 otherwise. $p_{k,n}$ is then set to be 0 for any $\rho_{k,n} = 0$. Note that $\boldsymbol{\lambda_1}$ is actually not necessary in the optimization, which can be initialized to be $\mathbf{0}$ and does not need to be updated. The other multipliers can be updated using the subgradient method [104] as

$$\lambda^{(i+1)}_{2,k} = \left[\lambda^{(i)}_{2,k} - s^{(i)} \left(\hat{P}_k - \sum_{n=1}^{N} p^{(i)}_{k,n} \right) \right]^+, \tag{7.28}$$

$$\lambda_{3,n}^{(i+1)} = \left[\lambda_{3,n}^{(i)} - s^{(i)}\left(\hat{I}_n - \sum_{k=1}^{K} q_{T_k,n}^{(B)} g'_{k,n} p_{k,n}^{(i)}\right)\right]^+, \tag{7.29}$$

$$\lambda_{4,k}^{(i+1)} = \left[\lambda_{4,k}^{(i)} - s^{(i)}\left(\sum_{n=1}^{N} \rho_{k,n} \bar{r}_{k,n}^{(i)} - \check{R}_k\right)\right]^+, \tag{7.30}$$

where $s^{(i)}$ is a small positive step size for the ith iteration.

Although the original problem seems to be non-convex, the duality gap between the primal and dual problems tends to be 0 with practical number of channels [70, 106, 103]. From our simulation, only a small number of iterations are needed before the subgradient search converges with appropriate step sizes. Therefore, we can achieve optimal resource allocation in the multi-user CR network by following the above procedure.

From (7.27)-(7.30), we can see clearly how the probabilities of channel availability, $q_{T_k,n}^{(B)}$ and $q_{R_k,n}^{(I)}$, act in the resource allocation algorithm. They both have weighting effects in allocating proper power to each channel for different users. The probabilistic resource allocation will be equivalent to the decision-based aggressive resource allocation if we replace N with N_0 and setting $q_{R_k,n}^{(I)} = 1$ and $q_{T_k,n}^{(B)} = 0$ for all $n \leq N_0$ in (7.22). Similarly, the probabilistic resource allocation will be equivalent to the decision-based conservative resource allocation if we replace N with N_0 and set $q_{R_k,n}^{(I)} = q_{T_k,n}^{(B)} = 1$ for all $n \leq N_0$ in (7.22). Neither the decision-based aggressive nor the decision-based conservative approach performs as well as the probabilistic approach since the flexibility of OSA is not fully exploited in the decision-based aggressive approach that channel availability is determined by thresholding the probabilities regardless of decision error or in the decision-based conservative approach that strict interference limit is applied regardless of channel availability. In other words, too much confidence is given in the decision-based aggressive approach and too little confidence is given in the decision-based conservative approach while appropriate confidence is given in the probabilistic approach that will yield the best performance.

Moreover, by carefully looking into the proposed solution, we find that the above algorithm actually leads to a distributed implementation shown below.

1. Each CR user, U_k, $1 \leq k \leq K$, obtains the probabilistic information, $q^{(B)}_{T_k,n}$ and $q^{(I)}_{R_k,n}$, and initializes $\lambda_{2,k}$, $\lambda_{3,n}$, and $\lambda_{4,k}$ to be any non-negative values for each channel n, $1 \leq n \leq N$, where only $\lambda_{3,n}$ should be the same for all the users.

2. Each CR user, U_k, $1 \leq k \leq K$, calculates $p_{k,n}$ and $v_{k,n}$ according to (7.27) and (7.25) for each channel n, $1 \leq n \leq N$, and then reports $v_{k,n}$ to the other users.

3. For each channel n, $1 \leq n \leq N$, the CR user with the largest $v_{k,n}$ notifies the other users to set the transmit power in this channel as 0, updates $\lambda_{3,n}$ according to (7.29), and reports to the other users for updating.

4. Each CR user, U_k, $1 \leq k \leq K$, updates $\lambda_{2,k}$ and $\lambda_{4,k}$ according to (7.28) and (7.30) for each channel n, $1 \leq n \leq N$.

5. Repeat Steps 2)–4) until the multipliers converge.

Note that the CR users do not need to exchange most of the local information during the above resource allocation except the utility information inherited in $v_{k,n}$ and the interference information involved in $\lambda_{3,n}$, both of which are necessary since the former is needed when selecting a most favorable user for communication over a certain channel and the later is needed to make sure that the interference from secondary communication is within the tolerant level of the licensed users.

In practice, the channel gains between the licensed users and the CR users can be obtained through successive spectrum sensing. Since the CR users acquire the received licensed user signal strengths during spectrum sensing, they may be able to estimate the channel gain as long as they have certain prior knowledge of the transmitted licensed user signal strengths. If the channel gains cannot be obtained, an alternative approach is to deploy several measuring points for the CR network [107]. With known channel gains between the measuring points and CR users, we can instead limit the interference level at

these points. We may also consider quantizing the conditional probabilities using a few bits to reduce the overhead of reporting over the control channel.

If the licensed activity appears and disappears frequently, the licensed channel state may change during secondary communication. In this case, we may divide the whole frame of the secondary communication into several time slots and associate different $q^{(B)}_{T_k,n}$ and $q^{(I)}_{R_k,n}$ for each time slot according to the acquired licensed activity statistics 3. Then the same resource allocation procedure can be applied to each time slot.

7.5 Simulation Results

In this section, we present simulation results in three different scenarios. Given spectrum sensing information, the probabilistic resource allocation approach is compared with both decision-based aggressive and conservative resource allocation approaches. In the decision-based resource allocation approaches, Bayesian decision rule is used to determine the availability of Channel n at User k by comparing $\frac{P(\Omega_{T_k,n}|\mathcal{H}_{B,n})}{P(\Omega_{R_k,n}|\mathcal{H}_{I,n})}$ with $\frac{P_{I,n}}{P_{B,n}}$ [97], which is equivalent to comparing $q^{(B)}_{T_k,n}$ in (7.9) with $q^{(I)}_{R_k,n}$ in (7.10).

In the first scenario, we consider a single CR user opportunistically utilizing 4 licensed channels each with a bandwidth of 100 KHz. The maximum transmit power for the CR user is 10 mW and the interference constraint for each channel is 0.7 mW, which are normalized to zero path loss. The CR user has obtained the probabilistic information as $\mathbf{q}^{(I)}_{R_1} = [0.1,\ 0.2,\ 0.8,\ 0.9]^T$ and $\mathbf{q}^{(B)}_{T_1} = [0.9,\ 0.8,\ 0.2,\ 0.1]^T$ through spectrum sensing. In Figure 7.2, we compare the overall data rates of the CR user with different resource allocation approaches under different noise powers. When the noise power changes, the average SNR will change accordingly. All the channel gains are fixed to be 1, so we can focus on the impact of using probabilistic information from spectrum sensing on the performance of resource allocation. From the figure, the probabilistic approach achieves much higher throughput performance than decision-based conservative resource allocation. Although the overall data rate of decision-based aggressive resource allocation is close to that of the

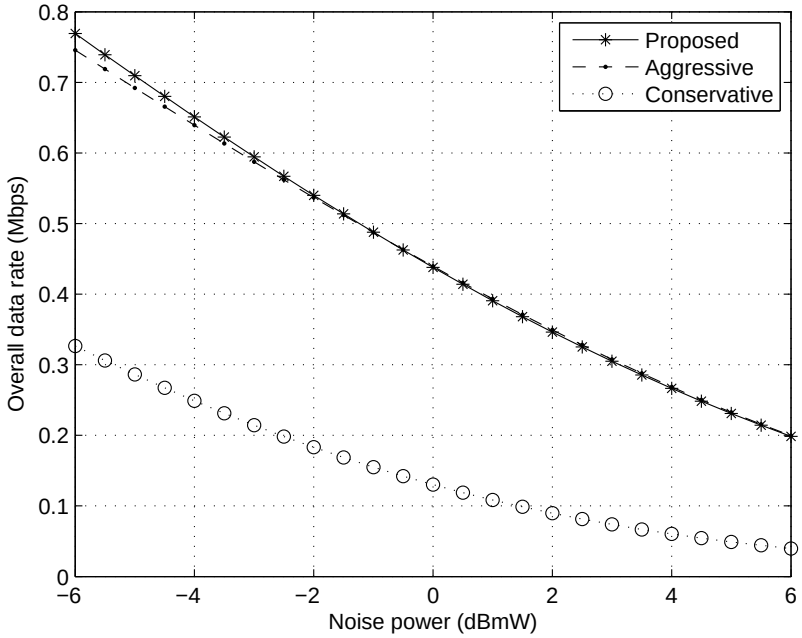

Figure 7.2. Overall data rates with respect to different noise powers with a single CR user.

proposed probabilistic approach, we observe in the simulation that the interference of the former with the licensed receiver in the third channel is as high as 1.0 mW, which exceeds the interference constraint and is thus harmful for the licensed communication. Therefore, the proposed probabilistic approach is the most favorable among the three approaches.

In the second scenario, we consider 2 CR users utilizing 16 licensed channels each with a bandwidth of 100 KHz. In this case, channel allocation has to be performed as well as power allocation. The maximum transmit power for the CR user is 10 mW and the interference constraint for each channel is 0.6 mW, which are normalized to zero path loss. The channels between the CR transmitters and receivers, and between the CR transmitters and licensed receivers are independent realizations of Rayleigh fading with unit power. The weights for the data rates of the two CR users are 1 and 2, and the minimum data rate requirements are 200 and 300 Kbps, respectively. Each CR user has obtained the same probabilistic information through spectrum sensing with $\mathbf{q}_{R_k}^{(I)}$ given in Table 7.1 under two different cases while $\mathbf{q}_{T_k}^{(B)} = \mathbf{1} - \mathbf{q}_{R_k}^{(I)}$. The weighted sum data rates under different noise

Table 7.1. Probabilistic information in resource allocation

Channel	1	2	3	4	5	6	7	8	9	10	11	12	13	14	15	16
Case 1	0.025	0.05	0.075	0.1	0.125	0.15	0.175	0.2	0.8	0.825	0.85	0.875	0.9	0.925	0.95	0.975
Case 2	0	0.0667	0.1333	0.2	0.2667	0.3333	0.4	0.4667	0.5333	0.6	0.6667	0.7333	0.8	0.8667	0.9333	1

powers with different resource allocation approaches are shown in Figures 7.3 and 7.4. It is obvious that the proposed probabilistic approach achieves the best throughput performance. The decision-based conservative and aggressive approaches using the hard decisions on the availability of licensed channels inherit decision errors from spectrum sensing, which results in the loss of spectrum opportunities. The throughput performance of decision-based conservative resource allocation is especially poor. Although the overall data rate of decision-based aggressive resource allocation is close to that of the proposed probabilistic approach, we observe that the interference of the former with the licensed receivers in certain channels exceeds the interference constraint as shown in Figure 7.5. Therefore, it is also preferable to use the proposed probabilistic approach in multi-user CR networks. The advantage of the proposed approach in Case 2 becomes more obvious from Figure 7.4 since there is much uncertainty under such probabilistic information so that resource allocation using the hard decisions from spectrum sensing will inherit plenty of decision errors and lose many spectrum opportunities.

In the third scenario, we consider 8 CR users utilizing 16 licensed channels each with a bandwidth of 100 KHz. Each CR user combines spectrum sensing information from 4 nearby cooperative CR nodes providing local hard decisions on licensed channel availability and the probability of incorrect local decision is 0.1. Meanwhile, the stable probability of presence of licensed user signal in each channel is 0.5. The required probabilistic information for the proposed resource allocation approach is computed according to (7.9) and (7.10). The weights for the data rates of the CR users are all set to be 1, and the minimum data rate requirements are 100 Kbps. Other parameters are the same as in the previous scenario. The weighted sum data rates, which turn into sum data rates in this scenario, under

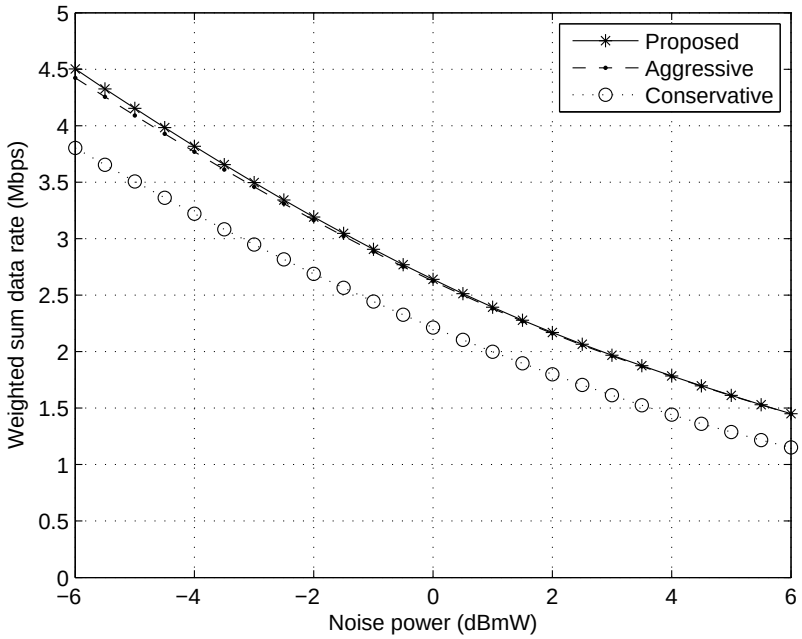

Figure 7.3. Weighted sum data rates with respect to different noise powers with 2 CR users in Case 1.

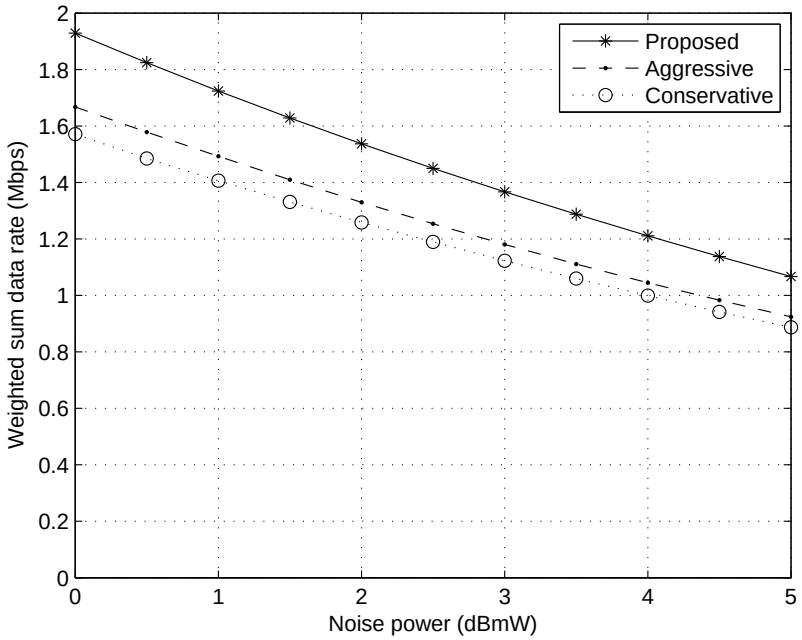

Figure 7.4. Weighted sum data rates with respect to different noise powers with 2 CR users in Case 2.

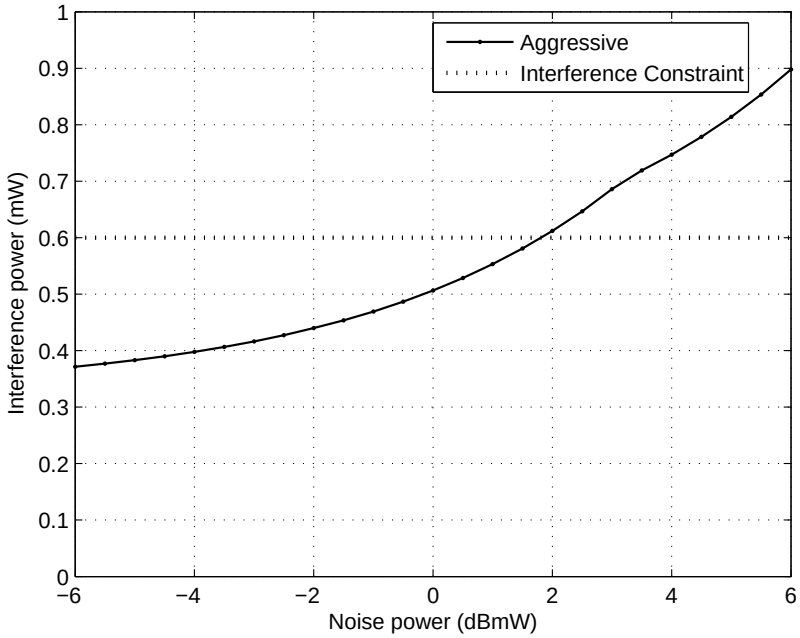

Figure 7.5. Received interference power in Channel 15 with respect to different noise powers in Case 1.

different noise powers with different resource allocation approaches are shown in Figure 7.6, which also implies that it is preferable to use the proposed probabilistic approach in multi-user CR networks. The proposed probabilistic approach achieves the best throughput performance, especially when it is compared with decision-based conservative resource allocation. Similarly, the interference of decision-based aggressive resource allocation with the licensed receivers does not always satisfy the interference constraint.

Figure 7.7 shows how the weighted sum data rate evolves in the iterations with the proposed algorithm in the third scenario when the noise power is -6 dBmW. The number of iterations required to reach convergence and achieve optimal resource allocation is around tens. Therefore, the proposed resource allocation algorithm converges fast and is practical for implementation.

7.6 Conclusion

In this chapter, we have provided a new resource allocation approach for OSA based on the probabilities of licensed channel availability obtained from spectrum sensing. Different

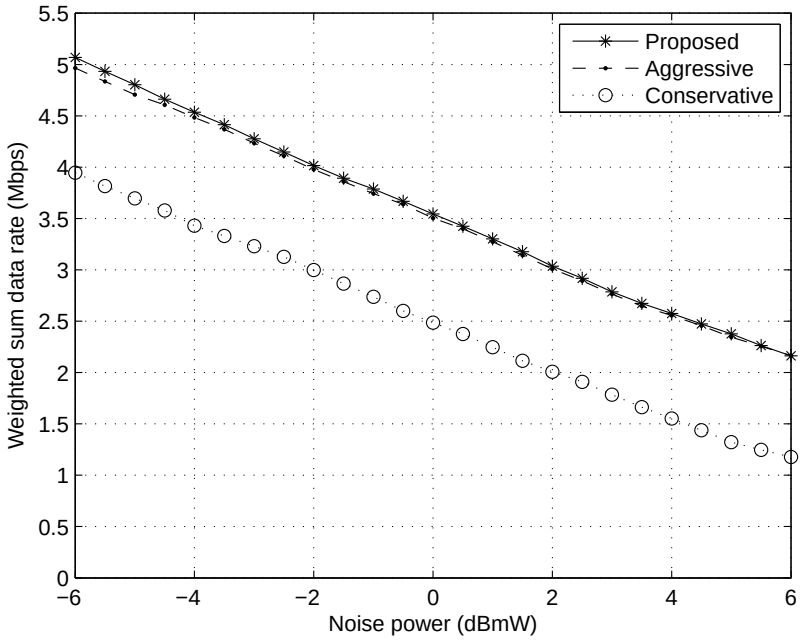

Figure 7.6. Weighted sum data rates with respect to different noise powers with 8 CR users.

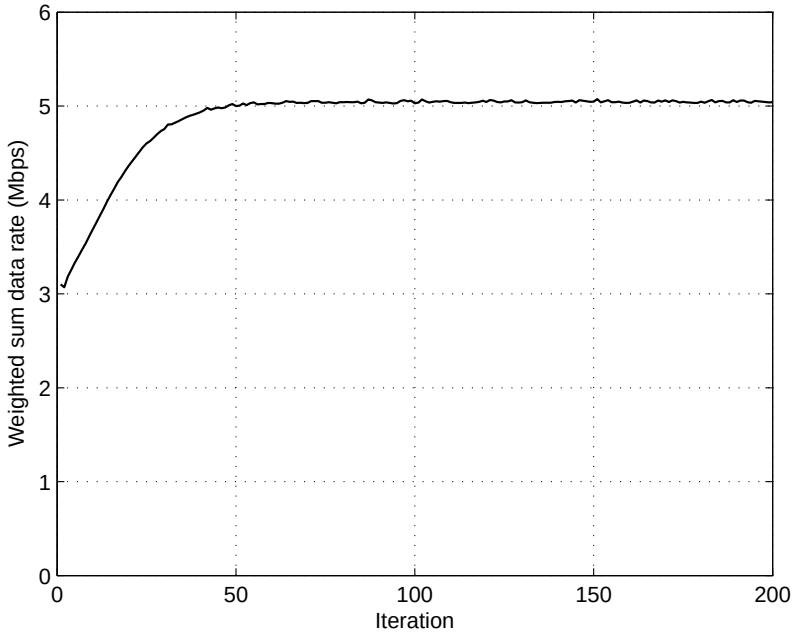

Figure 7.7. Evolution of weighted sum data rate in probabilistic resource allocation.

from conventional approaches, the probabilistic approach exploits the flexibility of OSA to ensure efficient spectrum usage and protect licensed users from unacceptable interference at the same time. It also supports diverse QoS requirements in multi-user networks and can be implemented in a distributed manner.

CHAPTER 8

CONCLUSION

In this dissertation, we focus on efficient spectrum sensing and utilization techniques for high-performance OSA. The main contribution is summarized as follows.

We have investigated both local spectrum sensing and cooperative spectrum sensing by exploring probabilistic information unique for CR. We have proposed probability-based periodic spectrum sensing by utilizing the statistical characteristics of licensed channel occupancy, which achieves nearly optimal performance with relatively low complexity. For the first time, the possibility that a licensed user appears in the middle of a sensing block has been taken into account. Based on the statistical model of licensed channel occupancy, we have also proposed periodic spectrum sensing scheduling to determine the optimal inter-sensing duration. Quick capture of spectrum opportunity is ensured when the licensed user signal is detected, and the spectrum efficiency is maximized under a given interference level when the licensed user signal is declared absent. The statistical information of licensed channel activity has been further used to vary the transmit power at each data sample to enhance throughput and reduce interference. Moreover, we have developed a probability-based scheme for combination of local sensing information collected from cooperative CR users, which enables combination of both synchronous and asynchronous sensing information. To satisfy the stringent bandwidth constraint for reporting, we have also proposed to simultaneously send local sensing data to a combining node through the same narrowband channel. The optimal local processing functions at the CR users and final decision rule at the combining node have been discussed when the reporting channel is Gaussian and experiences fading, respectively. Calculation of probabilistic information involved has been given as well. In the proposed approach, the bandwidth required for reporting does not change with the number of cooperative users. With proper preprocessing at individual users, such a design still maintains reasonable detection performance.

We have also addressed spectrum utilization including spectrum shaping and resource allocation by exploring probabilistic information. We have proposed a low-complexity spectrum shaping scheme for OFDM-based CR systems by mapping antipodal symbol pairs onto adjacent subcarriers at the edges of the utilized subbands. Sidelobe suppression and system throughput can be well balanced by adjusting the coding rate of the corresponding spectral precoder while power control on different sets of subcarriers has been introduced to further lower the sidelobes. We have also proposed a spectral precoding scheme for multiple OFDM-based CR users to enhance spectral compactness. By constructing individual precoders to render selected spectrum nulls, our scheme ensures user independence and provides sufficient OOB radiation suppression without BER performance loss. We have considered the selection of notched frequencies to further increase the bandwidth efficiency. The proposed schemes enable efficient spectrum sharing between CR and licensed users and exhibit the advantages of both simplicity and flexibility. We have also provided a new resource allocation approach for OSA based on the probabilities of licensed channel availability obtained from spectrum sensing. Different from conventional approaches, the probabilistic approach exploits the flexibility of OSA to ensure efficient spectrum usage and protect licensed users from unacceptable interference at the same time. The proposed approach supports diverse QoS requirements in multi-user networks and can be implemented in a distributed manner.

APPENDIX A

PROOF FOR CHAPTER 2

A.1 Proof of Proposition 2.2.1

The likelihood ratio between $\mathcal{H}_I$ and $\mathcal{H}_B$ given in (2.8) can be rewritten as

$$LR(\mathbf{R}) = \sum_{m=1}^{M} p'(m) e^{\nu}, \tag{A.1}$$

where

$$\nu = \frac{\gamma}{1+\gamma} \sum_{i=m}^{M} |r_i|^2 - (M - m + 1) \ln(1+\gamma). \tag{A.2}$$

In low SNR region where $\gamma \ll 1$,

$$\begin{aligned} \nu &\approx (M - m + 1)[\gamma - \ln(1+\gamma)] \\ &\approx \frac{\gamma^2 (M - m + 1)}{2} \ll 1, \end{aligned} \tag{A.3}$$

where the second approximation comes from the Taylor expansion of $\ln(1+\gamma)$ and the fact that $\gamma \ll 1$. Since $0 < \nu \ll 1$, $e^{\nu} \approx 1 + \nu$ and thus $LR(\mathbf{R})$ can be approximated by

$$\begin{aligned} LR(\mathbf{R}) &\approx \sum_{m=1}^{M} p'(m)(1+\nu) \\ &= 1 - \ln(1+\gamma) \sum_{m=1}^{M} p'(m)(M-m+1) + \frac{\gamma}{1+\gamma} T_P(\mathbf{R}), \end{aligned} \tag{A.4}$$

where

$$T_P(\mathbf{R}) = \sum_{m=1}^{M} \left(\sum_{i=1}^{m} p'(i) \right) |r_m|^2, \tag{A.5}$$

is the test statistics of the probability-based energy detection scheme. Since the first two items of (A.4) do not depend on the received signal vector, $\mathbf{R}$, the test statistics of the optimal detection scheme, $T_O(\mathbf{R})$, reduces to $T_P(\mathbf{R})$. In other words, the optimal detection scheme reduces to the probability-based energy detection scheme in low SNR region.

A.2 Proof of Proposition 2.3.1

To prove the proposition, we first show the following fact.

For any unbiased detection scheme, $c(n) + \varepsilon(1-a) - b(n) > 0$.

Proof

$$\begin{aligned}
& c(n) + \varepsilon(1-a) - b(n) \\
=& \sum_{m=1}^{M} p(m) P_{M,n}(m) + (1-P_F)\left(1 - \sum_{m=1}^{M} p(m)\right) - P_{M,n}(1) \\
>& P_{M,n}(1) \sum_{m=1}^{M} p(m) - P_{M,n}(1) + (1-P_F)\left(1 - \sum_{m=1}^{M} p(m)\right) \\
=& \left(1 - \sum_{m=1}^{M} p(m)\right)\left[P_{D,n}(1) - P_F\right], \qquad \text{(A.6)}
\end{aligned}$$

where the inequality comes from the fact that $P_{M,n}(m) > P_{M,n}(1)$, $1 < m \leq M$, since $P_{M,n}(m)$ increases with m, the location in the sensing block where the licensed user appears. In (A.6), P_F denotes the target false alarm probability and $P_{D,n}(1) = 1 - P_{M,n}(1)$ denotes the detection probability in the nth sensing block under $\mathcal{H}_B$. For any unbiased detection scheme, $P_{D,n}(1) > P_F$ and thus $c(n) + \varepsilon(1-a) - b(n) > 0$.

Proof of the proposition: According to (2.31),

$$\begin{aligned}
f'(x) &= \frac{df(x)}{dx} \\
&= \frac{\varepsilon b(1-a)}{\{[b-c-\varepsilon(1-a)]\, x + c + \varepsilon(1-a)\}^2} > 0, 0 \leq x \leq 1,
\end{aligned} \qquad \text{(A.7)}$$

which indicates that $f(x)$ is an increasing function. We further obtain the second order derivative of $f(x)$ as

$$f''(x) = \frac{d^2 f(x)}{dx^2} = \frac{2\varepsilon b(1-a)\,[c + \varepsilon(1-a) - b]}{\{[b-c-\varepsilon(1-a)]\, x + c + \varepsilon(1-a)\}^3}. \qquad \text{(A.8)}$$

According to Fact 1, $c + \varepsilon(1-a) - b > 0$. As a result, $f''(x) > 0$ for any $x \in [0,1]$, i.e., $f'(x)$ is also an increasing function of x. Since $f'(x) > 0$ and $f''(x) > 0$, $f(x)$ is a convex and monotonically increasing function, which completes the proof.

A.3 Proof of Proposition 2.3.2

To investigate the convergence of $x(n)$, we define $\Delta(n) = x(n) - x_c^*$ and then

$$\frac{\Delta(n+1)}{\Delta(n)} = \frac{x(n+1) - x_c^*}{x(n) - x_c^*} = \frac{f\left(x(n)\right) - f(x_c^*)}{x(n) - x_c^*}. \tag{A.9}$$

Since it has been shown that $f(x)$ is an increasing function in Appendix A.2, $\frac{\Delta(n+1)}{\Delta(n)} > 0$. With $x(1) = 0$, $x(n) < x_c^*$ for any n. Since $f(x)$ is a convex function and $x(n) < x_c^*$, we have

$$\frac{\Delta(n+1)}{\Delta(n)} = \frac{f\left(x(n)\right) - f(x_c^*)}{x(n) - x_c^*} < f'(x_c^*). \tag{A.10}$$

and

$$\left[f'(x_c^*)\right]^n \Delta(1) < \Delta(n+1) < 0, \quad n \geq 1, \tag{A.11}$$

where $f'(x_c^*) = \frac{df(x)}{dx}|_{x=x_c^*}$ is a constant independent of n. According to (2.35) and (A.7),

$$f'(x_c^*) = \begin{cases} \frac{\varepsilon(1-a)}{b}, & \text{if } \gamma \leq \gamma_c^*, \\ \frac{b}{\varepsilon(1-a)}, & \text{if } \gamma > \gamma_c^*, \end{cases} \tag{A.12}$$

which indicates that $0 < f'(x_c^*) \leq 1$ where the equality holds if and only if $\gamma = \gamma_c^*$. Thus Equation (A.11) verifies that $x(n)$ is an increasing sequence and converges at x_c^* linearly with the convergence ratio $f'(x_c^*)$, which completes the proof.

A.4 Proof of Proposition 2.3.3

To prove the convergence of $x(n)$ for the probability-based energy detection scheme when $\gamma > \gamma_p^*$, we first investigate the characteristic of function $\phi = h\left(x\right)$. According to the stable detection performance analysis of the fixed weight energy detection scheme, $\phi(n) = h(x(n))$ can be equivalently regarded as the stable probability of the presence of the licensed user at the beginning of each CR frame when the fixed weight is determined based on $x(n)$ as

$$w_i = \frac{\sum_{m=1}^{i} p_n(m)}{\sum_{m=1}^{M} p_n(m)}, \quad 1 \leq i \leq M, \tag{A.13}$$

where $p_n(m)$ is defined in (2.24).

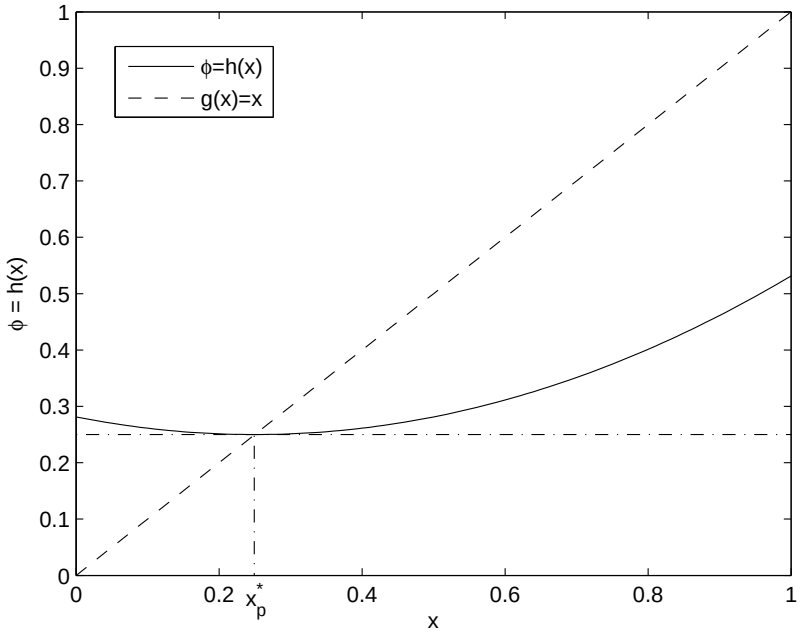

Figure A.1. Illustrative curve of $\phi = h(x)$

Figure A.1 shows the illustrative curve of $\phi = h(x)$ in which point $(x, h(x))$ denotes that the fixed weight is determined based on x and $x(n)$ converges at $\phi = h(x)$ accordingly. As analyzed, the probability-based energy detection scheme is nearly optimal in the sense that it maximizes the detection probability for a given false alarm probability. Therefore, the best stable detection performance is achieved when x, based on which the fixed wight is obtained, equals the limit of $x(n)$ since, in this case, the weight obtained is optimal.[1] In other words, $\phi = h(x)$ reaches its minimum value when it intersects with $g(x) = x$, as indicated in Figure A.1. Denote (x_p^*, x_p^*) as the intersection of $h(x)$ and $g(x)$, and then $h(x) \geq x_p^*$, where the equality holds if and only if $x = x_p^*$. If $x < x_p^*$, $h(x) > x$; if $x > x_p^*$, $h(x) < x$.

In the following, we utilize the characteristics of function $\phi = h(x)$ analyzed above to prove the convergence of $x(n)$ at x_p^*. To that end, two different scenarios are considered.

Scenario 1: suppose that $x(n) \leq x_p^*$ for any n. In this case, $\phi(n) = h(x(n)) \geq x(n)$. Since

[1] Suppose that $h(x)$ reaches its minimum value at $(x^*, h^*(x))$ where $h^*(x) \neq x^*$. Since $h^*(x) \neq x^*$, the weight based on x^* is not optimal and a smaller value of $h(x)$ can be achieved by adjusting the weight appropriately.

$\delta(n) \propto \phi(n) - x(n)$, $\delta(n) \geq 0$ for any n, where the equality holds if and only if $x(n) = x_p^*$. Hence, $x(n)$ is an increasing sequence and converges at x_p^*.

Scenario 2: suppose that $x(n) < x_p^*$ for any $n < N$ and $x(N) \geq x_p^*$, $N \geq 1$. In this case, it can be proved that $x(n)$ for $n \geq N$ is a decreasing sequence and converges at x_p^*.

Proof We prove it with induction.

Step 1: Obviously $x(N) \geq x_p^*$ holds.

Step 2: Suppose that $x(n) \geq x_p^*$, $n \geq N$, and then $\phi(n) = h(x(n)) \leq x(n)$. Since $-1 < \frac{x(n)-1}{\varphi(n)-x(n)} < 0$, based on (2.38), $\phi(n) - x(n) \leq \delta(n) \leq 0$. In other words, $\phi(n) \leq x(n+1) \leq x(n)$. Since $\phi(n) = h(x(n)) \geq x_p^*$, $x_p^* \leq x(n+1) \leq x(n)$, which, when $x(n) = x_p^*$, reduces to $x(n+1) = x(n) = x_p^*$.

Combine Steps 1 and 2, and then it is proved that $x(n)$ for $n \geq N$ is a decreasing sequence and converges at x_p^*.

Summarize Scenarios 1 and 2, and then we complete the proof of the proposition.

APPENDIX B

PROOF FOR CHAPTER 4

B.1 Proof of Proposition 4.3.1

Since all users have the same detection and false alarm probabilities and obtain sensing information at the same time, $P_{D,k} = P_D$, $P_{F,k} = P_F$, $t_k = t - \Delta t$, and $u_k = 0$ or 1, $k = 1, 2, ..., K$. Accordingly, the log-likelihood ratio can be obtained based on (4.1) as

$$\log Y = A \sum_{k=1}^{K} u_k + B(K - \sum_{k=1}^{K} u_k). \tag{B.1}$$

where $A = \log \frac{P_D e^{-\alpha\Delta t} + P_F(1-e^{-\alpha\Delta t})}{P_D(1-e^{-\beta\Delta t}) + P_F e^{-\beta\Delta t}}$ and $B = \log \frac{(1-P_D)e^{-\alpha\Delta t} + (1-P_F)(1-e^{-\alpha\Delta t})}{(1-P_D)(1-e^{-\beta\Delta t}) + (1-P_F)e^{-\beta\Delta t}}$. Let $D = \log \frac{P_I C_F}{P_B C_M}$, then the decision rule in (5.6) can be simplified as

$$\sum_{k=1}^{K} u_k \underset{\mathcal{H}_I}{\overset{\mathcal{H}_B}{\gtrless}} \frac{D - KA}{A - B}, \tag{B.2}$$

Equation (B.2) verifies that the optimal combination scheme reduces to the "K_0-out-of-K" scheme where $K_0 = \left\lceil \frac{D-KA}{A-B} \right\rceil$ and $\lceil x \rceil$ denotes the smallest integer greater than x.

APPENDIX C

PROOF FOR CHAPTER 5

C.1 Proof of (5.18)

C in (4.2) can be expressed as

$$
\begin{aligned}
C = & \sum_{q_1,q_2,...,q_K} C_F P(d=\mathcal{H}_B|q_1,q_2,...,q_K)P(q_1,q_2,...,q_K|\mathcal{H}_I)P_I \\
& + \sum_{q_1,q_2,...,q_K} C_M P(d=\mathcal{H}_I|q_1,q_2,...,q_K)P(q_1,q_2,...,q_K|\mathcal{H}_B)P_B \\
= & \sum_{q_1,q_2,...,q_K} C_F \int_{\varsigma}^{\infty} f(|z|^2|q_1,q_2,...,q_K)d|z|^2 \int_{R_{K,q_K}}...\int_{R_{2,q_2}}\int_{R_{1,q_1}} f(y_1,y_2,...,y_K|\mathcal{H}_I)dy_1dy_2...dy_K P_I \\
& + \sum_{q_1,q_2,...,q_K} C_M \int_{0}^{\varsigma} f(|z|^2|q_1,q_2,...,q_K)d|z|^2 \int_{R_{K,q_K}}...\int_{R_{2,q_2}}\int_{R_{1,q_1}} f(y_1,y_2,...,y_K|\mathcal{H}_B)dy_1dy_2...dy_K P_B \\
= & \sum_{q_1,q_2,...,q_K} C_F \int_{\varsigma}^{\infty} f(|z|^2|q_1,q_2,...,q_K)d|z|^2 \prod_{k=1}^{K}\int_{R_{k,q_k}} f(y_k|\mathcal{H}_I)dy_k P_I \\
& + \sum_{q_1,q_2,...,q_K} C_M \int_{0}^{\varsigma} f(|z|^2|q_1,q_2,...,q_K)d|z|^2 \prod_{k=1}^{K}\int_{R_{k,q_k}} f(y_k|\mathcal{H}_B)dy_k P_B \\
= & \sum_{A_i}\sum_{q_1,q_2,...,q_{j-1},q_{j+1},...,q_K} C_F \int_{\varsigma}^{\infty} f(|z|^2|q_1,q_2,...,q_{j-1},q_j=A_i,q_{j+1},...,q_K)d|z|^2 \\
& \cdot \int_{R_{j,A_i}} f(y_j|\mathcal{H}_I)dy_j \prod_{k=1,k\neq j}^{K}\int_{R_{k,q_k}} f(y_k|\mathcal{H}_I)dy_k P_I \\
& + \sum_{A_i}\sum_{q_1,q_2,...,q_{j-1},q_{j+1},...,q_K} C_M \int_{0}^{\varsigma} f(|z|^2|q_1,q_2,...,q_{j-1},q_j=A_i,q_{j+1},...,q_K)d|z|^2 \\
& \cdot \int_{R_{j,A_i}} f(y_j|\mathcal{H}_B)dy_j \prod_{k=1,k\neq j}^{K}\int_{R_{k,q_k}} f(y_k|\mathcal{H}_B)dy_k P_B, \qquad \text{(C.1)}
\end{aligned}
$$

where the first equation holds according to Bayes' theorem [84] and the third equation follows from the conditional independence of local observations from different CR users. The last equation results from expanding the cost C with respect to the local processing function of the jth CR user. Therefore, with (5.19) and (5.20), C can be written as in (5.18).

APPENDIX D

PROOF FOR CHAPTER 7

D.1 Proof of Proposition 7.3.1

We prove it by showing a counterexample.

In the decision-based aggressive resource allocation, the power allocation is in a water-filing fashion such that

$$p_{1,n} = \left[\frac{B}{\lambda \ln 2} - \frac{\sigma^2}{g_{1,n}} \right]^+, \tag{D.1}$$

where λ satisfies

$$\sum_{n=1}^{N_0} p_{1,n} = \hat{P}_1. \tag{D.2}$$

Therefore, if a certain channel, say n', is much more favorable than the others, it is possible that

$$p_{1,n} = \begin{cases} \hat{P}_1, & n = n', \\ 0, & \text{otherwise} \end{cases} \tag{D.3}$$

when the maximum transmit power is low. In the case that

$$q_{T_1,n'}^{(B)} g'_{1,n'} \hat{P}_1 > \hat{I}_{n'}, \tag{D.4}$$

the average interference will be beyond the acceptable level.

D.2 Proof of Proposition 7.3.2

Formulate a modified probabilistic resource allocation by changing N to N_0 in (7.11) as the following optimization problem

$$\begin{aligned} \max_{\mathbf{p}} \quad & \sum_{n=1}^{N_0} \bar{r}_{1,n} \\ \text{subject to} \quad & \sum_{n=1}^{N_0} p_{1,n} \le \hat{P}_1, p_{1,n} \ge 0, \forall n, \\ & q_{T_1,n}^{(B)} g'_{1,n} p_{1,n} \le \hat{I}_n, \forall n. \end{aligned} \tag{D.5}$$

When the interference constraints are inactive, the constraints for the decision-based aggressive resource allocation and the modified probabilistic resource allocation are the same. The objective of the modified probabilistic resource allocation is to maximize the average data rate $\sum_{n=1}^{N_0} \bar{r}_{1,n}$ while the decision-based aggressive resource allocation is with a different objective, to maximize $\sum_{n=1}^{N_0} r_{1,n}$. So the average data rate of the modified probabilistic resource allocation, $\bar{r}_1^{(m)}$, is of course not smaller than that of the decision-based aggressive resource allocation, $\bar{r}_1^{(a)}$. Meanwhile, the modified probabilistic resource allocation is suboptimal by limiting the transmit power to be within the N_0 channels, the average data rate of which is obviously no more than that of the original probabilistic resource allocation, $\bar{r}_1$. Therefore,

$$\bar{r}_1^{(a)} \leq \bar{r}_1^{(m)} \leq \bar{r}_1, \tag{D.6}$$

which completes the proof.

D.3 Proof of Proposition 7.3.3

Compare the optimization problem of the modified resource allocation defined above and the decision-based conservative resource allocation, we can find that the only difference is in the interference constraints. When the maximum power constraint is inactive for both, the allowed transmit power in each channel of the modified probabilistic resource allocation is not smaller than that of the decision-based conservative resource allocation since $q_{T_1,n}^{(B)} \leq 1$. So the average data rate of the latter, $\bar{r}_1^{(c)}$, is no more than that of the former, $\bar{r}_1^{(m)}$, due to the fact that the average data rate is monotone increasing with the allocated transmit powers. Meanwhile, the modified probabilistic resource allocation is suboptimal by limiting the transmit power to be within the N_0 channels, the average data rate of which is no more than that of the original probabilistic resource allocation, $\bar{r}_1$. Therefore,

$$\bar{r}_1^{(c)} \leq \bar{r}_1^{(m)} \leq \bar{r}_1, \tag{D.7}$$

which completes the proof.

REFERENCES

[1] FCC, "Spectrum policy task force report," *ET Docket No. 02-135*, Nov. 2002.

[2] FCC, "Spectrum policy task force report," *ET Docket No. 02-155*, Nov. 2002.

[3] J. Mitola, "Software radios: survey, critical evaluation and future directions," *IEEE Aerosp. Electron. Syst. Mag.*, vol. 8, pp. 25–31, Apr. 1993.

[4] J. Mitola and G. Q. Maguire, "Cognitive radio: making software radios more personal," *IEEE Personal Commun.*, vol. 6, p. 13, Aug. 1999.

[5] S. Haykin, "Cognitive radio: brain-empowered wireless communications," *IEEE J. Sel. Areas Commun.*, vol. 23, pp. 201–220, Feb. 2005.

[6] I. F. Akyildiz, W. Y. Lee, M. C. Vuran, and S. Mohanty, "Next generation dynamic spectrum access cognitive radio wireless networks: a survey," *Comput. Netw. J. (Elsevier)*, vol. 50, pp. 2127–2159, Sept. 2006.

[7] Q. Zhao and B. M. Sadler, "A survey of dynamic spectrum access: signal processing, networking, and regulatory policy," *IEEE Signal Process. Mag.*, vol. 24, pp. 79–89, Mar. 2007.

[8] J. Mitola, A. Attar, H. Zhang, O. Holland, H. Harada, and H. Aghvami, "Special issue on achievements and the road ahead: the first decade of cognitive radio," *IEEE Trans. Veh. Tech.*, vol. 59, May 2010.

[9] B. Wang and K. J. R. Liu, "Advances in cognitive radio networks: a survey," *IEEE J. Sel. Topics Signal Process.*, vol. 5, pp. 5–23, Feb. 2011.

[10] C. Cordeiro, K. Challapali, D. Birru, and N. S. Shankar, "IEEE 802.22: an introduction to the first wireless standard based on cognitive radios," *J. Commun.*, vol. 1, pp. 38–47, Apr. 2006.

[11] R. V. Prasad, P. Pawelczak, J. A. Hoffmeyer, and H. S. Berger, "Cognitive functionality in next generation wireless networks: standardization efforts," *IEEE Commun. Mag.*, vol. 46, pp. 72–78, Apr. 2008.

[12] FCC, "Notice of proposed rule making and order," *ET Docket No. 03-322*, Dec. 2003.

[13] D. Cabric, S. M. Mishra, and R. W. Brodersen, "Implementation issues in spectrum sensing for cognitive radios," in *Proc. IEEE Asilomar Conf. Signals, Syst. and Comput., Pacific Grove, CA*, pp. 772–776, Nov. 2004.

[14] S. Haykin, D. J. Thomson, and J. H. Reed, "Spectrum sensing for cognitive radio," *Proc. IEEE*, vol. 97, pp. 849–877, May 2010.

[15] A. Ghasemi and E. S. Sousa, "Collaborative spectrum sensing for oppotunistic access in fading environments," in *Proc. IEEE Int. Symp. New Frontiers in Dynamic Spectrum Access Networks, Baltimore, MD*, pp. 131–136, Nov. 2005.

[16] T. Clancy, "Achievable capacity under the interference temperature model," in *Proc. IEEE Int. Conf. Comput. Commun. (INFOCOM)*, May 2007.

[17] H. V. Poor, *An Introduction to Signal Detection and Estimation*. New York: Springer-Verlag, 2nd ed., 1994.

[18] M. Ghozzi, F. Marx, M. Dohler, and J. Palicot, "Cyclostatilonarilty-based test for detection of vacant frequency bands," in *Proc. Int. Conf. Cognitive Radio Oriented Wireless Networks and Commun., Mykonos Island, Greece*, June 2006.

[19] P. D. Sutton, K. E. Nolan, and L. E. Doyle, "Cyclostationary signature in practial cognitive radio applications," *IEEE J. Sel. Areas Commun.*, vol. 26, pp. 13–24, Jan. 2008.

[20] Z. Quan, W. Zhang, S. J. Shellhammer, and A. H. Sayed, "Optimal spectral feature detection for spectrum sensing at very low SNR," *IEEE Trans. Commun.*, vol. 51, pp. 201–212, Jan. 2011.

[21] A. V. Dandawate and G. B. Giannakis, "Statistical tests for presence of cyclostationarity," *IEEE Trans. Signal Process.*, vol. 42, pp. 2355–2369, Sept. 1994.

[22] W. Gardner, "Signal interception: a unifying theoretical framework for feature detection," *IEEE Trans. Commun.*, vol. 8, pp. 897–906, Aug. 1988.

[23] Z. Tian and G. B. Giannakis, "A wavelet approach to wideband spectrum sensing for cognitive radios," in *Proc. IEEE Int. Conf. Cognitive Radio Oriented Wireless Networks and Commun., Mykonos Island, Greece*, June 2006.

[24] Y. Zeng and Y. C. Liang, "Maximum-minimum eigenvalue detection for cognitive radio," in *Proc. IEEE Int. Symp. Personal, Indoor and Mobile Radio Commun., Athens, Greece*, Sept. 2007.

[25] A. Kortun, T. Ratnarajah, Sellathurai, C. M., Zhong, and C. B. Papadias, "On the performance of eigenvalue-based cooperative spectrum sensing for cognitive radio," *IEEE J. Sel. Topics Signal Process.*, vol. 5, pp. 49–55, Feb. 2011.

[26] M. Ghozzi, M. Dohler, F. Marx, and J. Palicot, "Cognitive radio: methods for the detection of free bands," *Comptes Rendus Physique*, vol. 7, no. 7, pp. 74–81, 2006.

[27] A. T. Hoang and Y.-C. Liang, "Adaptive scheduling of spectrum sensing periods in cognitive radio networks," in *Proc. IEEE Global Telecommun. Conf., Washington, DC*, pp. 3128–3132, Nov. 2007.

[28] A. T. Hoang, Y.-C. Liang, and Y. Zeng, "Adaptive joint scheduling of spectrum sensing and data transmission in cognitive radio networks," *IEEE Trans. Commun.*, vol. 58, pp. 235–246, Jan. 2010.

[29] Q. Zhao, S. Geirhofer, L. Tong, and B. M. Sadler, "Optimal dynamic spectrum access via periodic channel sensing," in *Proc. IEEE Wireless Commun. and Networking Conf., Hong Kong*, pp. 33–37, Mar. 2007.

[30] P. Wang, L. Xiao, S. Zhou, and J. Wang, "Optimization of detection time for channel efficiency in cognitive radio systems," in *Proc. IEEE Wireless Commun. and Networking Conf., Hong Kong*, pp. 111–115, Mar. 2007.

[31] H. Kim and K. G. Shin, "Efficient discovery of spectrum opportunities with MAC-layer sensing in cognitive radio networks," *IEEE Trans. Mobile Comput.*, vol. 7, pp. 533–545, May 2008.

[32] Y. Pei, A. T. Hoang, and Y.-C. Liang, "Sensing-throughput tradeoff in cognitive radio networks: how frequently should spectrum sensing be carried out," in *Proc. IEEE Int. Symp. Personal, Indoor and Mobile Radio Commun., Athens, Greece*, pp. 1–5, Sept. 2007.

[33] W. Y. Lee and I. F. Akyildiz, "Optimal spectrum sensing framework for cognitive radio networks," *IEEE Trans. Wireless Commun.*, vol. 7, pp. 3845–3857, Oct. 2008.

[34] Z. Quan, S. Cui, and A. H. Sayed, "Optimal linear cooperation for spectrum sensing in cognitive radio networks," *IEEE J. Sel. Topics Signal Process.*, vol. 2, pp. 28–40, Feb. 2008.

[35] G. Taricco, "Optimization of linear cooperative spectrum sensing for cognitive radio networks," *IEEE J. Sel. Topics Signal Process.*, vol. 5, pp. 77–86, Feb. 2011.

[36] R. Fan and H. Jiang, "Optimal multi-channel cooperative sensing in cognitive radio networks," *IEEE Trans. Wireless Commun.*, vol. 9, pp. 1128–1138, Mar. 2010.

[37] G. Ganesan and Y. (G.) Li, "Cooperative spectrum sensing in cognitive radio - Part I: two user networks," *IEEE Trans. Wireless Commun.*, vol. 6, pp. 2204–2213, June 2007.

[38] G. Ganesan and Y. (G.) Li, "Cooperative spectrum sensing in cognitive radio - Part II: multiuser networks," *IEEE Trans. Wireless Commun.*, vol. 6, pp. 2214–2222, June 2007.

[39] L.S. Cardoso, M. Debbah, P. Bianchi, and J. Najim, "Cooperative spectrum sensing using random matrix theory," in *Proc. Int. Symp. Wireless Pervasive Computing*, pp. 334–338, May 2008.

[40] J. Ma, G. D. Zhao, and Y. (G.) Li, "Soft combination and detection for cooperative spectrum sensing in cognitive radio networks," *IEEE Trans. Wireless Commun.*, vol. 7, pp. 4502–4507, Nov. 2008.

[41] E. C. Y. Peh and Y.-C. Liang, "Optimization for cooperative sensing in cognitive radio networks," in *Proc. IEEE Wireless Commun. and Networking Conf.*, 2007.

[42] P. K. Varshney, *Distributed detection and data fusion*. New York: Springer-Verlag, 1997.

[43] E. C. Y. Peh, Y.-C. Liang, Y. L. Guan, and Y. Zeng, "Optimization of cooperative sensing in cognitive radio networks: a sensing-throughput tradeoff view," *IEEE Trans. Veh. Tech.*, vol. 58, pp. 5294–5299, Sept. 2010.

[44] W. Han, J. Li, Z. Tian, and Y. Zhang, "Efficient cooperative spectrum sensing with minimum overhead in cognitive radio," *IEEE Trans. Wireless Commun.*, vol. 9, pp. 3006–3010, Oct. 2010.

[45] E. C. Y. Peh, Y.-C. Liang, Y. L. Guan, and Y. Zeng, "Cooperative spectrum sensing in cognitive radio networks with weighted decision fusion schemes," *IEEE Trans. Wireless Commun.*, vol. 9, pp. 3838–3847, Dec. 2010.

[46] A. Ghasemi and E. S. Sousa, "Opportunistic spectrum access in fading channels through collaborative sensing," *J. Commun.*, vol. 2, pp. 71–82, Mar. 2007.

[47] J. Lunden, V. Koivunen, A. Huttunen, and H. V. Poor, "Censoring for collaborative spectrum sensing in cognitive radios," in *Proc. Asilomar Conf. Signals, Syst. and Comput., Pacific Grove, CA*, pp. 772–776, Nov. 2007.

[48] A. W. Min, X. Zhang, and K. G. Shin, "Detection of small-scale primary users in cognitive radio networks," *IEEE J. Sel. Areas Commun.*, vol. 29, pp. 349–361, Feb. 2011.

[49] A. Anandkumar and L. Tong, "Type-based random access for distributed detection over multiaccess fading channels," *IEEE Trans. Signal Process.*, vol. 55, pp. 5032–5043, Oct. 2007.

[50] C. Song and Q. Zhang, "Sliding-window algorithm for asynchronous cooperative sensing in wireless cognitive networks," in *Proc. IEEE Int. Conf. Commun.*, pp. 3432–3436, May 2008.

[51] X. Zhang, Z. Qiu, and D. Mu, "Asynchronous cooperative spectrum sensing in cognitive radio," in *Proc. IEEE Int. Conf. Signal Process.*, pp. 2020–2023, Oct. 2008.

[52] J. Ma, G. Y. Li, and B. H. Juang, "Signal processing in cognitive radio," *Proc. IEEE*, vol. 97, pp. 805–823, May 2009.

[53] T. A. Weiss and F. K. Jondral, "Spectrum pooling: an innovative strategy for the enhancement of spectrum efficiency," *IEEE Commun. Mag., Radio Commun. Suppl.*, pp. 8–14, Mar. 2004.

[54] D. Chen, Q. Zhang, and W. Jia, "Aggregation aware spectrum assignment in cognitive ad-hoc networks," in *Proc. IEEE Int. Conf. Cognitive Radio Oriented Wireless Networks and Commun., Sigapore*, May 2008.

[55] T. Weiss, J. Hillenbrand, A. Krohn, and F. K. Jondral, "Mutual interference in OFDM-based spectrum pooling systems," in *Proc. IEEE Veh. Tech. Conf., Milan, Italy*, vol. 4, pp. 1873–1877, May 2004.

[56] H. A. Mahmoud and H. Arslan, "Sidelobe suppression in OFDM-based spectrum sharing systems using adaptive symbol transition," *IEEE Commun. Let.*, vol. 12, pp. 133–135, Feb. 2008.

[57] H. Yamaguchi, "Active interference cancellation technique for MB-OFDM cognitive radio," in *Proc. Eur. Microw. Conf., Amsterdam, Netherlands*, vol. 2, pp. 1105–1108, Oct. 2004.

[58] I. Cosovic, S. Brandes, and M. Schnell, "Subcarrier weighting: a method for sidelobe suppresion in OFDM systems," *IEEE Commun. Let.*, vol. 10, pp. 444–446, June 2006.

[59] S. Ahmed, R. U. Rehman, and H. Hwang, "New techniques to reduce sidelobes in OFDM system," in *Proc. Int. Conf. Convergence Hybrid Inform. Tech.*, pp. 117–121, Nov. 2008.

[60] M. Ohta, A. Iwase, and K, Yamashita, "Improvement of the error characteristics of N-continuous OFDM system by SLM," *IEICE Electronics Express*, vol. 7, pp. 1354–1358, Sept. 2010.

[61] C.-D. Chung, "Spectral precoding for rectangularly pulsed OFDM," *IEEE Trans. Commun.*, vol. 56, pp. 1498–1510, Sept. 2008.

[62] J. van de Beek and F. Berggren, "EVM-constrained OFDM precoding for reduction of out-of-band emission," in *Proc. IEEE Veh. Tech. Conf., Anchorage, AK*, Sept. 2009.

[63] J. van de Beek, "Sculpting the multicarrier spectrum: a novel projection precoder," *IEEE Commun. Let.*, vol. 13, pp. 881–883, Dec. 2009.

[64] R. Zhang, "On peak versus average interference power constraints for protecting primary users in cognitive radio networks," *IEEE Trans. Wireless Commun.*, vol. 8, pp. 2112–2120, Apr. 2009.

[65] Q. Zhao, L. Tong, and A. Swami, "Decentralized cognitive MAC for dynamic spectrum access," in *Proc. IEEE Int. Symp. New Frontiers in Dynamic Spectrum Access Networks, Baltimore, MD*, pp. 224–232, Nov. 2005.

[66] Y. Xing, R. Chandramouli, S. Mangold, and N. S. Shankar, "Dynamic spectrum access in open spectrum wireless networks," *IEEE J. Sel. Areas Commun.*, vol. 24, pp. 626–637, Mar. 2006.

[67] J. Huang, R. A. Berry, and M. L. Honig, "Distributed interference compensation for wireless networks," *IEEE J. Sel. Areas Commun.*, vol. 24, pp. 1074–1084, May 2006.

[68] L. M. C. Hoo, B. Halder, J. Tellado, and J. M. Cioffi, "Multiuser transmit optimization for multicarrier broadcast channels: asymptotic FDMA capacity region and algorithms," *IEEE Trans. Commun.*, vol. 52, pp. 922–930, June 2004.

[69] D. P. Palomar and M. Chiang, "A tutorial on decomposition methods for network utility maximization," *IEEE J. Sel. Areas Commun.*, vol. 24, pp. 1439–1451, Aug. 2006.

[70] K. Seong, M. Mohseni, and J. M. Cioffi, "Optimal resource allocation for OFDMA downlink systems," in *Proc. IEEE Int. Symp. Inform. Theory, Seattle, WA*, pp. 1394–1398, June 2006.

[71] A. T. Hoang and Y.-C. Liang, "Maximizing spectrum utilization of cognitive radio networks using channel allocation and power control," in *Proc. IEEE Veh. Tech. Conf., Montreal, Canada*, Sept. 2006.

[72] A. Attar, O. Holland, M. R. Nakhai, and A. H. Aghvami, "Interference-limited resource allocation for cognitive radio in orthogonal frequency-division multiplexing networks," *IET Commun.*, vol. 2, pp. 806–814, July 2008.

[73] D. Huang, C. Miao, and C. leung, "Resource allocation of MU-OFDM based cognitive radio systems under partial channel state information," *Computer Research Repository*, Aug. 2008.

[74] P. Mitran, L. Le, C. Rosenberg, and A. Girard, "Resource allocation for downlink spectrum sharing in cognitive radio networks," in *Proc. IEEE Veh. Tech. Conf., Calgary, Canada*, Sept. 2008.

[75] G. Bansal, M. J. Hossain, and V. K. Bhargava, "Optimal and suboptimal power allocation schemes for ofdm-based cognitive radio systems," *IEEE Trans. Wireless Commun.*, vol. 7, pp. 4710–4718, Nov. 2008.

[76] X. Kang, Y.-C. Liang, A. Nallanathan, H. K. Garg, and R. Zhang, "Optimal power allocation for fading channels in cognitive radio networks: ergodic capacity and outage capacity," *IEEE Trans. Wireless Commun.*, vol. 8, pp. 940–950, Feb. 2009.

[77] V. Asghari and S. Aissa, "Adaptive rate and power transmission in spectrum-sharing systems," *IEEE Trans. Wireless Commun.*, vol. 9, pp. 3272–3280, Oct. 2010.

[78] S. wook Han, H. Kim, Y. Han, and J. M. Cioffi, "Efficient power allocation schemes for nonconvex sum-rate maximization on gaussian cognitive MAC," *IEEE Trans. Commun.*, vol. 58, pp. 753–757, Mar. 2010.

[79] K. Son, B. C. Jung, S. Chong, and D. K. Sung, "Power allocation for OFDM-based cognitive radio systems under outage constraints," in *Proc. IEEE Int. Conf. Commun.*, 2010.

[80] X. Kang, H. K. Garg, Y.-C. Liang, and R. Zhang, "Optimal power allocation for OFDM-based cognitive radio with new primary transmission protection criteria," *IEEE Trans. Wireless Commun.*, vol. 9, pp. 2066–2075, June 2010.

[81] J. Hillenbrand, T. A. Weiss, and F. K. Jondral, "Calculation of detection and false alarm probabilities in spectrum pooling systems," *IEEE Commun. Let.*, vol. 9, pp. 349–351, Apr. 2005.

[82] P. K. Varshney, *Distributed Detection and Data Fusion*. New York: Springer-Verlag, 1997.

[83] H. L. V. Trees, *Detection, Estimation and Modulation Theory: Part I*. John Wiley & Sons Inc., 2001.

[84] A. Papoulis, *Probability, Random Variables, and Stochastic Process*. New York: McGraw-Hill, 4th ed., 2002.

[85] F. F. Digham, M. -S. Alouini, and M. K. Simon, "On the energy detection of unknown signals over fading channels," in *Proc. IEEE Int. Conf. Commun., Anchorage, AK*, vol. 5, pp. 3575–3579, May 2003.

[86] A. H. Nuttall, "Some integrals invloving the Q_M-function," in *Naval Underwater Systems Center (NUSC) Technical Report*, May 1974.

[87] I. S. Gradshteyn and I. M. Ryzhik, *Table of Integrals, Series, and Products*. San Diego, CA: Academic, 6th ed., 2000.

[88] B. Vujitic, N. Cackov, S. VujiCic, and L. Trajkovid, "Modeling and characterization of traffic in public safety wireless networks," in *Proc. Int. Symp. Performance Evaluation of Comput. and Telecommun. Syst., Philadelphia, PA*, pp. 214–223, July 2005.

[89] N. Matloff, "Renewal theory and some applications," in *University of California, Davis*, 2006.

[90] L. Yang, L. Cao, and H. Zheng, "Proactive channel access in dynamic spectrum networks," in *Proc. Int. Conf. Cognitive Radio Oriented Wireless Networks and Commun., Orlando, FL*, Aug. 2007.

[91] T. M. Cover and J. A. Thomas, *Elements of Information Theory*. New York: Wiley, 2nd ed., 1991.

[92] T. K. Moon and W. C. Stirling, *Mathematical Methods and Algorithms for Signal Processing*. New Jersey: Prentice Hall, 2000.

[93] Z. Chair, P. K. Varshney, "Optimal data fusion in multiple sensor detection systems," *IEEE Trans. Aerospace and Electron. Syst.*, vol. 1, pp. 98–101, Jan. 1986.

[94] D. Čabrić, S. M. Mishra, D.Willkomm, R. Brodersen, and A. Wolisz, "A cognitive radio approach for usage of virtual unlicensed spectrum," in *Proc. IST Mobile and Wireless Commun. Summit*, June 2005.

[95] K. Liu and A. M. Sayeed, "Optimal distributed detection strategies for wireless sensor networks," in *Proc. Allerton Conf. Commun., Control and Computing, Monticello, IL*, Sept. 2004.

[96] V. A. Vaishampayan, "Design of multiple description scalar quantizers," *IEEE Trans. Inf. Theory*, vol. 39, pp. 821–834, May 1993.

[97] Z. Chair and P. K. Varshney, "Distributed bayesian hypothesis testing with distributed data fusion," *IEEE Trans. Systems, Man Cybern.*, vol. 18, pp. 695–699, Sept. 1988.

[98] A. L. Stolyar, "Maximizing queueing network utility subject to stability: greedy primal-dual algorithm," *Queueing Systems*, vol. 50, no. 4, pp. 401–457, 2005.

[99] CEPT Report 31, "Frequency (channelling) arrangements for the 790-862 MHz band," in *http://www.erodocdb.dk/doks/relation.aspx?docid=2326*, Oct. 2009.

[100] S. J. Shellhammer, A. K. Sadek, and W, Zhang, "Technical challenges for cognitive radio in the TV white space spectrum," in *Proc. Inform. Theory and Applications Workshop, San Diego, CA*, Feb. 2009.

[101] P. J. Kolodzy, "Interference temperature: a metric for dynamic spectrum utilization," *Int. J. Netw. Management*, vol. 16, pp. 103–113, Mar. 2006.

[102] A. Ghasemi and E. S. Sousa, "Impact of user collaboration on the performance of opportunistic spectrum schemes," in *Proc. IEEE Veh. Tech. Conf., Montreal, Canada*, pp. 1–6, Sept. 2006.

[103] D. Bertsekas, *Nonlinear Programming*. New Hampshire: Athena Scientific, 1999.

[104] Y. Wei and R. Lui, "Dual methods for nonconvex spectrum optimization of multicarrier systems," *IEEE Trans. Commun.*, vol. 54, pp. 1310–1322, July 2006.

[105] X. Liu, E. K. P. Chong, and N. B. Shroff, "A framework for opportunistic scheduling in wireless networks," *Comput. Netw. J. (Elsevier)*, vol. 41, pp. 451–474, Mar. 2003.

[106] L. Li and A. J. Goldsmith, "Capacity and optimal resource allocation for fading broadcast channels - Part I: ergodic capacity," *IEEE Trans. Inf. Theory*, vol. 47, pp. 1083–1102, Mar. 2001.

[107] Y. Xing, C. N. Mathur, M. A. Haleem, R. Chandramouli, and K. P. Subbalakshmi, "Dynamic spectrum access with QoS and interference temperature constraints," *IEEE Trans. Mobile Computing*, vol. 6, pp. 423–433, Apr. 2007.

VITA

Xiangwei Zhou was born in Nanjing, Jiangsu Province, China. He received his B.S. degree in 2005 from the School of Electronic Engineering and Optoelectronic Techniques, Nanjing University of Science and Technology, Nanjing, China, and his M.S. degree in 2007 from the Department of Information Science and Electronic Engineering, Zhejiang University, Hangzhou, China. In 2011, he received the Ph.D. degree from the School of Electrical and Computer Engineering, Georgia Institute of Technology, Atlanta, Georgia.